ZSoil
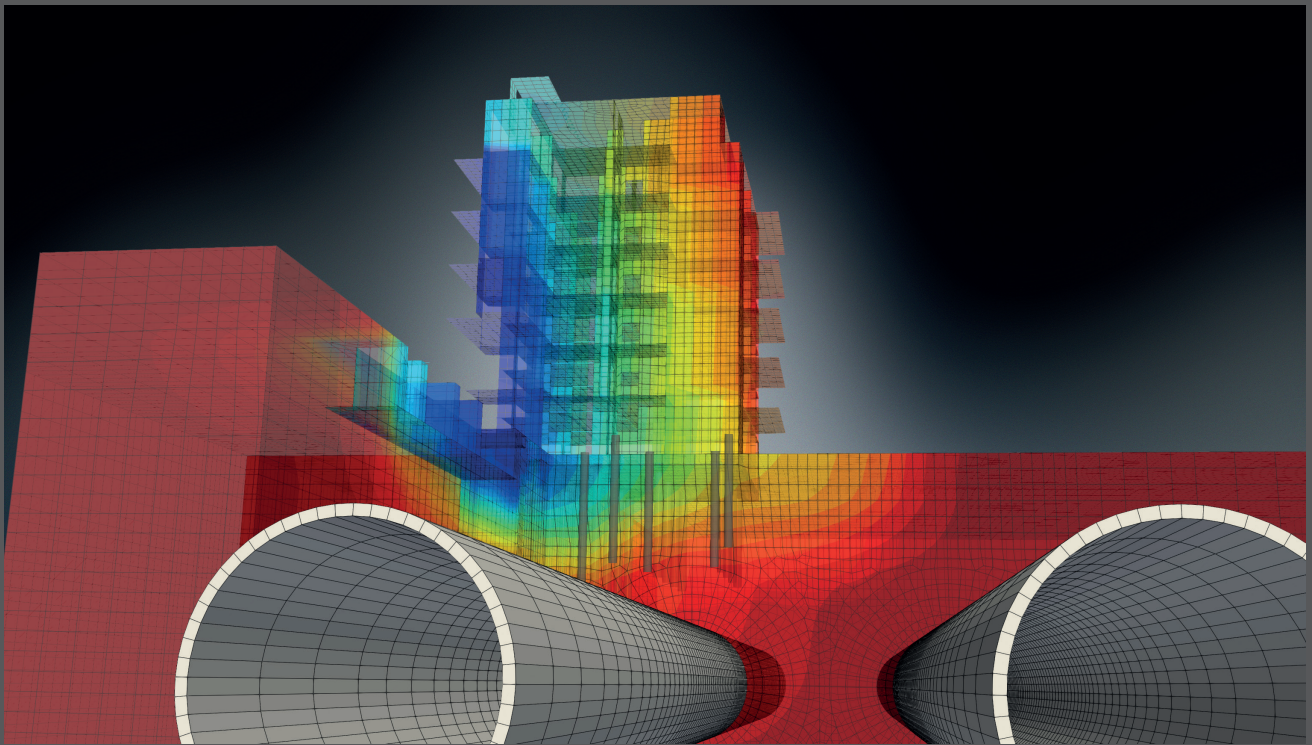
for geotechnics & structures

User manual
BENCHMARKS

Soil, rock and structural mechanics in dry or partially saturated media

ZSoil

for geotechnics & structures

BENCHMARKS
User manual
ZSoil®2026

A. Truty Th. Zimmermann K. Podleś R. Obrzud
with contribution by A. Urbański and S. Commend

WARNING

ZSoil is regularly updated for minor changes. We recommend that you send us your e-mail, as ZSoil owner, so that we can inform you of latest changes. Otherwise, consult our site regularly and download free upgrades to your version.

Latest updates to the manual are always included in the online help, so that slight differences with your printed manual will appear with time; always refer to the online manual for latest version, in case of doubt.

ZSoil 2026 manual:
1. Data preparation
2. Tutorials and benchmarks
3. Theory

END-USER LICENSE AGREEMENT FOR GeoDev's ZSoil® SOFTWARE

Applicable to all V2026 versions: professional & academic, single user & networks, under Windows 10, 11.

Read carefully this document, it is a binding agreement between you and GeoDev Sarl (GeoDev) for the software product identified above. By installing, copying, or otherwise using the software product identified above, you agree to be bound by the terms of this agreement. If you do not agree to the terms of this agreement, promptly return the unused software product to the place from which you obtained it for full refund of price paid. GEODEV SARL OFFERS A 60 DAYS MONEY-BACK GUARANTEE ON ZSOIL.

ZSOIL (the Software & associated hotline services when applicable) SOFTWARE PRODUCT LICENSE:

ZSOIL Software is protected by copyright laws and international copyright treaties, as well as other intellectual property laws and treaties. The **ZSOIL** software product is licensed, not sold.

1. GRANT OF LICENSE

   A: **GeoDev Sarl** grants you, the customer, a non-exclusive license to use N_{bought} (= the number of licenses bought) copies of **ZSOIL**. You may install copies of **ZSOIL** on an unlimited number of computers, provided that you use only N_{bought} copies at the time.

   B: You may make an unlimited number of copies of documents accompanying **ZSOIL**, provided that such copies shall be used only for internal purposes and are not republished or distributed to any third party.

   C: Duration of the agreement may be limited or unlimited, depending on license purchased. Installation of time unlimited licenses of ZSOIL V2026 will be supported for a period of 3 years starting from date of purchase. This support is limited to ZSOIL V2026 upgrades, under Windows 10 and 11.

2. COPYRIGHT

   All title and copyrights in and to **the Software** product (including but not limited to images, photographs, text, applets, etc.), the accompanying materials, and any copies of **ZSOIL** are owned by **GeoDev Sarl**. **ZSOIL** is protected by copyright laws and international treaties provisions. Therefore, you must treat **ZSOIL** like any other copyrighted material except that you may make copies of the software for backup or archival purposes or install the software as stipulated under section 1 above.

3. OTHER RIGHTS AND LIMITATIONS

   A: Limitations on Reverse Engineering, Decompilation, Disassembly. You may not reverse engineer, decompile, or disassemble **the Software**.

   B: No separation of components. **ZSOIL** is licensed as a single product and neither **the Software's** components, nor any upgrade may be separated for use by more than N_{bought} user(s) at the time.

   C: Rental. You may not lend, rent or lease the software product.

   D: Software transfer. You may permanently transfer all of your rights under this agreement and within the territory (country of purchase and delivery), provided you do not retain any copies, and the recipient agrees to all the terms of this agreement.

   E: Termination. Without prejudice to any other rights, **GeoDev Sarl** may terminate this agreement if you fail to comply with the conditions of this agreement. In such event, you must destroy all copies of **the Software**.

WARRANTIES & LIMITATIONS TO WARRANTIES

1. DISCLAIMER
   ZSOIL, developed by **GeoDev Sarl** is a finite element program for the analysis of above- and underground structures in which soil/rock & structural models are used to simulate the soil, rock and/or structural behaviour. The **ZSOIL** code and its soil/rock & structural models have been developed with great care. Although systematic testing and validation have been performed, it cannot be guaranteed that the **ZSOIL** code is free of errors. Moreover, the simulation of geotechnical and/or structural problems by means of the finite element method implicitly involves some inevitable numerical and modelling errors. **ZSOIL** is a tool intended to be used by trained professionals only and is not a substitute for the user's professional judgment or independent testing. The accuracy at which reality is approximated depends highly on the expertise of the user regarding the modelling of the problem, the understanding of the soil and structural models and their limitations, the selection of model parameters, and the ability to judge the reliability of the computational results. Hence, **ZSOIL** may only be used by professionals that possess the aforementioned expertise. The user must be aware of his/her responsibility when he/she uses the computational results for geotechnical design purposes. **GeoDev Sarl** cannot be held responsible or liable for design errors that are based on the output of **ZSOIL** calculations. The user is solely responsible for establishing the adequacy of independent procedures for testing the reliability, accuracy and completeness of any output of **ZSOIL** calculations.

2. LIMITED WARRANTY
   GeoDev Sarl warrants that **ZSOIL** will a) perform substantially in accordance with the accompanying written material for a period of 90 days from the date of receipt, and b) any hardware accompanying the product will be free from defects in materials and workmanship under normal use and service for a period of one year, from the date of receipt.

3. CUSTOMER REMEDIES
   GeoDev Sarl entire liability and your exclusive remedy shall be at **GeoDev's** option, either a) return of the price paid, or b) repair or replacement of the software or hardware component which does not meet **GeoDev**'s limited warranty, and which is returned to **GeoDev Sarl**, with a copy of proof of payment. This limited warranty is void if failure of **the Software** or hardware component has resulted from accident, abuse, or misapplication. Any replacement of software or hardware will be warranted for the remainder of the original warranty period or 30 days, whichever is longer.

NO OTHER WARRANTIES.

YOU ACKNOWLEDGE AND AGREE THAT **ZSOIL** IS PROVIDED ON AN "AS IS" AND "AS AVAILABLE" BASIS AND THAT YOUR USE OF OR RELIANCE UPON **ZSOIL** AND ANY THIRD PARTY CONTENT AND SERVICES ACCESSED THEREBY IS AT YOUR SOLE RISK AND DISCRETION. **GeoDev Sarl** AND ITS AFFILIATES, PARTNERS, SUPPLIERS AND LICENSORS HEREBY DISCLAIM ANY AND ALL REPRESENTATIONS, WARRANTIES AND GUARANTIES REGARDING **ZSOIL** AND THIRD PARTY CONTENT AND SERVICES, WHETHER EXPRESS,IMPLIED OR STATUTORY. TO THE MAXIMUM EXTENT PERMITTED BY APPLICABLE LAW, **GeoDev Sarl** DISCLAIMS ALL OTHER WARRANTIES, EITHER EXPRESS OR IMPLIED, INCLUDING, BUT NOT LIMITED TO, IMPLIED WARRANTIES OF MERCHANTABILITY AND FITNESS FOR A PARTICULAR PURPOSE, WITH REGARD TO THE SOFTWARE PRODUCT, AND ANY ACCOMPANYING HARDWARE.

NO LIABILITY FOR CONSEQUENTIAL DAMAGES.

TO THE MAXIMUM EXTENT PERMITTED BY LAW, IN NO EVENT SHALL **GeoDev Sarl** HAVE ANY LIABILITY (DIRECTLY OR INDIRECTLY) FOR ANY SPECIAL INCIDENTAL, INDIRECT, OR CONSEQUENTIAL DAMAGES WHATSOEVER (INCLUDING, WITHOUT LIMITATION, DAMAGES FOR LOSS OF BUSINESS, PROFITS, BUSINESS INTERRUPTION, LOSS OF BUSINESS INFORMATION, OR ANY OTHER PECUNIARY LOSS) ARISING OUT OF THE USE OF OR INABILITY TO USE ZSOIL, EVEN IF **GeoDev Sarl** HAS BEEN ADVISED OF THE POSSIBILITY OF SUCH DAMAGES.

OTHER PROVISIONS.

SUPPORT: If included in license price, assistance will be provided by **GeoDev Sarl**, by e-mail exclusively, during the first year following purchase. This service excludes all forms of consulting on actual projects. Installation support is limited to initially supported OS and a four year duration.

PROFESSIONAL VERSIONS of **ZSOIL** are meant to be used in practice & in research centers.

ACADEMIC VERSIONS of **ZSOIL** are meant to be used exclusively for teaching and research in academic institutions.

ACADEMIC WITH CONSULTING VERSIONS of **ZSOIL** are meant to be used exclusively for teaching, research and consulting in academic institutions.

The terms of this agreement may be amended in the future, by **GeoDev Sarl**, when necessary. In such cases the revised agreement will be resubmitted for user approval on the software's front screen.

APPLICABLE LAW AND JURISDICTION THIS AGREEMENT IS GOVERNED BY THE (SUBSTANTIVE) LAWS OF SWITZERLAND, ALL DISPUTES ARISING OUT OF OR IN CONNECTION WITH THIS AGREEMENT OR THE USE OF ZSOIL SHALL EXCLUSIVELY BE SETTLED BY THE ORDINARY COURTS OF CANTON DE VAUD (ARRONDISSEMENT DE LAUSANNE)

LAUSANNE 15.11.2025

Contents of Benchmarks

[1]concerns versions: **ACADEMIC, PROFESSIONAL, EXPERT** only

PREFACE

Document *BENCHMARKS* provides a set of examples where ZSoil® results are compared with another available results.

More complicated examples explaining different aspects of building computational model, related to practical problems may be found in *TUTORIALS* part.

The quickest approach to data preparation consists in loading an existing file, saving it under a different name (option SAVE AS in FILES) and then modifying it.

For the theoretical background see *THEORETICAL MANUAL*.

INTRODUCTION

ELEMENTARY BOUNDARY VALUE PROBLEMS

SOIL MECHANICS BENCHMARKS

FLOW BENCHMARKS

HEAT BENCHMARKS

STRUCTURAL BENCHMARKS

SOIL-STRUCTUREINTERACTION BENCHMARKS

Chapter 1

INTRODUCTION

Z_SOIL uses several yield criteria characterized by two parameters C, the cohesion, and ϕ, the friction angle. Various size adjustments of the yield criterion are possible which are discussed below and, more extensively, in the theoretical section.

- **DRUCKER-PRAGER CRITERION**

  Plane strain

  The following size adjustment is adopted by default in the program:

  $$k = C \cdot \cos \phi$$
  $$a_\phi = \sin \phi / 3.$$

  This corresponds to matching the collapse loads of Drucker–Prager and Mohr–Coulomb criteria under plane–strain conditions, assuming deviatoric plastic flow.

  It is sometimes preferable to adopt a different matching obtained by assuming coincidence of elastic domains and Poisson's ratio ν_t equal to 0.5 in the transverse direction, i.e.:

  $$k = C \cdot \cos \phi$$
  $$a_\phi = \sin \phi / 3$$
  $$\nu_t = 0.5.$$

  This results in:

  $$\sigma_3 = \sigma; \quad \sigma - \text{mean pressure}$$

  and

  $$s_3 = 0, \quad s_3 - \text{transverse deviatoric stress}$$

  σ_3 is then always the intermediate stress and the failure mechanism occurs in the plane Π_{12}.

  Axisymmetry

  Axisymmetry corresponds to a three–dimensional stress state. The default matching adopted in the program corresponds the average calibration given by

  $$k = \frac{6\sqrt{3} \cdot C \cdot \cos \sigma}{\left(9 - \sin^2 \phi\right)}$$
  $$a_\phi = \frac{2\sqrt{3} \cdot C \cdot \sin \sigma}{\left(9 - \sin^2 \phi\right)}$$

- **SMOOTH MOHR-COULOMB CRITERION**

  The smooth Mohr–Coulomb criterion also needs a size adjustment in principle. As a particular case, when the friction angle tends to zero, the smooth Mohr–Coulomb criterion transforms into von Mises criterion (identical to a Drucker–Prager criterion at $\phi = 0$). This corresponds to:

  $$\sqrt{J_2} = \frac{2}{\sqrt{3}}k$$

  Plane strain

 For the plane strain failure adjustment see theoretical section.

  Axisymmetry

  No size adjustment

- **INITIAL STATE**

  Some soil mechanics problems are characterized by a stress state which lies on the yield surface, i.e., on the limit of instability. It is therefore important to adopt appropriate material data to avoid triggering instability by an inappropriate choice of data. This is illustrated next.

  ZSoil® offers a box–shaped medium by default. Under initial gravity loading, when tectonic stresses are present, care must be taken to apply a value of the coefficient of earth pressure at rest K_0 which is acceptable. This can easily be done with the help of Figure a) In the figure Drucker–Prager 1 corresponds to the hypothesis that the horizontal stresses σ_1, σ_3 are equal. Drucker–Prager 2 corresponds to $\sigma_3 = 0.5 \cdot (\sigma_1 + \sigma_2)$.
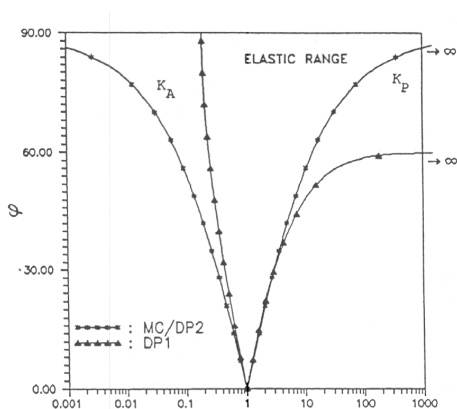
a) M–C & D–P horizontal surface
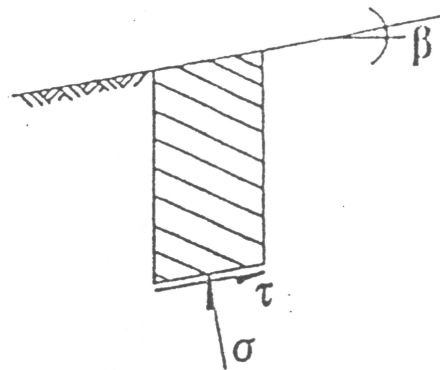
b)Infinite slope inclined at angle β
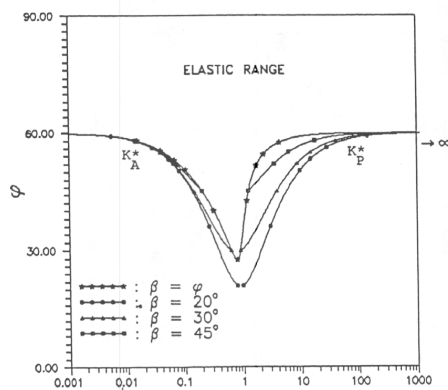
c) D–P~1, inclined surface
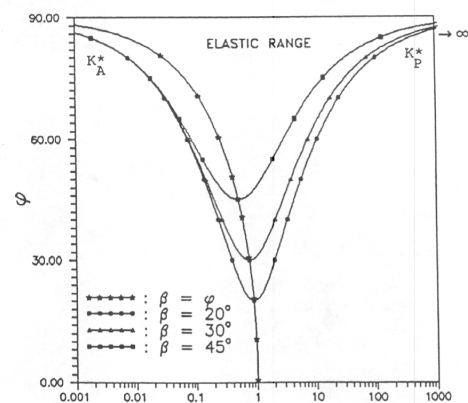
d) M–C & D–P2, inclined surface

When no tectonic stresses are applied, a function $\phi(\nu)$ can be derived for each adjustment of the yield criteria (see theoretical part), which corresponds to the onset of plastic behaviour. **As a general rule, the first step of the analysis should always be elastic in order to avoid overshooting the collapse load with the initial conditions.** This is illustrated later for several boundary–value problems.

Chapter 2

ELEMENTARY BOUNDARY VALUE PROBLEMS

BOX-SHAPED MEDIUM :

PLANE STRAIN AND AXISYMMETRY

WITH WATER BOUNDARY CONDITIONS

WITH OVERPRESSURE

2.1   BOX-SHAPED MEDIUM, PLANE STRAIN AND AXISYMME-TRY

The following derivation is valid for a dry medium or, in terms of effective stresses, for a saturated medium. For many problems the soil half-space can be conveniently approximated by a box shaped medium with smooth lateral boundaries.
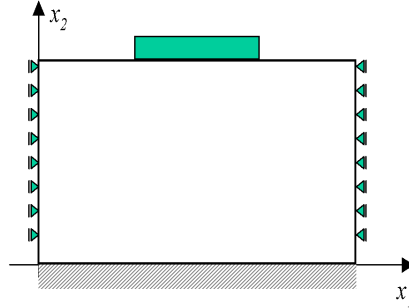

Figure 2.1: Box-shaped medium

The particular stress-strain state which results can easily be derived, for plane strain and the given lateral boundary conditions :
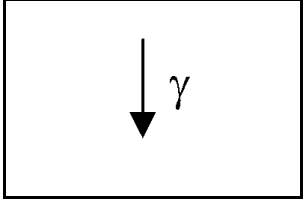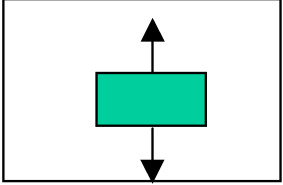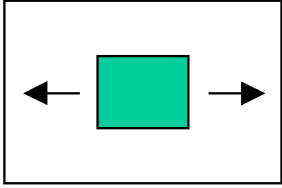
$$\varepsilon_3 = 0 \implies \sigma_3 = \nu(\sigma_1 + \sigma_2)$$
$$\varepsilon_1 = 0 \implies \sigma_1 = \nu(\sigma_2 + \sigma_3)$$

Therefore:

$$\sigma_1 = \frac{\nu}{1-\nu}\sigma_2 = K_0\sigma_2$$

The elastic stress-strain fields corresponding to some frequently encountered loading cases, for box-shaped medium with smooth lateral boundaries ($\varepsilon_1 = \varepsilon_3 = 0$) are summarized below:

No.	APPLICATION OF:	YIELDS:	WHERE:
1	**deadweight γ downwards** γ	$\sigma_2 = -\gamma h;$ $\sigma_1 = \sigma_3 = -\dfrac{\nu}{1-\nu}\gamma h;$ $\varepsilon_2 = -\dfrac{\gamma h}{E}(1 - \dfrac{2\nu^2}{1-\nu});$	**BOXD1.INP**
2	**vertical initial stress σ_{02}**	$\sigma_2 = 0;$ $\sigma_1 = \sigma_3 = -\dfrac{\nu}{1-\nu}\sigma_{02};$ $\varepsilon_2 = -\dfrac{\sigma_{02}}{E}(1 - \dfrac{2\nu^2}{1-\nu});$	**BOXD2.INP**

3	**horizontal initial stress** σ_{01} $\sigma_{01} = -0.5\gamma h$ 	$\sigma_1 = \sigma_{01}$; $\sigma_2 = \sigma_3 = 0$; $\varepsilon_2 = 0$;	**BOXD3.INP**
4	**gravity field,** $\sigma_{02} = -\gamma h$ $\sigma_{01} = K_0\sigma_{02}$; $\sigma_{03} = K_0\sigma_{02}$;	$\sigma_2 = -\gamma h$; $\sigma_1 = \sigma_3 = K_0\sigma_{02}$ $= -K_0\gamma h$; $\varepsilon_2 = 0$;	**BOXD4.INP**
5	**gravity field, automatically generated** as the initial state driver is activated in the program and K_0 is prescribed by the user (in a direction which is confined). (NB: $K_0 = \dfrac{\nu}{1-v}$, by default)		**BOXD5.INP**

As already mentioned, it is important to start always from an elastic state when performing either a load carrying capacity analysis or a stability analysis, this to avoid overshooting the limit load with the initial state. To help prevent this, Fig. 2.2 shows the limit of elastic behavior under gravity loading, which is the most common initial state. The elastic limit is reported for two possible matchings of the Drucker-Prager criterion with the Mohr-Coulomb criterion. When the data point (φ, ν) lies above the curve corresponding to the selected adjustment, behavior is elastic, otherwise it is plastic.

The first proposed adjustment corresponds to the matching of collapse loads under plane-strain conditions and deviatoric flow (the program's default option). The second one, corresponds to the matching of the elastic domain with Poisson's ratio equal to 0.5 in the transverse direction (orthotropic matching). The first matching seems physically more sensible, while the second is more favorable. Direct use of a Mohr-Coulomb criterion yields a result located in between.
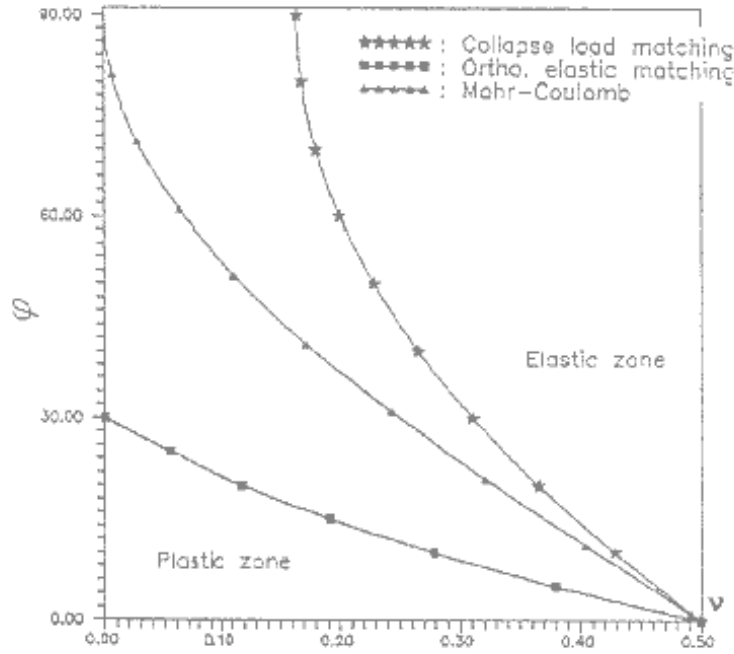
Figure 2.2: Influence of Poisson's ratio

2.2 BOX-SHAPED MEDIUM, WITH WATER BOUNDARY CONDITIONS

Data Files BOXW*.INP
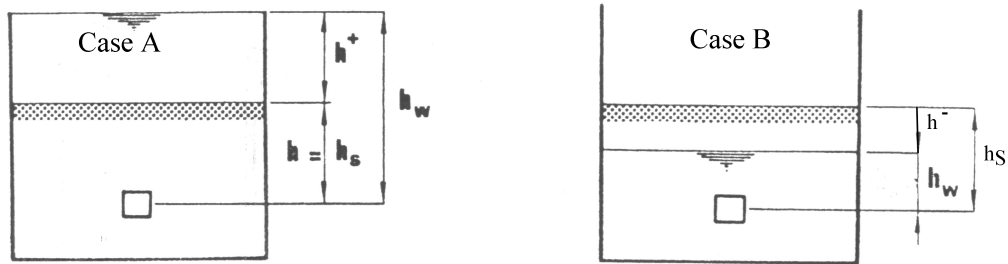
Figure 2.3: Box-shaped medium, with water table.

Appropriate water boundary conditions are applied on the top of the mesh. When necessary (BOXW1), a distributed force, acting on the solid and fluid phase, is added. Note that a coupled deformation and flow (steady-state) analysis is used here. The resulting effective stress state under gravity loading can then be derived as, assuming $\gamma = \gamma^{\mathsf{SAT}}$.

Case A:

$$\sigma'_2 = \sigma_2 - p^{\mathsf{F}} = -\gamma h_S - \gamma^{\mathsf{F}} h^+ + \gamma^{\mathsf{F}} h_W = -\gamma^{\mathsf{B}} h_S$$

$$\sigma'_1 = \sigma'_3 = \sigma_2 - p^{\mathsf{F}} = -\frac{\nu}{1-\nu} \gamma^{\mathsf{B}} h_S$$

$$\gamma^{\mathsf{B}} = \gamma^{\mathsf{SAT}} - \gamma^{\mathsf{F}}$$

Case B:

$$\sigma'_2 = \sigma_2 - p^{\mathsf{F}} = -\gamma h_S + \gamma^{\mathsf{F}} h_W = -\gamma(h_W + h^-) + \gamma^{\mathsf{F}} h_W$$
$$= -h_S(\gamma - \gamma^{\mathsf{F}}) - h^- \gamma$$
$$= -\gamma^{\mathsf{B}} h_S - \gamma h^-$$
$$\sigma'_1 = \sigma'_3 = \frac{\nu}{1 - \nu} \sigma'_2$$

When the water table is the only applied load these expressions reduce to:

$$\sigma'_1 = \sigma'_3 = \frac{\nu}{1 - \nu} \sigma'_2$$
$$\sigma'_2 = -\gamma^{\mathsf{F}} h_S$$

These cases can be verified using data: BOXW*.INP. Results are listed in the following table.

SITUATION	DATA	RESULTS	FILE
1	h=6.0 $\quad \gamma^{\mathsf{F}} = 10$ h_W=8.0 $\quad \gamma_{\mathsf{d}} = 0$ $\nu = 0.5 \quad e_o = 0$ Altitude of stress point: $h_\sigma = 2.0$	$\sigma'_1 = \sigma'_3 = 60$ $\sigma'_2 = 60$ $p^{\mathsf{F}} = -80$	**BOXW1.INP**
2	All data identical but: $h_W = 6.0$	$\sigma'_1 = \sigma'_3 = 60$ $\sigma'_2 = 60$ $p^{\mathsf{F}} = -60$	**BOXW2.INP**
3	All data identical but: $h_W = 5.0$	$\sigma'_1 = \sigma'_3 = 50$ $\sigma'_2 = 50$ $p^{\mathsf{F}} = -50$	**BOXW3.INP**

Again, initial data for the nonlinear analysis must be carefully chosen to avoid plasticity at the initial state, unless so desired. Figure 2.4 illustrates the elastic limit corresponding to gravity loading;

Remark:

Pressure results in the above examples are given in the element centers. In order to obtain them, go to postprocessor and use option `Info/Element results`. In the following table pressure will be given as p^F.
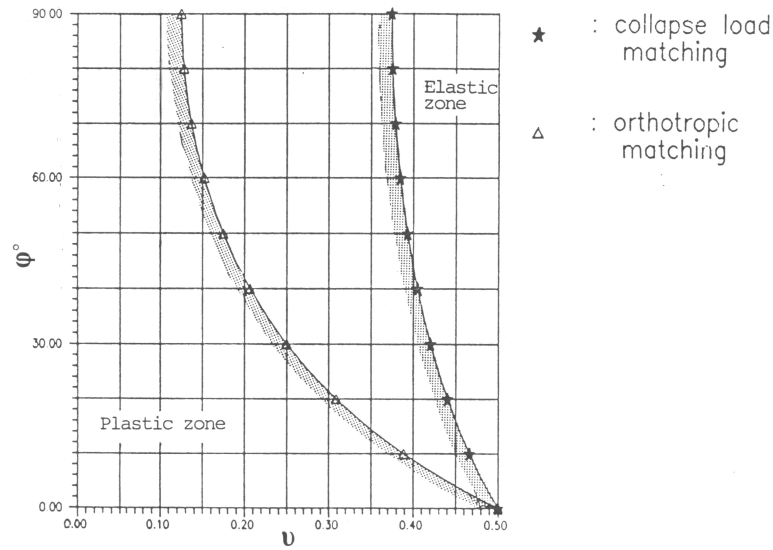
Figure 2.4: Influence of Poisson's ratio, saturated medium (cohesionless soil)

2.3 PLANE STRAIN BOX-SHAPED MEDIUM WITH OVERPRESSURE
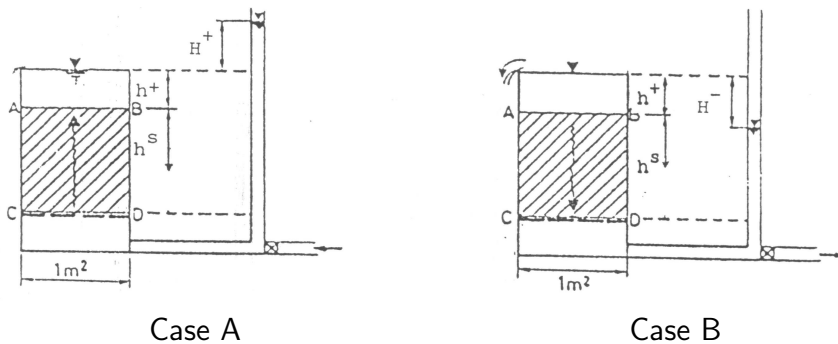
Case A   Case B

Figure 2.5: Downstream flow

Total and effective stresses :

Case A	Case B
$\sigma_2 = -(\gamma^\mathsf{F} h^+ + \gamma h_S)$	$\sigma_2 = -(\gamma^\mathsf{F} h^+ + \gamma h_S)$
$p^\mathsf{F} = -(h^+ + h_S + H^+)\gamma^\mathsf{F}$	$p^\mathsf{F} = -(h^+ + h_S - H^-)\gamma^\mathsf{F}$
$\sigma_2' = \sigma_2 - p^\mathsf{F} = -\gamma^\mathsf{B} h_S + \gamma^\mathsf{F} H^+$	$\sigma_2' = \sigma_2 - p^\mathsf{F} = -\gamma^\mathsf{B} h_S - \gamma^\mathsf{F} H^-$

For case A and B:

$$\sigma_1' = \frac{\nu}{1-\nu}\sigma_2'$$
$$\sigma_3' = \nu(\sigma_1' + \sigma_2')$$

N.B. : $H^+\gamma^F = (H^+/h_S \cdot h_S)\gamma^F = (i\gamma^F) \cdot h_S$ = seepage force; this shows equivalence of the seepage force with an overpressure.

In the program, overpressures are introduced through nodal values and computed at the center of elements.

CASE	DATA	RESULTS	FILE
A	$h_S = 1;\quad h^+ = 0.40$ $H^+ = 0.50$ $\gamma^F = 10 \quad \gamma = 18$ $K_o = 0.5 \quad (\nu = 0.333)$	$\sigma'_1 = \sigma'_3 = -1.5 kPa$ $\sigma'_2 = -3.0 kPa$ $p^F = -19 kPa$	**CASEA.INP**
B	$H^- = 0.50$	$\sigma'_1 = \sigma'_3 = -6.5 kPa$ $\sigma'_2 = -13.0 kPa$ $p^F = -9 kPa$	**CASEB.INP**

Remark:

Pressure results in the above examples are given in the element centers. In order to obtain them go to postprocessor and use option `Info/Element results`. In the resulting tabular output pressure is denoted by p^F.

Chapter 3

SOIL MECHANICS BENCHMARKS

LOAD CARRYING AND SETTLEMENTS OF FOUNDATIONS

STABILITY ANALYSIS

PRESTRESS

EXCAVATION AND CONSTRUCTION STAGES

CONSOLIDATION PROBLEMS

CREEP

SWELLING [1]

INFINITE MEDIA

---

[1]concerns versions: **ACADEMIC, PROFESSIONAL, EXPERT** only

3.1 LOAD CARRYING AND SETTLEMENTS OF FOUNDATIONS

SUPERFICIAL FOUNDATION (PLANE STRAIN)

EMBEDDED FOUNDATION

AXISYMMETRIC SUPERFICIAL FOUNDATION

3.1.1 SUPERFICIAL FOUNDATION (PLANE STRAIN)

This problem has been studied intensively by several authors. results for the rough and smooth footing are shown in the figure. The smaller upper bound obtained using Prandtl and Hill mechanism is reported from[2]. Additional results from[3], [4] are superposed, along with results from ZSoil®.
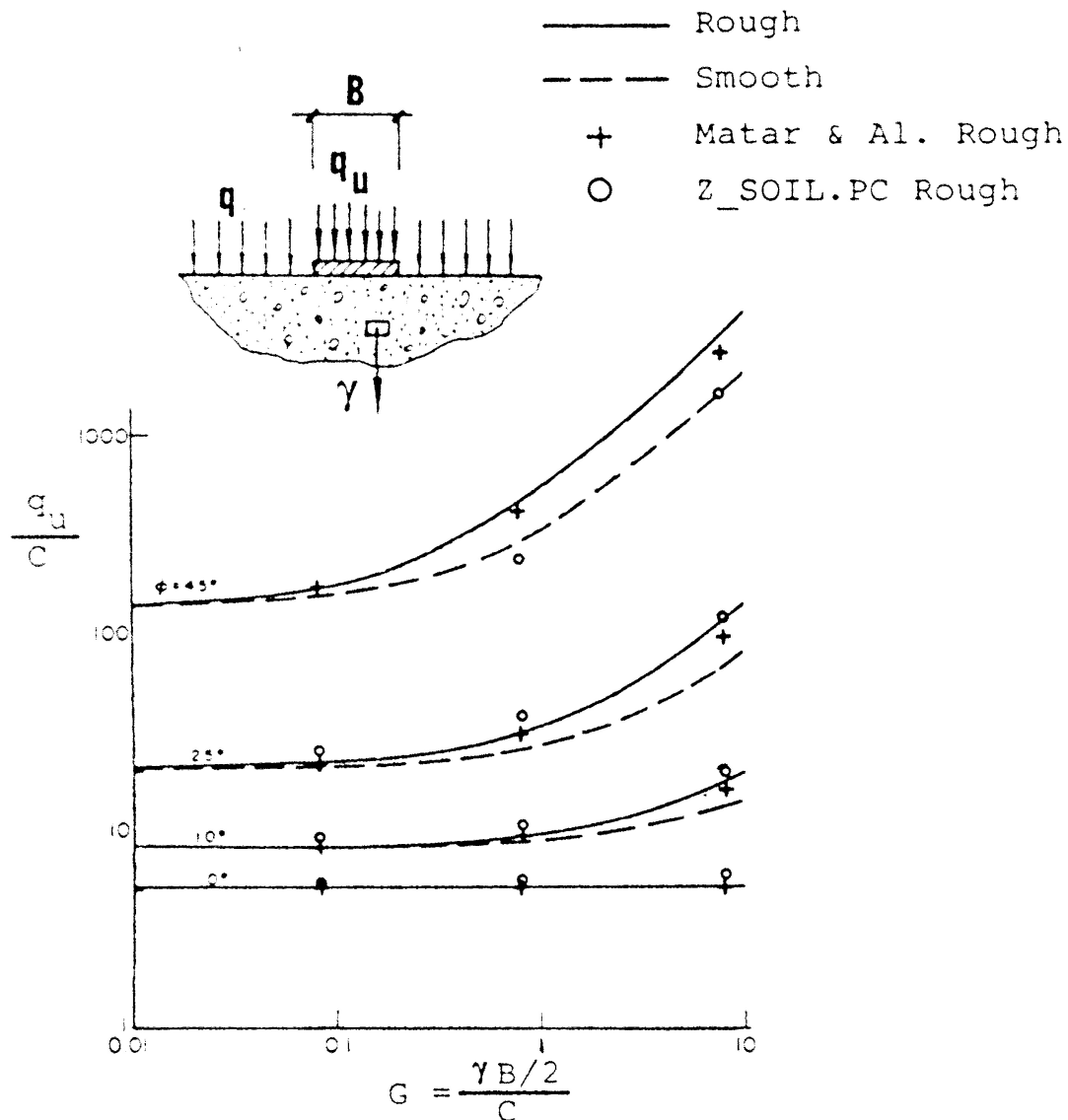

Figure 3.1: Bearing capacity of surface footing for $\phi = 0°$, $10°$, $25°$, $45°$

---

[2]W.F. Chen, Limit analysis and soil plasticity, Elsevier (1975).

[3]M. Matar and J.Salençon, Capacité portante des semelles filantes, Revue Française de Géotechnique, No.9 (1979).

[4]J. Salençon and M. Matar, Capacité portante des superficielles circulaires, Journal dé Méchanique Théorique et Appliqué, No.2 (1982).

- **Application 1:** Input file **FOOT.INP, FOOT-AUTO-STEP-CTRL.INP** (plane strain)

The meaningful data is set in the following tables:

Material	Model	Data group	Properties	Unit	Value
1 soil	Drucker-Prager	Elastic	E	[kN/m^2]	30000
			ν	—	0.38
		Nonlinear	ϕ	[°]	20
			Ψ	[°]	0
			C	[kN/m^2]	1
			Adjustment		Plane strain
2 concrete footing	Elastic	Elastic	E	[kN/m^2]	25000000
			ν	—	0.2

With B=2m a theoretical solution of $q_u = 15.6$ is obtained from J. Salençon & M. Matar paper. Using ZSoil$^®$, the solution converges at 15.6 but fails to converge at 15.8. In the data file **FOOT.INP** we use constant time step $\Delta t = 0.5$ but the load time function varies from zero to value 15.0 in the time period $t = 0 \div 3$ and then it varies from value 15.0 to 20.0 in the time range $t = 3 \div 8$. In the data file **FOOT-AUTO-STEP-CTRL.inp** we use the option of automatic time step reduction and restart the computation with the reduced step (by default by factor of 2.0) with maximum 3 reduction trials. In this data set we assume that the load time function varies from value 0 to 20.0 in the time range $t = 0 \div 4$. In both cases same ultimate load is obtained.
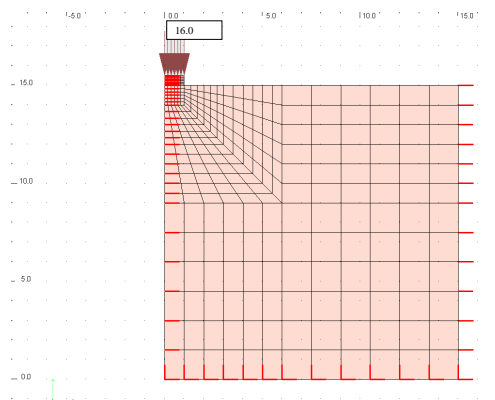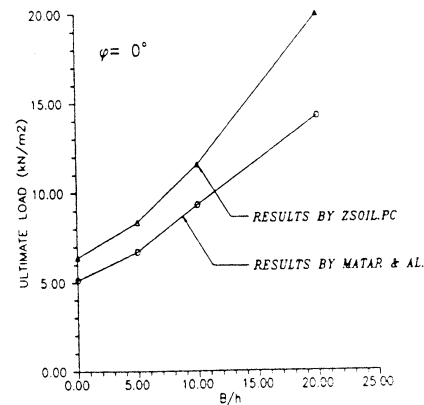

Figure 3.2: Mesh and geometry

Figure 3.3: Influence of distance to rigid layer (B/h)

In the numerical analysis the theoretical (J. Salençon & M. Matar paper) ultimate load is applied with a load multiplication factor varying between 0.5 to 1.5.

At low friction angles the numerical results show a safety factor F of about 1.2 w.r.t. the solution of J. Salençon & M. Matar paper. At high friction angles ($45°$) they undershoot the analytical solution $F = 0.7$.

The results obtained for small footing on an infinite medium with a rather crude mesh are reported in Fig. 1. In additon a study of influence of B/h was performed. Results are compared to the ones (J. Salençon & M. Matar paper) in Fig. 3.2. The overshoot of the analytical solution varies between 20% ($B/h = 0$) and 35% ($B/h = 0.2$).

- **Application 2:** Input file **FOOT-UNDRAINED.INP** (plane strain)

The same test as in Application 1 is run assuming undrained conditions. The analysis mode is changed to `Deformation+Flow` and `Driven Load (undrained)` driver is used with automatic step reduction activated. The analytical solution given by Prandtl yields the ultimate limit load of value $q_{ult} = (\pi + 2)\,c$. For cohesion $c = 20$ kPa the $q_{ult} = 102.8$ kN/m². The computed limit load is 105 kN/m². In the considered case the penalty fluid bulk modulus is set as $10^6 K$ and K is the elastic solid bulk modulus. The cut-off for suction pore pressure can be deactivated by setting large value for this parameter (here it is 10^6 kPa). Both parameters are kept in group `Flow`.

3.1.2 EMBEDDED FOUNDATION

• EMBEDDED FOUNDATION, DRY (PLANE STRAIN CASE)

A foundation embedded at a depth of 1.5 [m] is analyzed.
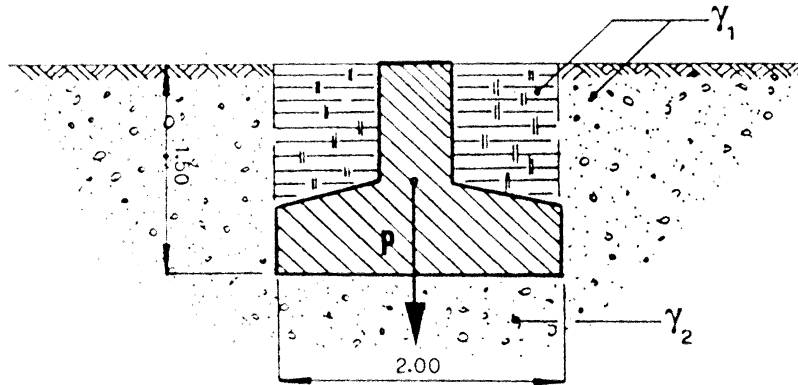

Figure 3.4: Embedded foundation

The bearing capacity expression following Terzaghi is:

$$q_u = c \cdot N_c + q \cdot N_q + \gamma \frac{B}{2} N_\gamma$$

where

$$p = q_u \cdot B.$$

Application: (input files: EMFT.INP, EMFT-AUTO-STEP-CTRL.INP)

$$\gamma_1 = \gamma_2 = 17 \left[\frac{\text{kN}}{\text{m}^3}\right], \quad C = 26 \left[\frac{\text{kN}}{\text{m}^3}\right], \quad \Phi = 28°$$

$$B = 2.00 \; [\text{m}] \; (\text{foundation width}),$$

$$h = 1.5 \; [\text{m}] \; (\text{foundation depth}).$$

Then:

a) using Terzaghi's parameters:

$$N_c = 34, \; N_q = 18, \; N_\gamma = 14, \; q_u = 1649 \left[\frac{\text{kN}}{\text{m}^2}\right]$$

b) using Meyerhof's parameters:

$$N_c = 28, \; N_q = 18, \; N_\gamma = 14, \; q_u = 1425 \left[\frac{\text{kN}}{\text{m}^2}\right].$$

Matar and Salençon propose an alternative expression for the bearing capacity:

$$q_u = q + \mu_c \left(C_0 + q \cdot \tan \Phi\right) \cdot \left(\frac{1}{2} \cdot \frac{g + \gamma \tan \Phi}{C_0 + q \tan \Phi} \cdot B \cdot N'_\gamma + C_0 \tan \Phi + N'_c\right)$$

which takes the form for the constant cohesion $C_0 = C$ $(g = 0)$:

$$q_u = q + \mu_c \left(C_0 + q \cdot \tan \Phi\right) \cdot \left(\frac{1}{2} \cdot \frac{\gamma B N'_\gamma}{C + q \tan \Phi} + N'_c\right).$$

Then:

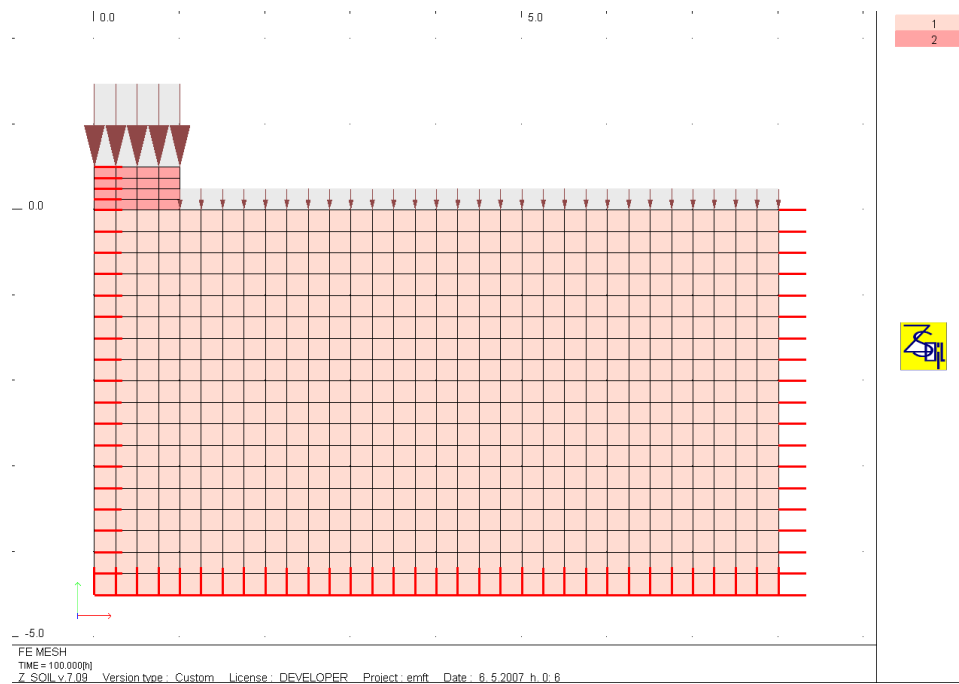$$\mu_c = 1.115, \ N'_\gamma = 11, \ N'_c = 34, \ q_u = 1868 \left[\frac{\text{kN}}{\text{m}^2}\right]$$
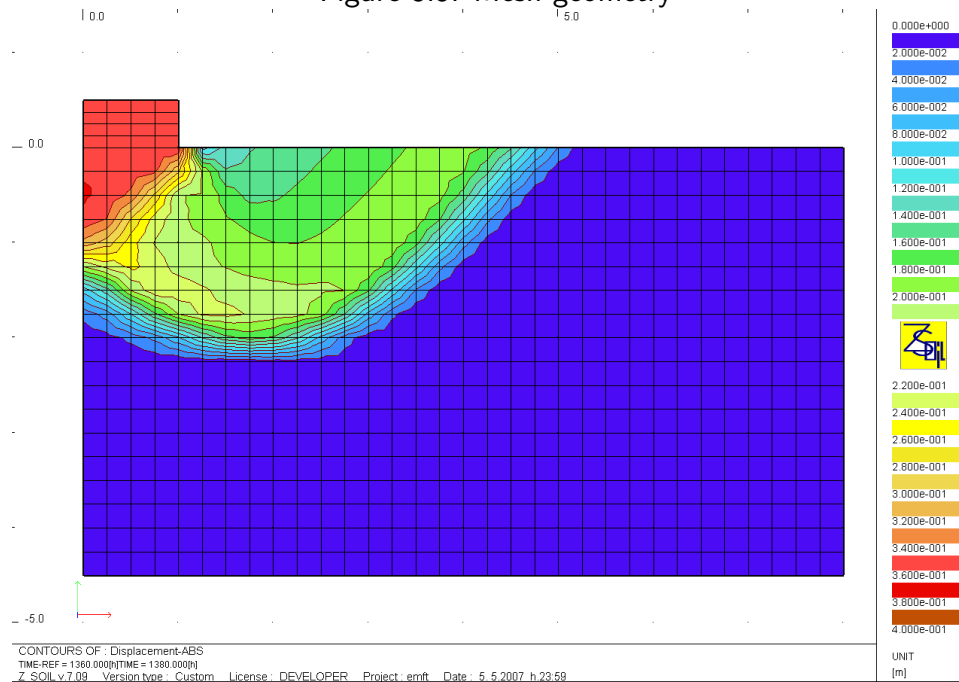

Figure 3.5: Mesh geometry

Figure 3.6: Failure mechanism

Material	Model	Data group	Properties	Unit	Value
1 soil	Drucker-Prager	Elastic	E	[kN/m^2]	10000
			ν	—	0.35
		Density	γ	[kN/m^3]	17
		Nonlinear	ϕ	[°]	28
			Ψ	[°]	0
			C	[kN/m^2]	26
			Adjustment		Plane strain
2 concrete footing	Elastic	Elastic	E	[kN/m^2]	25000000
			ν	–	0.2

The q load simulates the 1.5 [m] soil layer while p load, applied to concrete footing is increased until collapse. The calculated bearing capacity is equal to: $p = 1360 \left[\frac{kN}{m^2}\right]$ for the first model (here the load at which failure state was generated is equal to 1380) and $p = 1369 \left[\frac{kN}{m^2}\right]$ for data set with automatic step reduction. Comparison with the theoretical solution yields the following results:

	Terzaghi	Meyerhof	Matar–Salençon
$\dfrac{p}{(q_u)_{\text{theor}}}$	0.82	0.95	0.73

Note that this analysis is performed with an initial state followed by a driven load.

- **EMBEDDED FOUNDATION, DRY (AXISYMMETRIC CASE)**

The same problem is solved for the axisymmetric case (input file: **EMFTA.INP).** The ultimate load corresponds to: $p = 2275 \left[\frac{kN}{m^2}\right]$ which can be compared to the analytical solutions:

	Terzaghi	Matar–Salençon
$\dfrac{p}{(q_u)_{\text{theor}}}$	1.02	0.94

- **EMBEDDED FOUNDATION, DRAINED WITH WATER BOUNDARY CONDITIONS (PLANE STRAIN CASE)**

A foundation embedded at 1.5 [m] depth with a water table at the foundation level is analyzed.
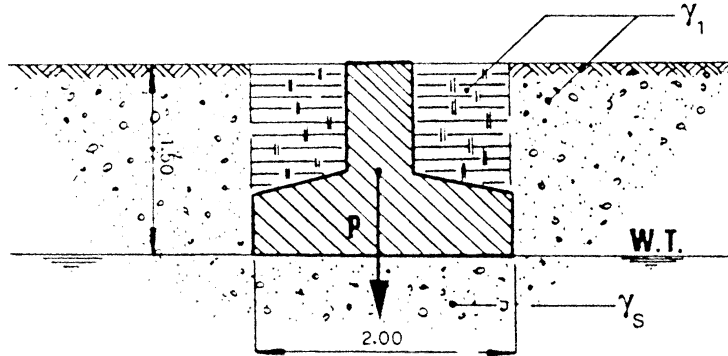

Figure 3.7: Embedded foundation with water table

Solution

The bearing capacity factor of Terzaghi and of Meyerhof are the same as for the dry case but the parameters of Matar & Salençon change, then: $q_u = 1423 \left[\frac{kN}{m^2}\right]$.

Application

a) Terzaghi:

$$q_u = 1604 \left[\frac{kN}{m^2}\right]$$

b) Meyerhof:

$$q_u = 1408 \left[\frac{kN}{m^2}\right]$$

c) Matar & Salençon:

$$(\mu_b = 1.1), \text{ then } q_u = 1423 \left[\frac{kN}{m^2}\right].$$

Computation of the bearing capacity gives the following results (file: **EMFTW.INP**):

$$p = 1155 \left[\frac{kN}{m^2}\right].$$

Compared to the theoretical solution, the following ratios result:

	Terzaghi	Meyerhof	Matar–Salençon
$\dfrac{p}{(q_u)_{\text{theor}}}$	0.72	0.82	0.81

3.1.3   AXISYMMETRIC SUPERFICIAL FOUNDATION

File: FOOTA.INP

This problem is similar to the one discussed under Superficial foundation (plane strain), except for the axisymmetric geometry. The influence of several parameters is analyzed here and comparizons are made with results of other authors.

Fig. 3.2 shows the geometry. Material data are $E = 3000 \left[\frac{kN}{m^2}\right]$, Poisson's ratio $\nu = 0.38$, cohesion $C = 1.0 \left[\frac{kN}{m^2}\right]$ and dilatancy $\psi = 0°$ (incompressible plastic flow). The value of the friction angle is first varied between $20°$ and $45°$ and the corresponding bearing capacities are illustrated in Fig. 3.9 for different yield surfaces: smooth Mohr–Coulomb, internal and external Drucker–Prager adjustments to Mohr–Coulomb. These numerical predictions are compared with the analytical results given by three different methods. Two of these methods are based on limit analysis, that is Terzaghis method adjusted by Vesic[5] for circular footings and the method developed by Salençon and Matar. The third analytical method is based on the slip–line method and was developed by Cox[6]. All the results are presented in Fig. 3.9 for comparison. It can be seen that all the theoretical and numerical methods predict the same increase of the ultimate bearing stress with increase of the friction angle. However, this increase varies depending on the considered method and that variation is not only observed for the numerical methods but also for the analytical ones illustrating the sensitivity of the problem. From Fig. 3.9 it can be seen that the ultimate bearing stress is bounded by the values obtained with the Drucker–Prager material calibrated to the two extreme values. For a friction angle greater than $36.8°$ no clear failure could be obtained with the external Drucker–Prager criterion as illustrated by the vertical asymptotic trend. It can also be observed that the bearing stress predicted with the smooth Mohr–Coulomb condition and the one obtained with the method developed by Salençon and Matar are in a very close agreement. Furthermore, the agreement is improved for increasing friction angle. This is probably due to the fact that the smooth Mohr–Coulomb condition approximates the original Mohr–Coulomb one (used by Salençon and Matar) more closely for higher values of the friction angle as illustrated in Cox, Eason & Hopkins paper.
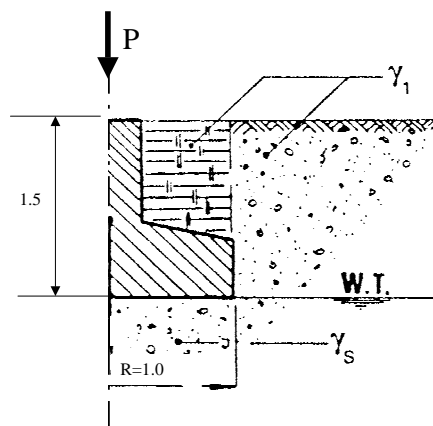

Figure 3.8: Axisymmetric embedded foundation with water table

The analysis of the above results suggests that the calibration of the Drucker–Prager surface

---

[5]Vesic, Foundation Engineering Handbook, Chapter 3, Bearing capacity of Shallow Foundations (pp.121–147), Van Nostrand Reinhold (1975).

[6]Cox, Eason & Hopkins, Axially symmetric plastic deformation in soils, Phil.Trans. of the Royal Soc. of London, 254 (pp.1–45), (1961).

is best when using a mean value between the internal and external Mohr–Coulomb adjustment such as

$$a_\phi = \frac{2\sqrt{3} \cdot \sin\phi}{9 - \sin^2\phi}$$

$$k = \frac{6\sqrt{3} \cdot C \cdot \cos\phi}{9 - \sin^2\phi}$$
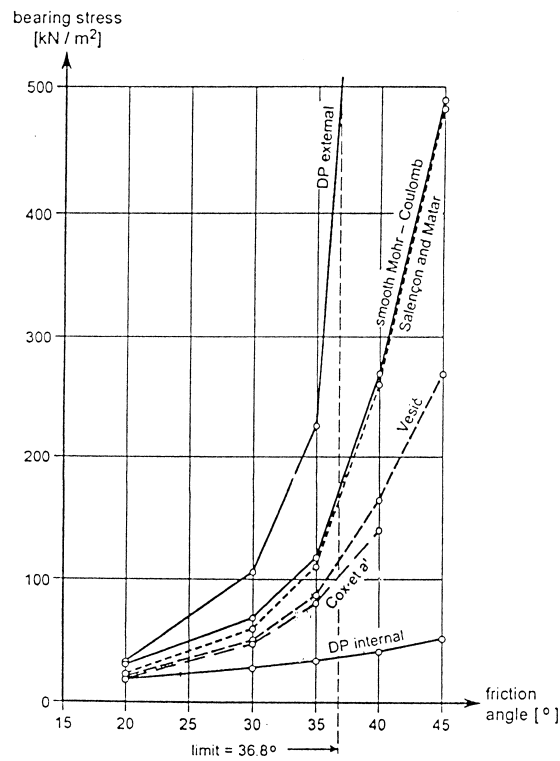

Figure 3.9: Comparison of the computed ultimate bearing stresses

This calibration will lead to results which are closer to the ones obtained with the Mohr–Coulomb criterion, especially for axisymmetric computations. It can be noted that this calibration is characterized by a limiting friction angle $45°$ for which the load carrying capacity tends to infinity. This adjustment covers most of the friction angles observed in soil. It is therefore adopted as default adjustment for axisymmetry.

3.2   STABILITY ANALYSIS

SLOPES

SEISMIC BEARING CAPACITY OF STRIP FOOTING ON SLOPES

SLOPE STABILITY IN PRESENCE OF SEEPAGE FLOW

3.2.1 SLOPES

- **Analytical solution**

a) Vertical cut

Let the theoretical safety factor be:

$$F_{\text{th}} = \frac{H_c}{H} \leq \frac{N_s \cdot C}{\gamma \cdot H}$$

given $\dfrac{C}{\gamma \cdot H} = 0.2$ (**CUT.INP**) the following theoretical result:

$\phi°$	0	10	20	30	40
F_{th}	0.77	0.92	1.1	1.34	1.66

b) Natural slope at $45°$

Several conventional approaches to slope stability are used and compared with results from **Z_SOIL PC**.
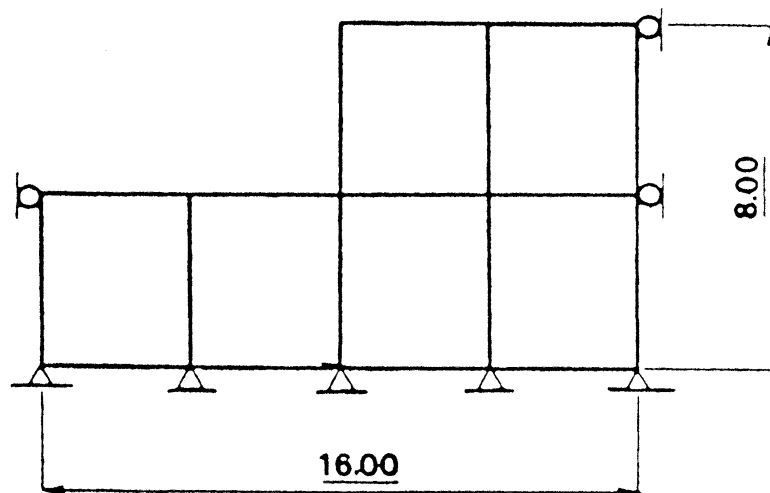
- **Z_SOIL simulation**

CUT.INP

Figure 3.10: Mesh and geometry

Material	Model	Data group	Properties	Unit	Value
1 soil	Drucker-Prager	Elastic	E	[kN/m^2]	10000
			ν	—	0.40
		Density	γ	[kN/m^3]	20
		Nonlinear	ϕ	[°]	30
			Ψ	[°]	0
			C	[kN/m^2]	26
			Adjustment		Plane strain

NSLOPE.INP
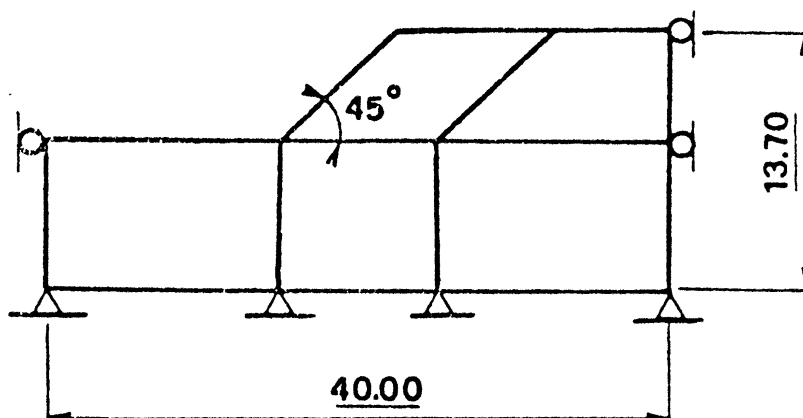
Figure 3.11: Mesh and geometry

Material	Model	Data group	Properties	Unit	Value
1 soil	Drucker-Prager	Elastic	E	[kN/m^2]	5000
			ν	—	0.30
		Density	γ	[kN/m^3]	24
		Nonlinear	ϕ	[°]	30
			Ψ	[°]	0
			C	[kN/m^2]	27.36
			Adjustment		Plane strain

- Comparison of results of **Z_SOIL PC** with conventional methods, and parametric study.
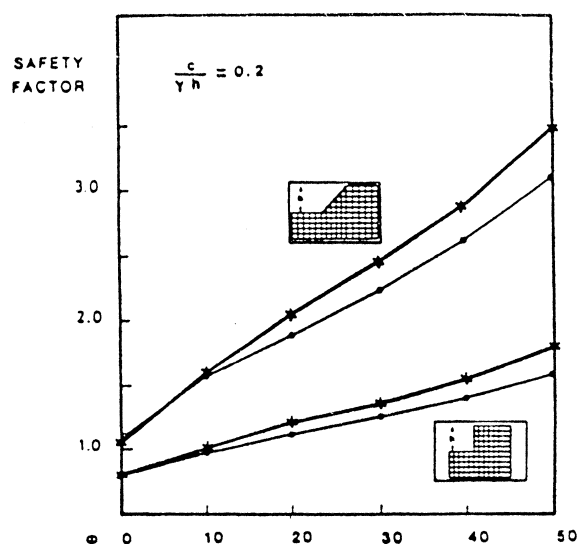
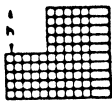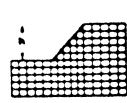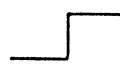Figure 3.12: Results by Z_Soil (last converged step, increments SF_2 by $0.05SF$)
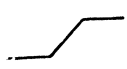
		Z_SOIL.PC		METHOD OF SLICES	
$\frac{C}{\gamma H}$	ϕ				
0.2	0	0.80	1.10	.801	1.10
	10	1.00	1.60	.967	1.57
	20	1.10	2.10	1.12	1.89
	30	1.30	2.50	1.26	2.23
	40	1.50	2.90	1.40	2.62
	50	1.70	3.40	1.59	3.11

Figure 3.13: Result comparison

$\tan\phi$ $\frac{c}{\gamma\cdot H}$	Simplified Bishop	Ord. Meth. of slices	Friction circle	Janbu procedure	**Z_SOIL**
2	1.17	1.12	1.14	1.10	1.20
5	1.83	1.73	1.78	1.70	2.00
8	2.48	2.30	2.36	2.26	2.60

Nondim. length between lat. bnd	Total number of nodes used to discretize the soil medium					
	25	55	91	136	190	253
0.75	2.3	2.3	2.2	2.2	2.2	2.2
1.00	2.4	2.4	2.3	2.2	2.2	2.2
1.25	2.4	2.4	2.4	2.3	2.3	2.2

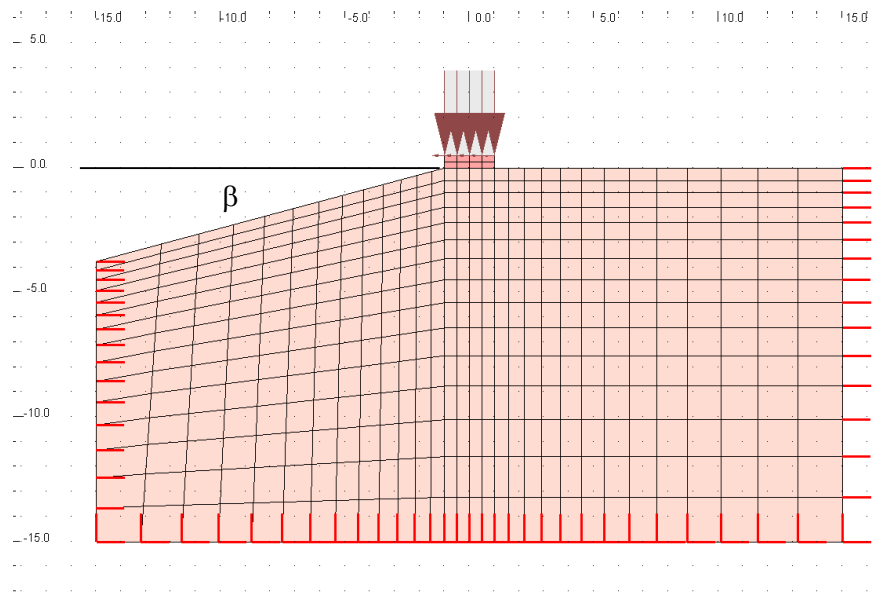## 3.2.2 SEISMIC BEARING CAPACITY OF STRIP FOOTING ON SLOPES

Figure 3.14: Problem geometry

The seismic bearing capacity of strip footings located on top of a slope is calculated and compared to results obtained by Soubra and Reynolds[7] using an approximate upper bound approach.

The geometry of the problem is shown in Fig. 3.14 and $B_0 = 2\,[\mathrm{m}]\,, \lambda = 0$. Material data are as follows:

Material	Model	Data group	Properties	Unit	Value
1 soil	Drucker-Prager	Elastic	E	[kN/m^2]	30000
			ν	—	0.30
		Density	γ	[kN/m^3]	20
		Nonlinear	ϕ	[°]	30
			Ψ	[°]	0 / 30
			C	[kN/m^2]	80÷400
		Adjustment			Plane strain
2 concrete footing	Elastic	Elastic	E	[kN/m^2]	20000000
			ν	–	0.15

Loads include gravity with a horizontal component $K_h \cdot \gamma$ and the footing loading with the same horizontal component.

---

[7]A.I. Soubra & F.Reynolds, Design charts for the seismic bearing capacity of strip footing slopes. In 'Slope Stability in Seismic Areas', ... Editions (1992).

The corresponding data files are:

seismic_b00_kh000	$(\beta = 0°, K_h - 0.00)$
seismic_b00_kh015	$(\beta = 0°, K_h - 0.15)$
seismic_b15_kh000	$(\beta = 15°, K_h - 0.00)$
seismic_b15_kh015	$(\beta = 15°, K_h - 0.15)$
seismic_b30_kh000	$(\beta = 30°, K_h - 0.00)$
seismic_b30_kh015	$(\beta = 30°, K_h - 0.15)$

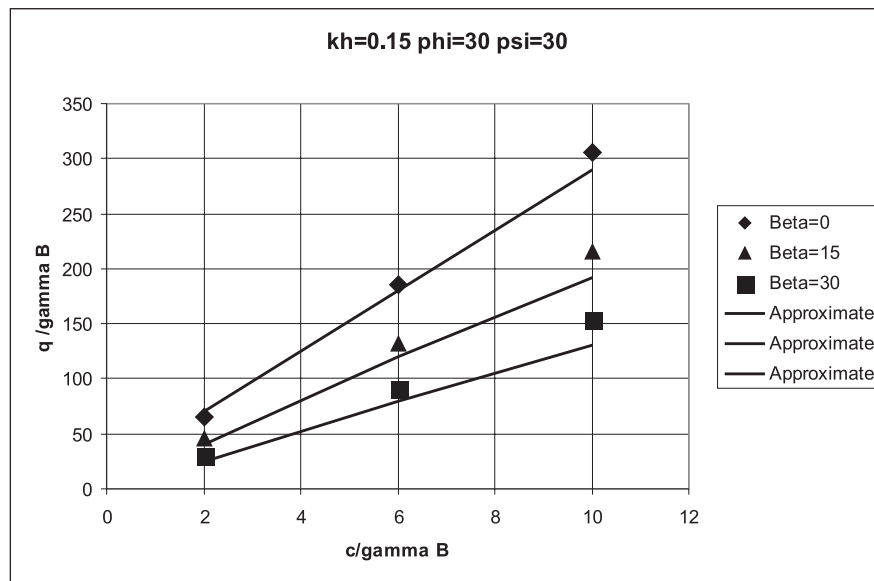The following charts are taken from A.I. Soubra & F.Reynolds paper and completed with results obtained with **Z_SOIL**.
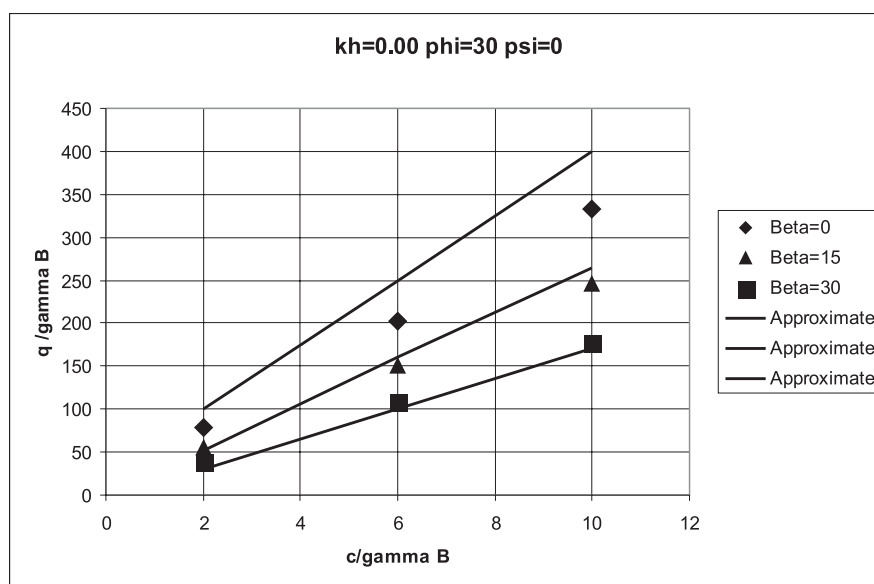

Figure 3.15: Seismic bearing capacity (1)

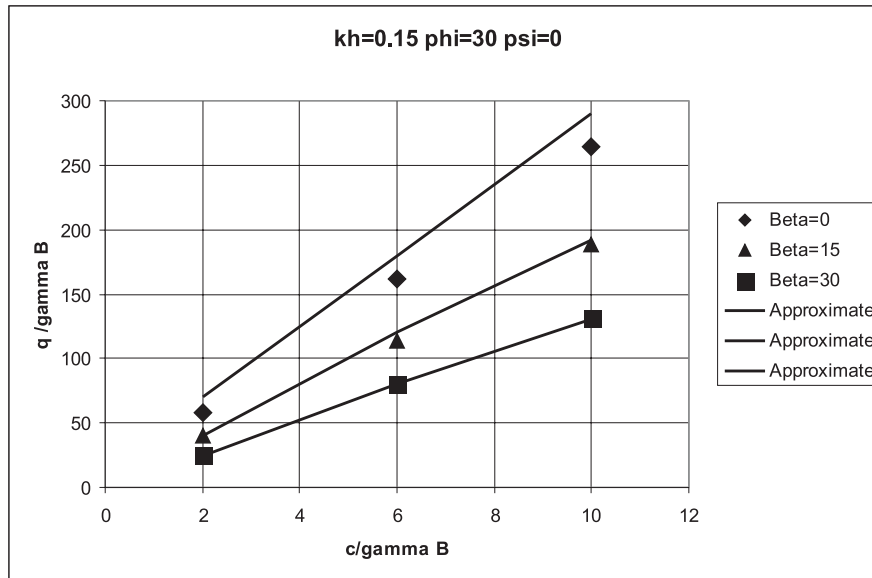Figure 3.16: Seismic bearing capacity (2)
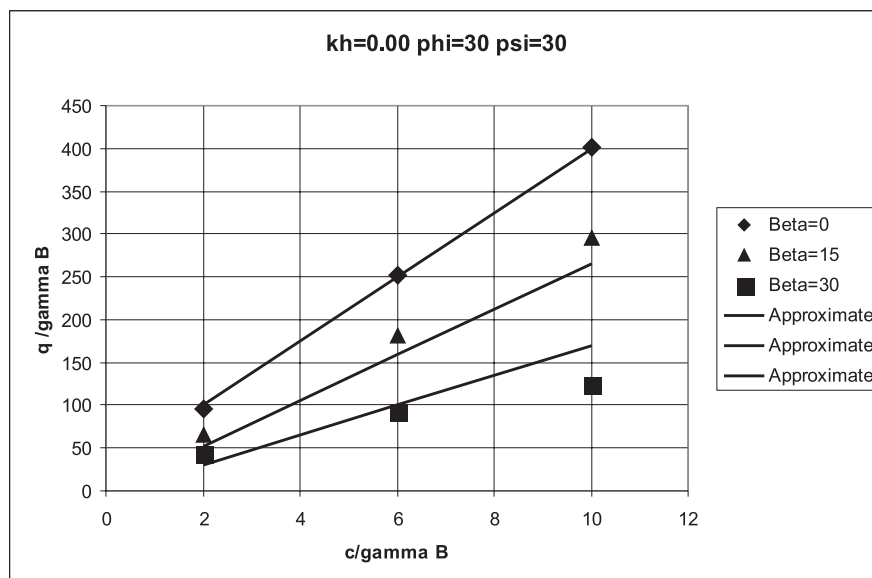
Figure 3.17: Seismic bearing capacity (3)

Figure 3.18: Seismic bearing capacity (4)
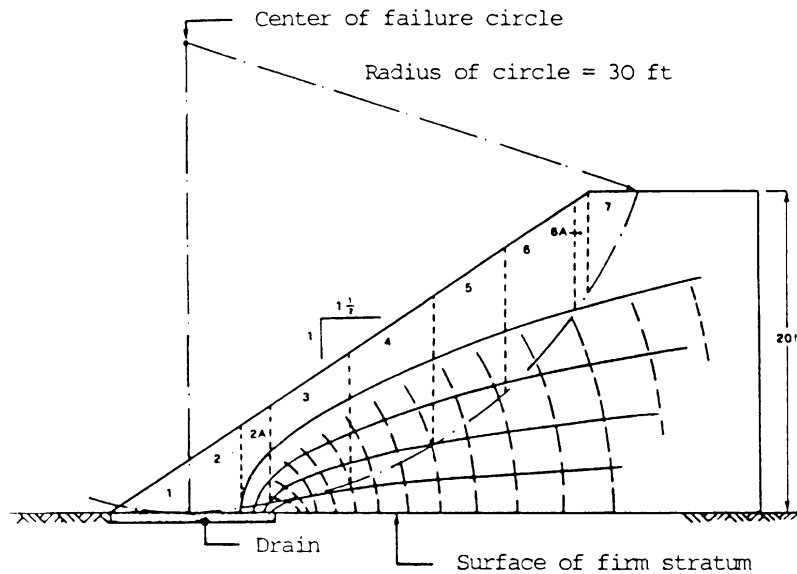
3.2.3   SLOPE STABILITY IN PRESENCE OF SEEPAGE FLOW

Figure 3.19: Earth slope with seepage flow

The problem is analyzed using the slip circle approach

- **Application**

Given a slope of $34°$, the flow boundary conditions and the following soil strength parameters

$$\gamma = 125 \left[\frac{\text{lb}}{\text{ft}^3} \right], \; C = 90 \left[\frac{\text{lb}}{\text{ft}^2} \right], \; \phi = 32°$$

The following safety factor is obtained: $F_{\text{th}} = 1.27$ (according Lambe & Whitman).

- **Z_SOIL PC simulation**

Data File: drain02.inp

One material set is used:

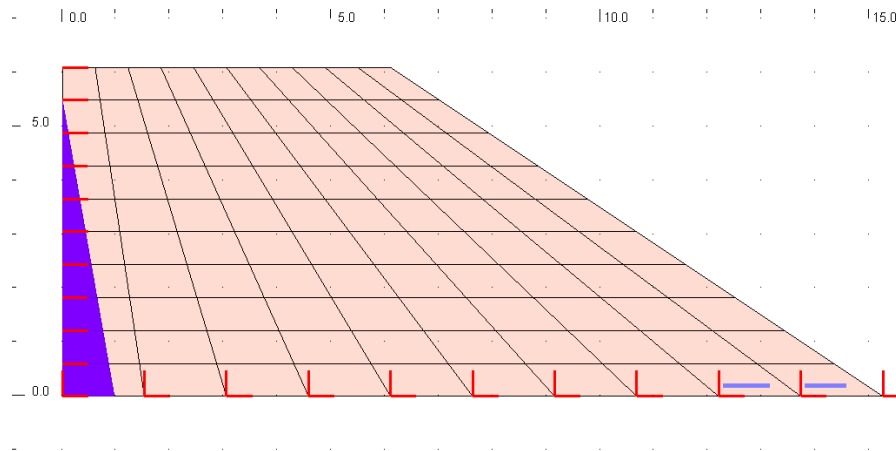| Material	Model	Data group	Properties	Unit	Value
1 soil	Drucker-Prager	Elastic	E	[kN/m^2]	100457
			ν	—	0.30
		Density	γ	[kN/m^3]	23.52
			γ^{F}	[kN/m^3]	10
		Nonlinear	ϕ	[°]	30
			Ψ	[°]	0
			C	[kN/m^2]	4.78
			Adjustment		Plane strain
		Flow	$k_x = k_y$	[m/day]	1
			K^{F}	[kN/m^2]	10^{38}
			S_r	–	0
			α	[1/m]	2

Figure 3.20: Mesh and geometry

A coupled deformation flow analysis is performed: first, an initial state is done, followed by a safety analysis. The failure occurs for F between $1.25 \div 1.30$.
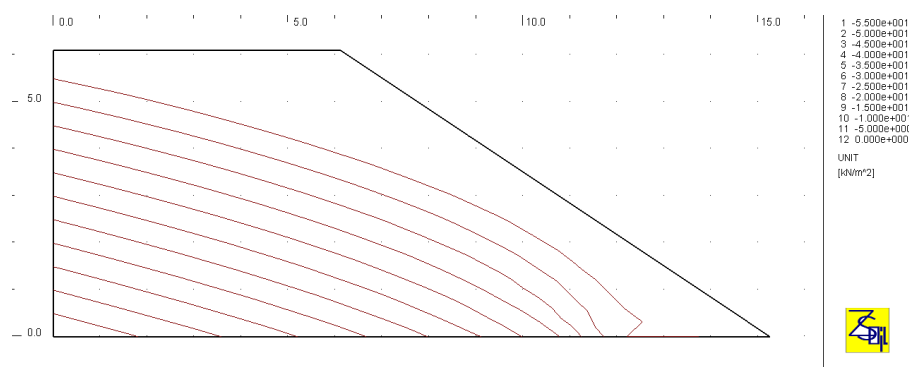

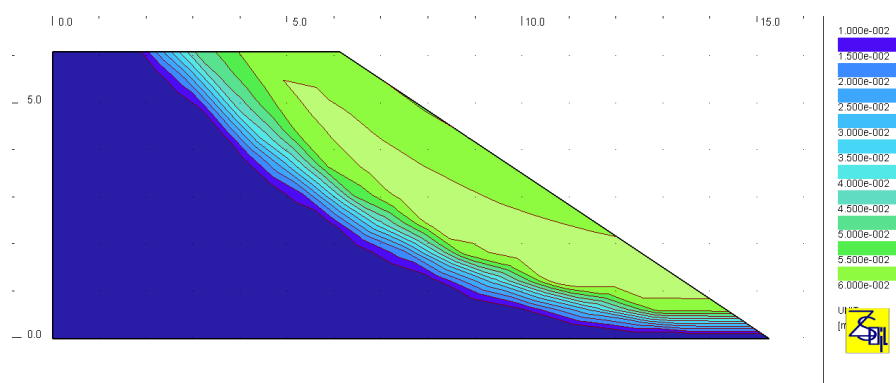Figure 3.21: Total pore pressure (steady state calculated from the water B.C.)

Figure 3.22: Stability failure circle for $SF = 1.3$

3.3 PRESTRESS

SINGLE ANCHOR

3.3.1 SINGLE ANCHOR

- **File: TA1.INP**

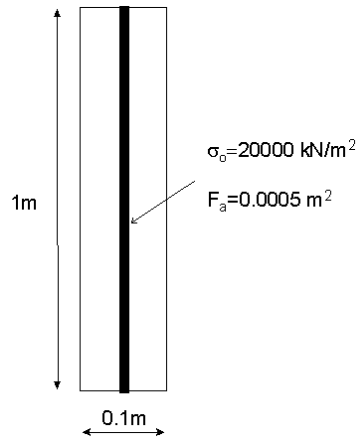- **Geometry and data:**

  Analysis type: *Plane strain*

Figure 3.23: Prestressed anchor, geometry

Material data:

	Material	Model	Data group	Properties	Unit	Value
1	concrete	Elastic	Elastic	E	[kN/m^2]	20000000
				ν	—	0.0
2	steel anchor	Elastic	Elastic	E	[kN/m^2]	200000000
				ν	–	0.0
				$Area$	[m^2]	0.0005

- **Problem description:**

  This test illustrates the application of prestress when stiffness of the anchor is taken into account. The analysis is performed over 4 time steps. At time $t = 1$ prescribed prestressing stress is applied, as indicated by the corresponding *LOADING FUNCTION* (Fig. 3.24). As long as the corresponding *EXISTENCE FUNCTION* (fig 3.24) is on ($t \leq 2$) no injection takes place and and prestress is monitored to stay at its nominal value. When the *EXISTENCE FUNCTION* value is set to 0, prestress is no more monitored, injected behavior is assumed ($t > 2$) and steel deforms with concrete. A compression load of 100 is applied at time $t = 3$

- **Results:**

  The solution of this problem is expressed by the following set of equations.

$$\sigma_a^o F_a + \sigma_c^o F_c = 0$$
$$\Delta\sigma_a F_a + \Delta\sigma_c F_c = -q F_c$$
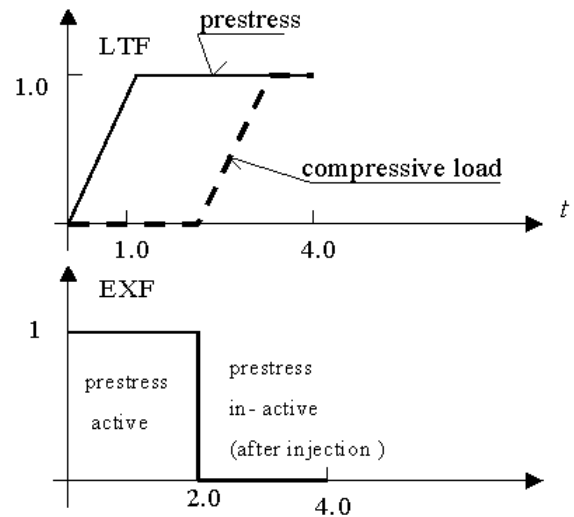$$\frac{\Delta\sigma_a}{E_a} = \frac{\Delta\sigma_c}{E_c}$$

Figure 3.24: Load functions and existence function for prestress

where: σ_a° is the assumed prestress value,

F_a is the steel cross section,

σ_c^o is the stress in concrete after prestressing,

F_c is the concrete cross section.

Starting from t=2 the prestress is not controlled anymore and additional vertical compressive load q applied to the top concrete surface induces additional stress/strain state change both in anchor and concrete. The second equation expresses force balance and the third one expresses strain increment compatibility.

t	σ_a [kN/m^2]	$N_a = \sigma_a F_a$ [kN]	σ_c [kN/m^2]	$N_c = \sigma_c F_c$ [kN]	$N = N_a + N_c$ [kN]
1	20000	10	-100	-10	0
2	20000	10	-100	-10	0
3	19047	9.52	-195.2	-19.52	-10

3.4 EXCAVATION AND CONSTRUCTION STAGES

EXCAVATION WITH PROGRESSIVE UNLOADING

3.4.1   EXCAVATION WITH PROGRESSIVE UNLOADING

Consider the following excavation in an elastic medium, with associated unloading function.

Gravity generates a uniform stress state (**UNL1.INP**) which is maintained after excavation until $t = 2$, due to the unloading function Unloading starts decreasing. At the time $t = 4$ the redistribution of stresses due to excavation has ended. The solution reached corresponds to the one obtained with a direct computation of excavated state (**UNL2.INP**).
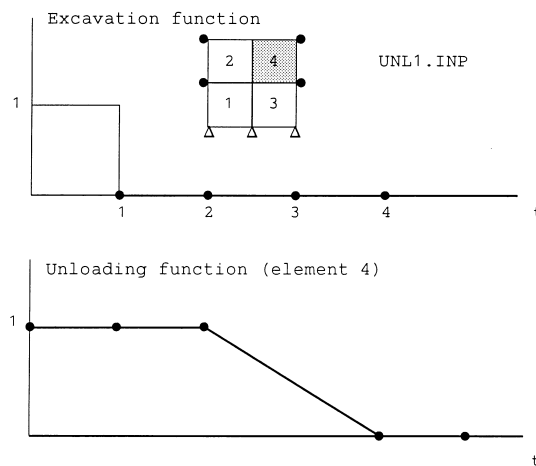
Figure 3.25: Excavation and unloading functions

3.5 CONSOLIDATION PROBLEMS

OEDOMETRIC TEST

TWO LAYERS MEDIUM

TWO LAYERS WITH WATER TABLE

TWO–DIMENSIONAL FOOTING SETTLEMENT

ELASTOPLASTIC COMPRESSION

3.5.1 TERZAGHI'S 1D CONSOLIDATION TEST

This problem illustrates the performance of the numerical model in the case of 1D consolidation. The analytical solution for excess pore pressure, given by Terzaghi, is taken from[8].

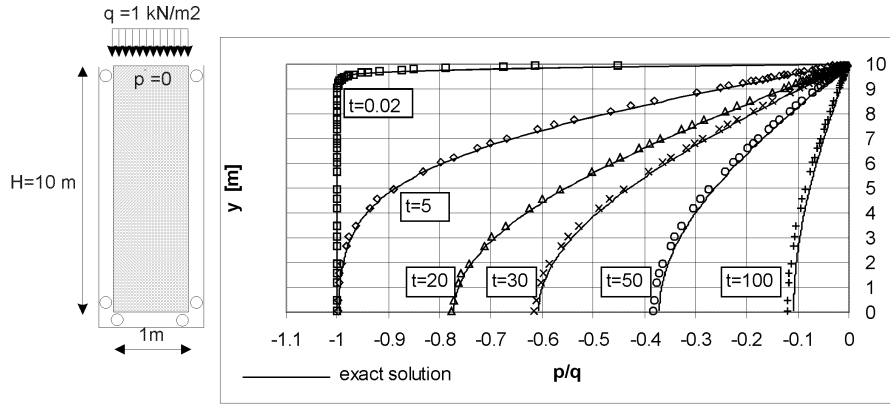Consolidation test **Input files: CNS1DPS.INP** (plain strain), **CNS1DAXS.INP** (axisymmetry)

Figure 3.26: Problem statement (left); Solution (right)

Analytical solution takes the following form:

$$\frac{p^{\mathsf{F}}(z,t)}{q} = \sum_{m=0}^{\infty} \left(\frac{2}{M}\right) \sin\left(\frac{M \cdot z}{H}\right) \exp\left(-M^2 \cdot T_v\right)$$

$$M = \frac{\pi(2m+1)}{2}$$

$$T_v = \left(\frac{C_v \cdot t}{H^2}\right); \qquad C_v = \left(\frac{E_{\mathsf{oed}} \cdot k}{\gamma^{\mathsf{F}}}\right) \ (=1).$$

Numerical solution

Critical time step[9]

$$\Delta t_{\mathsf{crit}} \geq \left(\gamma_c = \frac{1}{6}\right) \cdot \frac{h^2}{\alpha C_v}$$

(here $\alpha = 1, \gamma_c = \frac{1}{4}, \Delta t_{\mathsf{crit}} = 0.0039$ [d], $h = 0.125$ m (element size adjacent to the edge where pressure boundary condition is prescribed) and assumed initial time step $\Delta t = 0.025$ [d]. Both the analytical and the numerical solution are illustrated in the Fig. 3.26 for $T_v = (10^{-4})$ to 1)

Material	Model	Data group	Properties	Unit	Value
1 soil	Elastic	Elastic	E	[kN/m^2]	100
			ν	—	0.0
		Flow	$k_{x'}$	[m/day]	0.1
			$k_{y'}$	[m/day]	0.1
			K^{F}	[kN/m^2]	10^{38}

---

[8]Bowles, Physical and Geotechnical Properties of Soil, Mc Graw–Hill (1979)

[9]P. Vermeer, A. Verruijt, An accuracy condition for consolidation by finite elements, Int.J.Num.Anal.meth.Geomech., **5** (pp.1–14)

3.5.2   BIOT'S 1D CONSOLIDATION TEST

This problem illustrates the performance of the numerical model in the case of 1D consolidation taking into account the effect of Biot coefficient ($\tilde{\alpha} < 1$). The analytical solution for the excess pore pressure, is taken from[10].

Input files: CNS1DPS-BIOT-1.INP, **CNS1DPS-BIOT-1-STAB-OFF.INP**, **CNS1DPS-BIOT-1-STAB.INP**

Analytical solution takes the following form:

$$\frac{p^{\mathsf{F}}\left(z,t\right)}{q} = \frac{p_o}{q} \sum_{m=1,3..}^{\infty} \left(\frac{4}{m\pi}\right) \sin\left(\frac{m\pi z}{2H}\right) \exp\left(-m^2\pi^2\tau\right)$$

$$\tilde{\alpha} = 1 - \frac{K}{K_s}$$

$$B = 1 - \frac{n\left(\frac{K}{K_f} - \frac{K}{K_s}\right)}{\left(1 - \frac{K}{K_s}\right) + n\left(\frac{K}{K_f} - \frac{K}{K_s}\right)}$$

$$\nu_u = \frac{B\tilde{\alpha}\left(1-2\nu\right) + 3\nu}{3 - B\tilde{\alpha}\left(1-2\tilde{\alpha}\nu\right)}$$

$$\frac{p_o}{q} = \frac{B\left(1+\nu_u\right)}{3\left(1-\nu_u\right)}$$

$$c = \frac{k}{\gamma^F S}$$

$$\tau = \frac{c\,t}{4\,H^2}$$

$$M = \frac{2G\left(\nu_u - \nu\right)}{\tilde{\alpha}^2\left(1-2\nu_u\right)\left(1-2\nu\right)}$$

$$S = \frac{\left(1-2\nu_u\right)\left(1-2\nu\right)}{M\left(1-\nu\right)\left(1-2\nu_u\right)}$$

where porosity is denoted by n ($n = e_0/(1+e_0)$).

Data set used in this benchmark is given in table below

Material	Model	Data group	Properties	Unit	Value
1 soil	Elastic	Elastic	E	[kN/m^2]	20000000
			ν	—	0.25
		Density	γ_d	[kN/m^3]	22
			e_0	—	0.25
		Flow	$k_{x'}$	[m/day]	8.64e-06
			$k_{y'}$	[m/day]	8.64e-06
			K^{F}	[kN/m^2]	2000000
			$\tilde{\alpha}$	—	0.75

---

[10]Detournay, E. and Cheng, A.H.-D., "Fundamentals of poroelasticity," Chapter 5 in Comprehensive Rock Engineering: Principles, Practice and Projects, Vol. II, Analysis and Design Method, ed. C. Fairhurst, Pergamon Press, pp. 113-171, 1993
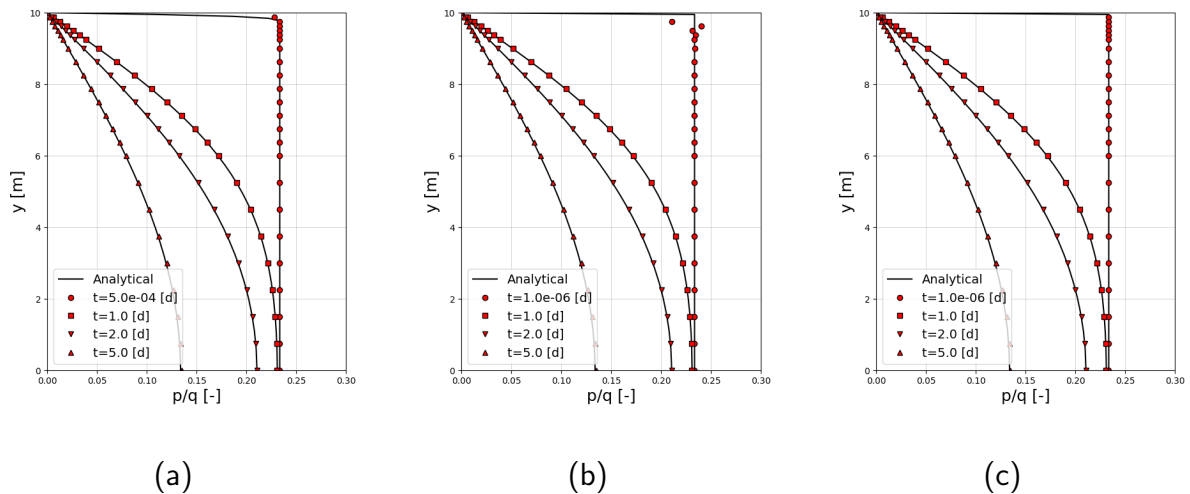
Figure 3.27: Profiles of excess pore pressures at different time instances. (a) initial time step larger than the critical one (b) nonstabilized solution (initial time step much smaller than the critical one) (c) stabilized solution (initial time step much smaller than the critical one)

3.5.3 TERZAGHI CONSOLIDATION, TWO LAYERS MEDIUM

This problem is similar to the single layer problem. The computed solution is compared to a finite difference solution[11].

Remark:

At both top and bottom surface the appropriate pressure boundary conditions are assumed to allow drainage through those surfaces.

Window 3-1: Input file: TWOLAY.INP

Excess pore pressure (a difference between pressure at given time instance and pressure at the initial state) results of both numerical solutions are compared in the figure below.

---

[11]G. Sanglerat, G. Olivari & B. Cambon, Practical problems in soil mechanics and foundation engineering, Elsevier (1984).
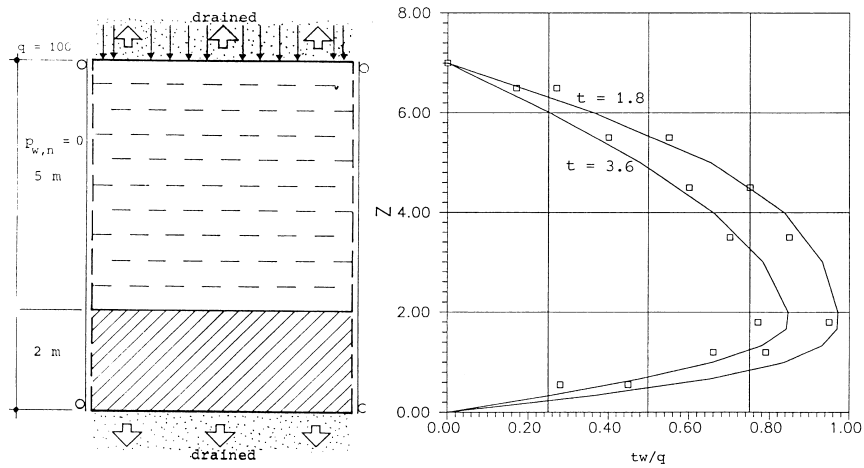
Consolidation of a two layer medium

Window 3-1

Material	Model	Data group	Properties	Unit	Value
1 soil	Elastic	Elastic	E	[MN/m^2]	16.36
			ν	—	0.0
		Flow	$k_{x'}$	[m/day]	0.095
			$k_{y'}$	[m/day]	0.095
			K^{F}	[kN/m^2]	10^{38}
			$\tilde{\alpha}$	—	1.0
2 soil	Elastic	Elastic	E	[MN/m^2]	73.63
			ν	—	0.0
		Flow	$k_{x'}$	[m/day]	0.19
			$k_{y'}$	[m/day]	0.19
			K^{F}	[kN/m^2]	10^{38}
			$\tilde{\alpha}$	—	1.0

3.5.4 TERZAGHI CONSOLIDATION, TWO LAYERS WITH WATER TABLE

The computed solution is compared with an analytical solution by R. Holtz & W. Kovacs[12]; alternatively the same formula as presented in 3.5.1 can be used.

Window 3-2: Input file: HOLTZ.INP
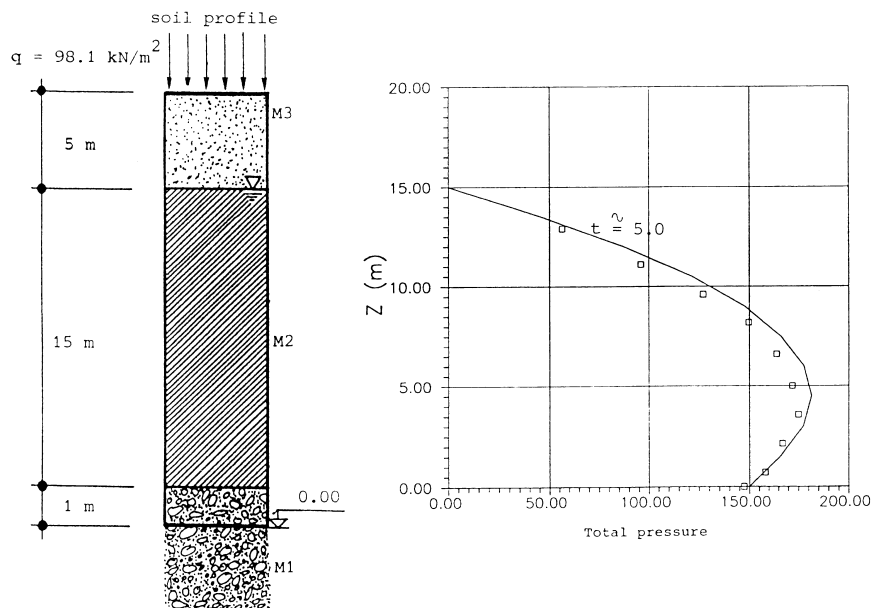
Consolidation of a two layers medium with water table; geometry (left) and computed vs. analytical results (right)

Window 3-2

Material	Model	Data group	Properties	Unit	Value
1 soil	Elastic	Elastic	E	[kN/m^2]	563
			ν	—	0.35
		Flow	$k_{x'}$	[m/day]	0.017
			$k_{y'}$	[m/day]	0.017
			K^{F}	[kN/m^2]	10^{38}
			$\tilde{\alpha}$	—	1.0
2 soil	Elastic	Elastic	E	[kN/m^2]	5000
			ν	—	0.3
		Flow	$k_{x'}$	[m/day]	10^6
			$k_{y'}$	[m/day]	10^6
			K^{F}	[kN/m^2]	10^{38}
			$\tilde{\alpha}$	—	1.0

[12]R. Holtz, W. Kovacs, An Introduction to Geotechnical Engineering, Prentice–Hall, New Jersey, (1981)

3.5.5   TWO–DIMENSIONAL FOOTING SETTLEMENT

This plane strain consolidation problem is compared with Schiffmann's analytical solution[13]

Window 3-3: Footing settlement – SCHIFF.INP

The computed results for the vertical and horizontal excess pore pressure distribution is compared with Schiffmann's solution.
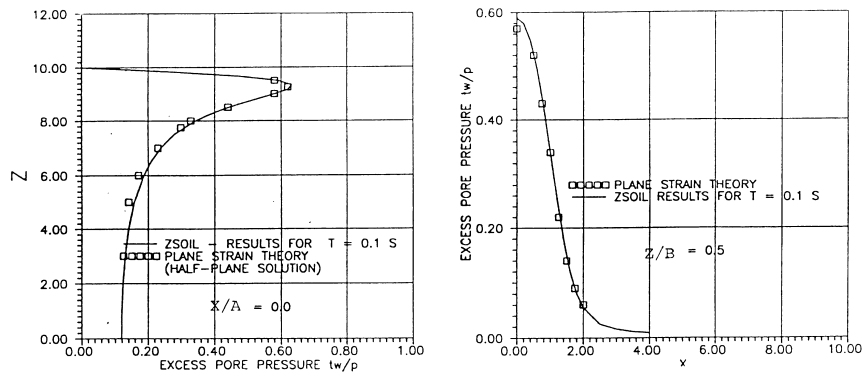
Distribution of excess pore water pressure; vertical distribution of p_w/p at axis (left); horizontal distribution of p_w/p at depth $z/a = 0$ (right)

Window 3-3

Material	Model	Data group	Properties	Unit	Value
1 soil	Elastic	Elastic	E	[MN/m^2]	100
			ν	—	0.0
		Flow	$k_{x'}$	[m/day]	0.1
			$k_{y'}$	[m/day]	0.1
			K^F	[kN/m^2]	10^{38}
			$\tilde{\alpha}$	—	1.0

---

[13]R.L. Schiffmann, A.T. Chen, J.C. Jordan, An analysis of consolidation theories, J. of the Soil Mech. and Found. Div., Vol.95 (1969).

3.5.6 ELASTOPLASTIC COMPRESSION (COMP.INP)

A column of soil subjected to elastoplastic compression is analyzed. The geometry of the structure and the initial state of stress are specified in the figure below. the following material data are assumed for calculation:

$\phi = 30°$, $a_\phi = \dfrac{\sin\phi}{3} = 0.167$, $M = 3\sqrt{3}$, $a_\phi = 0.866$

$E = 2820$, $\nu = 0.4$, $C = $ any, $e_0 = 1$

$E_{\text{oed}} = \dfrac{E(1-\nu)}{(1+\nu)(1-2\nu)} = 6043$, $\lambda = 0.383$, $\sigma_{\text{VM}} = 40\,[\text{kPa}]$ (from oedometer)
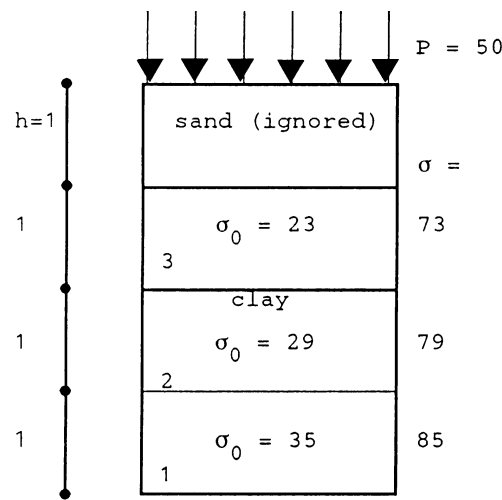
Figure 3.28: Geometry and load of the structure

Settlement calculation

$$\text{elastic} \qquad d^{\text{e}} = \frac{40 - \sigma_0}{E_{\text{oed}}} \cdot h$$

$$\text{plastic} \qquad d^{\text{p}} = \frac{\lambda}{1 + e_0} \ln\left(\frac{\sigma}{40}\right) \cdot h$$

where h is the layer thickness.

The following results are obtained for consecutive layers

Layer	h	d^{e}	d^{p}	**Z_SOIL**	d^{tot}
1	1	8.3×10^{-4}	0.144	$C = 0$	0.396
2	1	1.8×10^{-3}	0.130	$C = 2$	0.396
3	1	2.8×10^{-3}	0.115	$C = 10$	0.396

while the hand calculation gives $d^{\text{tot}} = 0.396$.

The cap model is needed for this analysis, the initial cap size defined by $\underline{p_c} = 34.15\,[\text{kPa}]$ is computed followng the procedure outlined in the manual. The settlement calculation can be done by hand, layer by layer, ignoring the sand and the results match satisfactorily with the numerical simulation and appeared to be insensitive to the value of the cohesion C.

3.6 CREEP (CREEP1.INP)

A simple symmetric creep test under variable load is performed. Numerical results are compared with the analytical solution.

- **Analytical solution**

$$d = -1.0 \cdot \left(\frac{1}{E} + A \cdot t^m \right) - 2.0 \cdot \left[\frac{1}{E} + A \left(t - 2000 \right)^m \right]$$
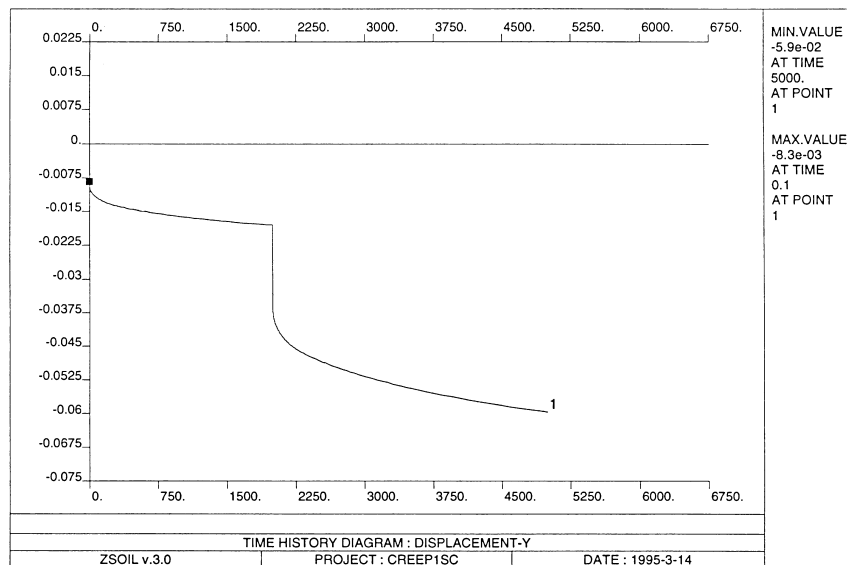
Figure 3.29: Time history diagram: displacement in y direction

Material	Model	Data group	Properties	Unit	Value
1 soil	Elastic	Elastic	E	[MN/m^2]	120
			ν	—	0.30
		Creep	Curve type		power
			A_V	–	0.001
			B_V	–	0.3
			EXF_V	–	0.0
			A_D	–	0.001
			B_D	–	0.3
			EXF_D	–	0.0
			a	–	0.0
			b	–	0.0

3.7 SWELLING [14]

OEDOMETER TEST UNDER FORCE CONTROL

OEDOMETER UNLOADING-LOADING TEST UNDER FORCE CONTROL

---

[14]concerns versions: **ACADEMIC, PROFESSIONAL, EXPERT** only

3.7.1   OEDOMETER TEST UNDER FORCE CONTROL (SWELL_FCTRL.INP)

An oedometric test under force control is considered here. The vertical pressure p=1 kN/m^2, scaled by the load time function starting from value $LTF(t=0)=500$, is applied to the top boundary.
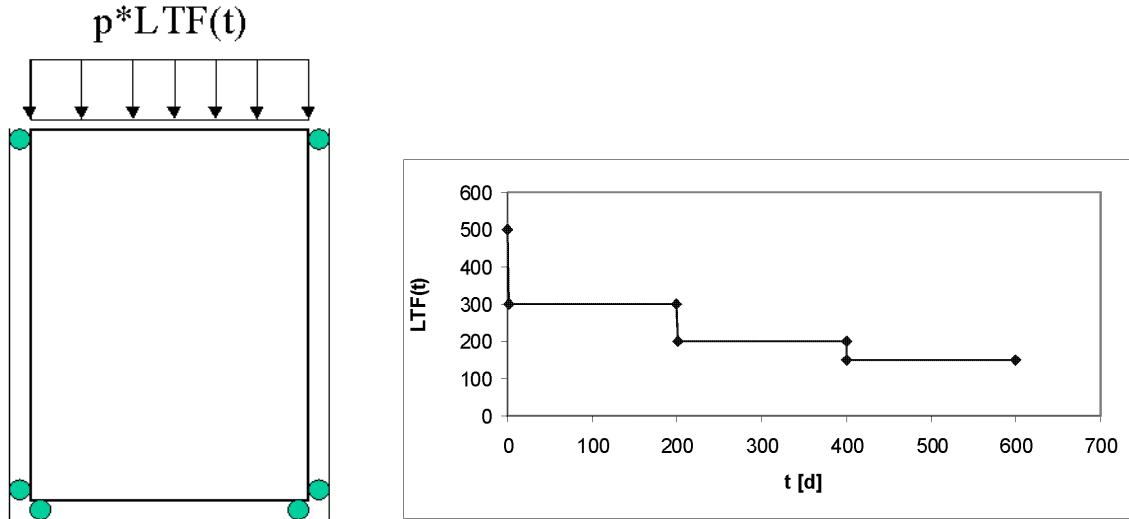
Material data set:

E=50000 [kN/m^2], $\nu = 0.2$, $\underline{\sigma}_{os}$=400 [kPa], $\underline{\sigma}_{cs}$=50 [kPa], $\kappa = 0.03$, $B = 75d$, $\alpha_s = 5$,

$$E_{\text{oed}} = \frac{1 - \nu}{(1 + \nu)(1 - 2\nu)}E = 5.555 \cdot 10^4 \text{ [kN/m}^2]$$

The constant time step has been used $\Delta t = \Delta t_o = 1$ d.

The asymptotic analytical solutions at time t=200 d, 400 d, 600 d are:

$$\varepsilon_y(t = 200) = \frac{500 - 300}{5.555 \cdot 10^4} - 0.03 \cdot \ln(\frac{300}{400}) = 1.22 \cdot 10^{-2}$$

$$\varepsilon_y(t = 400) = \frac{500 - 200}{5.555 \cdot 10^4} - 0.03 \cdot \ln(\frac{200}{400}) = 2.62 \cdot 10^{-2}$$

$$\varepsilon_y(t = 600) = \frac{500 - 150}{5.555 \cdot 10^4} - 0.03 \cdot \ln(\frac{150}{400}) = 3.57 \cdot 10^{-2}$$

The numerical solution

$\varepsilon_y(t = 200) = 1.22 \cdot 10^{-2}$,

$\varepsilon_y(t = 400) = 2.63 \cdot 10^{-2}$,

$\varepsilon_y(t = 600) = 3.60 \cdot 10^{-2}$

The evolution of the vertical strain $\varepsilon_y(t)$, relation $\varepsilon_y - \sigma_y$ and $\sigma_x(t)$ are shown in following figures.
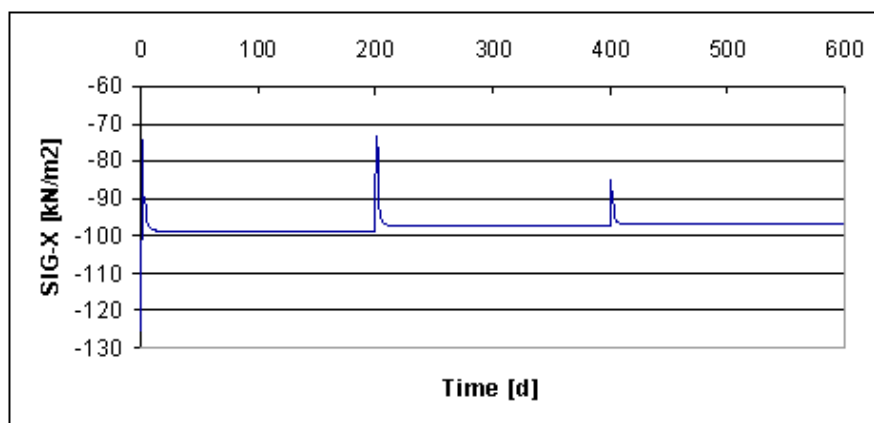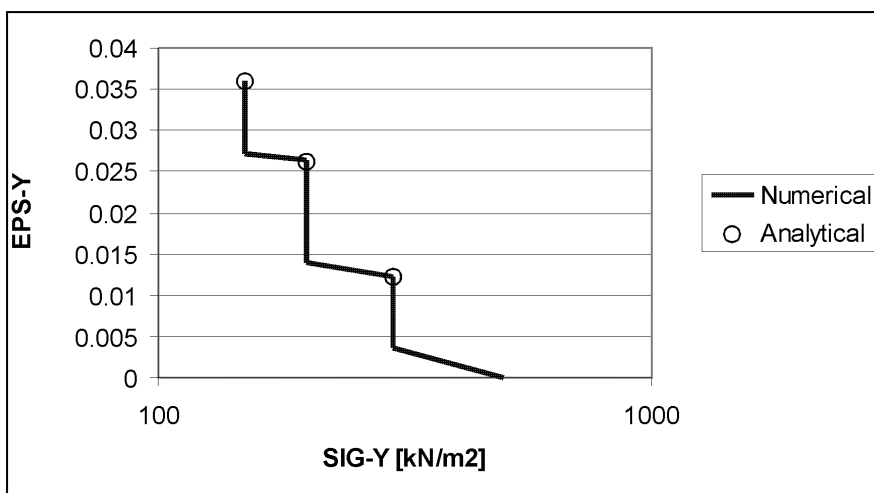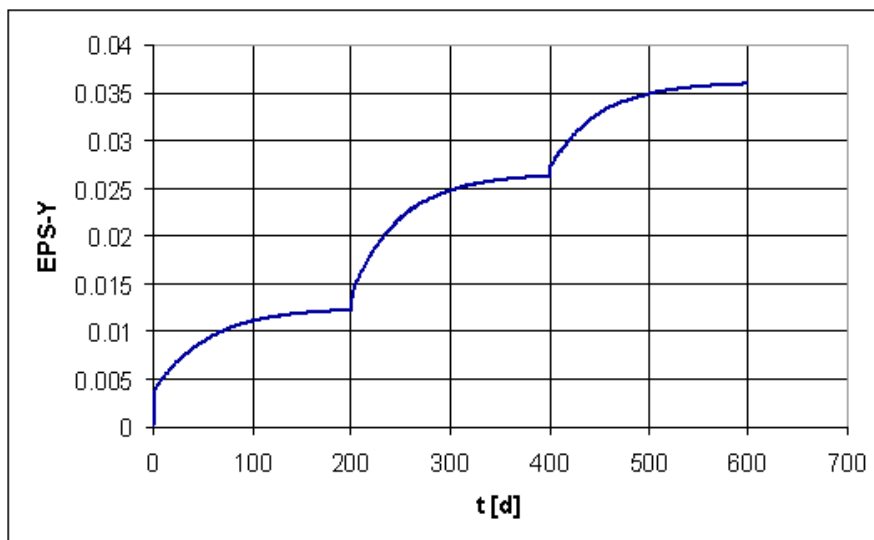
3.7.2 OEDOMETER UNLOADING-LOADING TEST UNDER FORCE CONTROL (SWELL_UNLREL.INP)

An oedometric unloading-reloading test under force control is considered here. The aim of this trest is to show that swelling may be stopped during reloading process. The vertical pressure p=1 kN/m^2, scaled by the load time function starting from value $LTF(t = 0) = 500$, is applied to the top boundary.
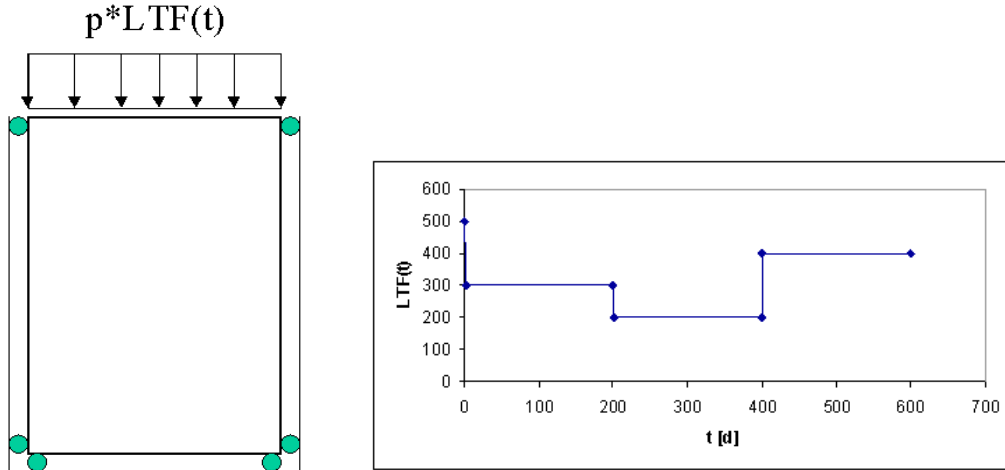
Material data is Material data set:

E=50000 [kN/m^2], $\nu = 0.2$, $\underline{\sigma}_{os}$=400 [kPa], $\underline{\sigma}_{cs}$=50 [kPa], $\kappa = 0.03$, $B = 75d$, $\alpha_s = 5$

$$E_{\text{oed}} = \frac{1 - \nu}{(1 + \nu)(1 - 2\nu)} E = 5.555 \cdot 10^4 \text{ kN/m}^2$$

The constant time step has been used $\Delta t = \Delta t_o = 1$ d.

The asymptotic analytical solutions:

$$\varepsilon_y(t = 200) = \frac{500 - 300}{5.555 \cdot 10^4} - 0.03 \cdot \ln(\frac{300}{400}) = 1.22 \cdot 10^{-2}$$

$$\varepsilon_y(t = 400) = \frac{500 - 200}{5.555 \cdot 10^4} - 0.03 \cdot \ln(\frac{200}{400}) = 2.62 \cdot 10^{-2}$$

$$\varepsilon_y(t = 600) = 2.62 \cdot 10^{-2} - \frac{400 - 200}{5.555 \cdot 10^4} = 2.26 \cdot 10^{-2}$$

The numerical solution:

$$\varepsilon_y(t = 200) = 1.22 \cdot 10^{-2}, \ \varepsilon_y(t = 400) = 2.63 \cdot 10^{-2}, \ \varepsilon_y(t = 600) = 2.27 \cdot 10^{-2}$$

The evolution of the vertical strain $\varepsilon_y(t)$ is shown in figure below:
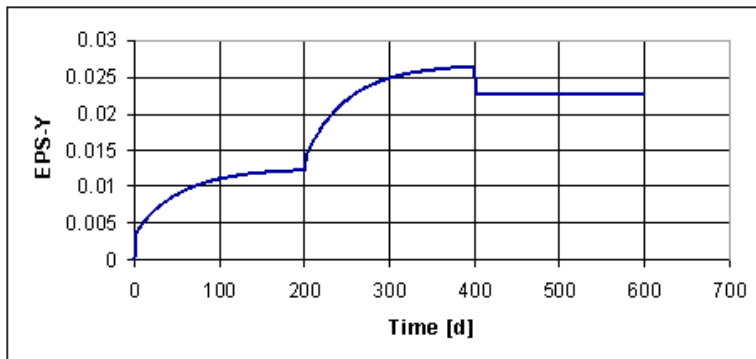
3.8 INFINITE MEDIA

HALF-SPACE UNDER COMPRESSIVE LOAD (3D)

A GAP IN INFINITE MEDIUM(PS)

CIRCULAR CAVITY UNDER THE PRESSURE (AXS)

3.8.1   A GAP IN INFINITE MEDIUM

Data File: GAPINFINITE-PS.INP

Problem description for plane strain model:

The problem of a gap of length $c = 2.5$m embedded in the elastic infinite medium and loaded by an internal pressure $p_0 = 1$kN/m^2 is considered here. The closed form solution for horizontal displacements of gap boundary is as follows

$$u_x(0,y) = \frac{2(1-\nu^2)}{E} p_0 \left(c^2 - y^2\right) \quad \text{for } |y| \le c$$

The solution is obtained by considering only one quarter of the model due to symmetry of the problem.

Geometry and discretization:

The numerical model including infinite elements with similarity center at (0,0) is shown in Fig. 3.30
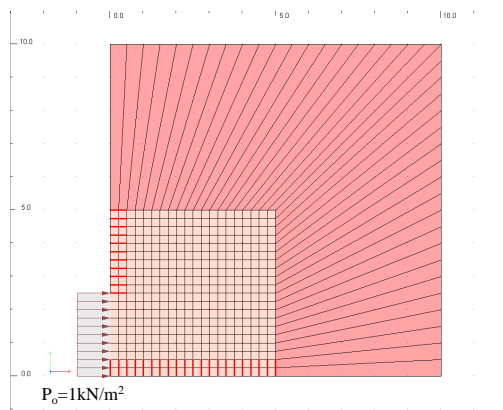
Figure 3.30: Gap in infinite medium
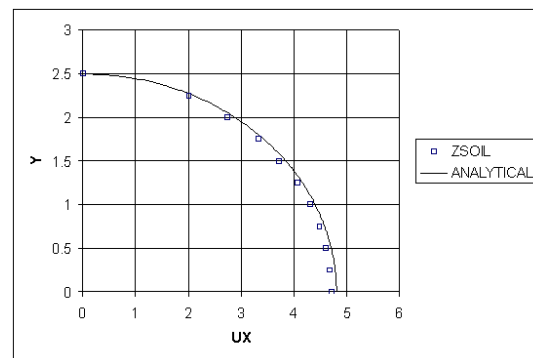
Figure 3.31: Distribution of horizontal displacements of a gap

Material:

Linear elastic, with Young modulus $E = 1.0$ and Poisson ratio $v = 0.2$

Results comparison

The comparison of computed horizontal displacements versus analytical solution is shown in Fig.3.31

3.8.2 HALF-SPACE UNDER COMPRESSIVE LOAD (3D)

Data File: INFELE3D.INP

Reference: Nowacki W. Theory of elasticity. Ed. PWN Warsaw 1970.

Problem description:

Elastic half-space is loaded with uniformly distributed load $p_y = -1.0$ [kN/m^2] within rectangular area $b \times a = 4.8$ m $\times$ 4.8 m. Due to quarter symmetry of the problem only one quarter is considered and on the two planes of symmetry appropriate kinematic boundary conditions are applied. The mesh of $6 \times 6 \times 6$ brick elements filling cubical domain 7.2 m $\times$ 7.2 m $\times$ 7.2 m. The solution obtained with aid of infinite elements is compared with closed form solution for this classical problem of elasticity theory.

Geometry and discretization:

The model is shown in Figure 3.32 (**INFELE3D.INP)**
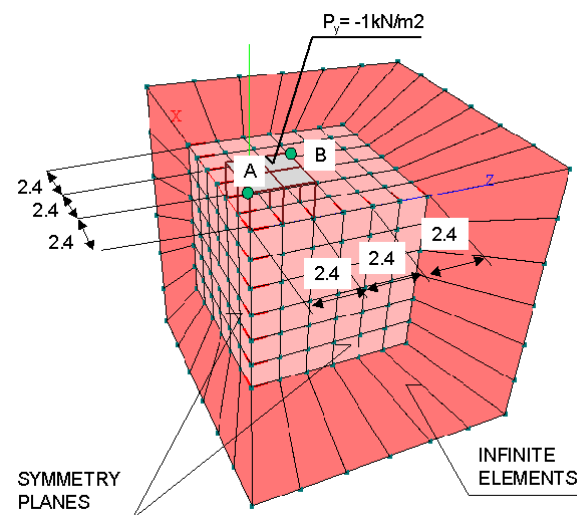
Figure 3.32: Infinite half-space. Model outlook

Material: Linear elastic, with Young modulus $E = 1.0e5$ [kPa] and Poisson ratio $\nu = 0.3$

Result comparison

The comparison concerns vertical displacements in the middle of the loaded area (p. A) and at its corner (p. B)

Theoretical values are evaluated according to the formula:

$$u_{yA} = 2u_{yB} = \frac{1 - v^2}{E} qb \cdot \frac{2}{\pi} (\alpha \ln \frac{1 + \sqrt{1 + \alpha^2}}{\alpha} + \ln(\alpha + \sqrt{1 + \alpha^2})) \text{ with } \alpha = \frac{a}{b} = 1$$

point:	Infinite medium	Theory
A	-4.899e-5	-4.902e-5
B	-2.443e-5	-2.451e-5

3.8.3   CIRCULAR CAVITY UNDER THE PRESSURE

Data File: INFINITECIRCLE-PS.INP

Problem description for plane strain model:

Elastic space (plane strain condition) with circular cavity (radius $R = 1$) is loaded with uniformly distributed pressure $p = 1.0$. This classical problem of elasticity theory is solved in closed form giving radial displacement on the boundary as:

$$u_r = \frac{1 + v}{E} \frac{pR^2}{r}$$

The solution is performed with use on infinite elements exclusively by taking only one quarter of the model due to symmetry of the problem.

Geometry and discretization:

The numerical model consisting of 16 infinite elements with similarity centre at (0,0) is shown in Fig. 3.33
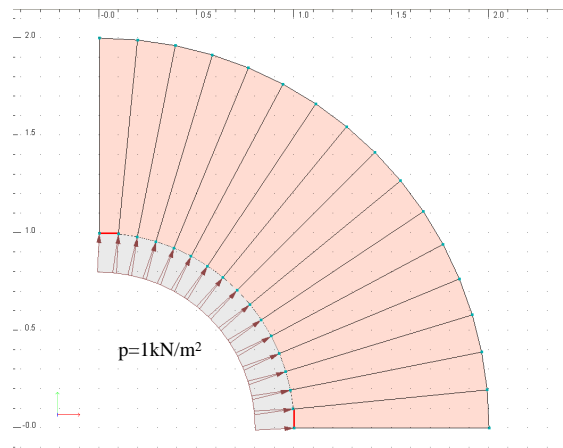
Figure 3.33: Circular cavity

Material: Linear elastic, with: Young modulus $E = 1.0$ and Poisson ratio $v = 0.3$

Result comparison

u_{exact}	1.3
u_{zsoil}	1.299

Data File: INFINITECIRCLE-AXS.INP

Problem description for axisymmetric model:

The same problem is analyzed here using an axisymmetric model which consists of a single infinite element.

Geometry and discretization:

The numerical model consisting of 1 infinite element created as an infinite layer with Direction vector (1.0,0.0) and length 1m is shown in Fig. 3.34
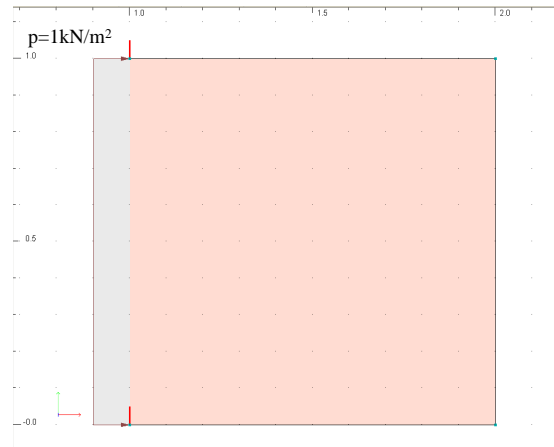
Figure 3.34: Circular cavity-axisymmetric model

Result comparison

u_{exact}	1.3
u_{zsoil}	1.3

Chapter 4

FLOW BENCHMARKS

RECTANGULAR DAM WITH TAIL–WATER

RECTANGULAR DAM WITH TOE–DRAIN

MODELLING BOUNDARY CONDITIONS

STEADY STATE FLOW FOR ASSUMED WATER TABLE CONFIGURATION

4.1   RECTANGULAR DAM WITH TAIL–WATER

Data File: SSF02.INP
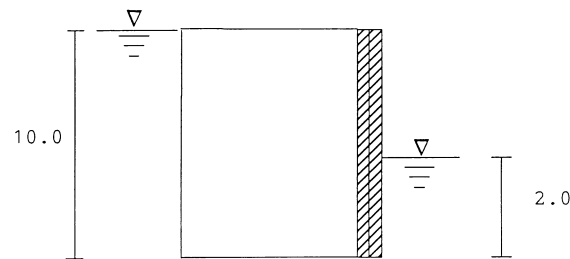
Figure 4.1: Problem illustration

Material	Model	Data group	Properties	Unit	Value
1 soil	Elastic	Unit weights	γ^F	[kN/m^3]	10
		Flow	$k_{x'}$	[m/h]	10^{-5}
			$k_{y'}$	[m/h]	10^{-5}
			β	–	0
			S_r	–	0
			α	[1/m]	2
			n	–	2
			k_r after	–	Irmay

The illustrated case is analyzed with a flow only option. A steady–state driver is used here. Water boundary conditions are applied where necessary, while a seepage surface is present or the right side of the dam.

The free surface solution is comparable with the solution of reference S.J. Lacy & J.H. Prevost, Flow through porous media: A procedure for locating the free water surface, Int.J. for Num. and Anal. meth. in Geomechanics, Vol.11, pp.585–601 (1987).
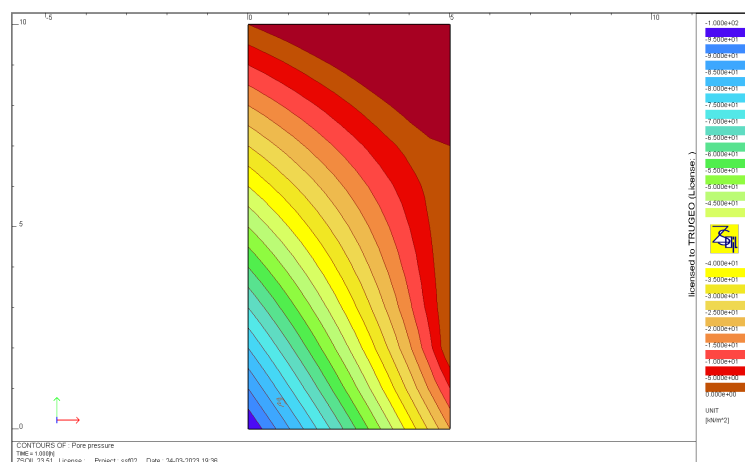
Figure 4.2: Pore pressure distribution

4.2 RECTANGULAR DAM WITH TOE–DRAIN

Data File: SSF01.INP
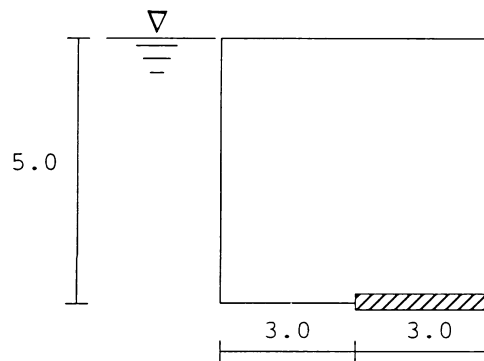
Figure 4.3: Problem illustration

Material	Model	Data group	Properties	Unit	Value
1 soil	Elastic	Unit weights	γ^{F}	[kN/m^3]	10
		Flow	$k_{x'}$	[m/h]	10^{-5}
			$k_{y'}$	[m/h]	10^{-5}
			β	–	0
			S_r	–	0
			α	[1/m]	2
			n	–	2
			k_r after	–	Irmay

A steady–state driver is activated under a flow only analysis of water boundary conditions is applied on the left part of the dam, while the drain is modelised by seepage surface elements.

The free surface solution is again comparable with Lacy's (S.J. Lacy & J.H. Prevost, Flow through porous media: A procedure for locating the free water surface, Int.J. for Num. and Anal. meth. in Geomechanics, Vol.11, pp.585–601 (1987)).
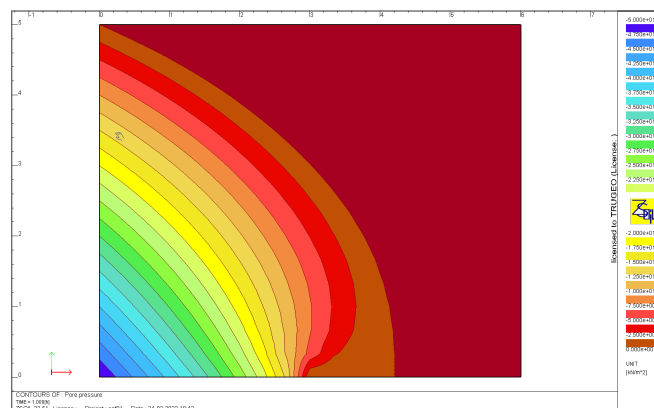
Figure 4.4: Pore pressure distribution

4.3 MODELLING BOUNDARY CONDITIONS FOR TRANSIENT AND STEADY STATE FLOW

Example: filling and drawdown

Data File: filldrawdown2d.*

The transient flow problem is considered here. First the initial state is generated through the initial state driver (it is equivalent to the steady state solution at time $t = 0$) and then the transient flow driver is activated. This example illustrates on how to model the effect of the filling and the drawdown with the aid of the total head type of the boundary condition applied to the seepage surface which is generated on both left and right contour of the domain. **It has to be emphasized here that the total head b.c. should be, in most cases applied to the seepage surface. The reason is that if some node, with which the total head b.c. is associated, is above free water surface then it will get automatically zero pressure b.c.**

The total head is defined as below:

$$h = -\frac{p^{\mathsf{F}}}{\gamma^{\mathsf{F}}} + y$$
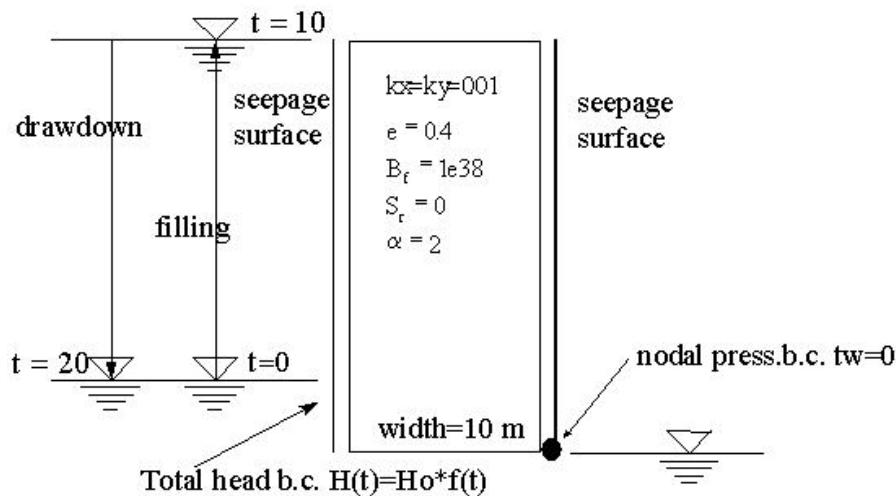
Figure 4.5: Filling and drawdown. Example outlook

The total head $H(t)$ evolution in time is governed by the load time function as given below:

$$H_0 = 1\,[\mathrm{m}]$$

$$f(t) = \begin{cases} t = 0, & H(0) = 5 \\ t = 10, & H(20) = 20 \\ t = 20, & H(5) = 5 \end{cases}$$

This evolution of the free water surface is shown for $t = 0$, $t = 10.6$, $t = 15.7$ and $t = 20.0$ in corresponding figures below.

Material	Model	Data group	Properties	Unit	Value
1 soil	Elastic	Unit weights	γ^{F}	[kN/m^3]	10
		Flow	$k_{x'}$	[m/h]	0.01
			$k_{y'}$	[m/h]	0.01
			β	–	0
			S_r	–	0
			α	[1/m]	2
			n	–	2
			k_r after	–	Irmay
			K^{F}	[kN/m^2]	2000000
			K_{air}	[kPa]	100
		Density	e_{o}	–	0.4
			γ^{F}	[kN/m^3]	10

Figure 4.6: Pore pressure distribution in time

4.4 STEADY STATE FLOW FOR ASSUMED WATER TABLE CON-FIGURATION

Example: steady state seepage for assumed water table configuration in fully saturated medium

Data File: ssf-bench-Domenico-he-4m.inp

The steady state flow problem in 200mx100m domain is considered here. The left, right and bottom boundaries are assumed as impermeable, while at the top boundary pressure head boundary condition is enforced (see fig.**??**). The pressure head $h(x)$ at $z = z_o = 100$ m is defined as follows

$$h(x) = A - B \, \cos\left(\pi x/L\right)$$

where:

$$
\begin{aligned}
B &= \cosh\left(\pi \, z_o/L\right) \\
A &= L/2 + B
\end{aligned}
$$

In the considered case $L = 200$ m and $z_o = 100$ m.
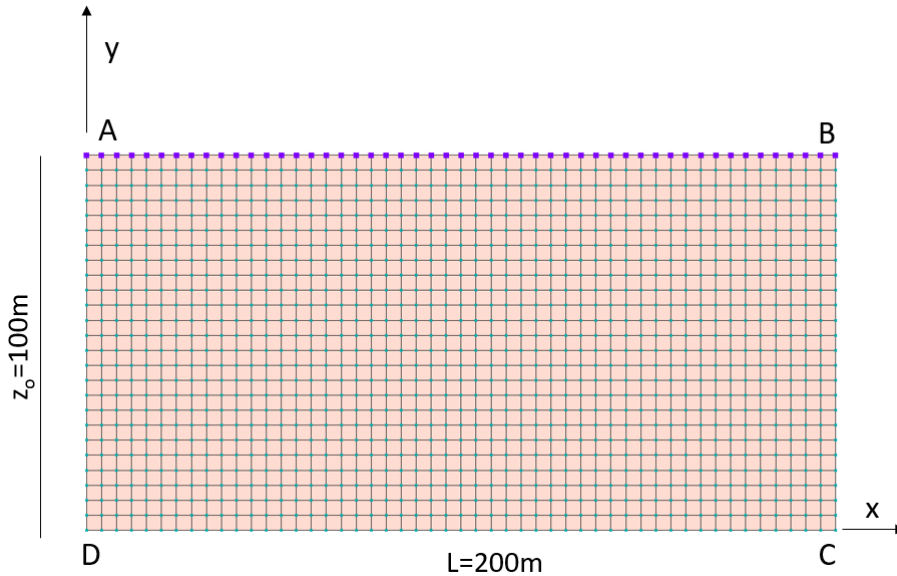
Figure 4.7: Geometry and BC for the benchmark

The analytical solution for spatial distribution of total heads $h(x,y)$, derived by Domenico and Palciauskas (Domenico, P.A. and Palciauskas, V.V. (1973). Theoretical Analysis of Forced Convective Heat Transfer in Regional Ground- Water Flow. Geol Soc Am Bull, 84, pp. 3803-3814.), is as follows (z is equivalent in 2D to y coordinate)

$$h(x,z) = A - B\frac{\cosh\left(\pi \, z/L\right)}{\cosh\left(\pi \, z_o/L\right)} \, \cos(\pi \, x/L) \tag{4.1}$$

Material properties used in this benchmark are given in the following table

Material	Model	Data group	Properties	Unit	Value
1 soil	Elastic	Unit weights	γ^F	[kN/m^3]	10
		Flow	$k_{x'}$	[m/day]	0.00432
			$k_{y'}$	[m/day]	0.00432
			β	–	0
			S_r	–	0
			α	[1/m]	2
			n	–	2
			k_r after	–	Irmay
			K^F	[kN/m^2]	2000000
			K_{air}	[kPa]	100
		Density	$e_{\circ}$	–	0.428571
			γ^F	[kN/m^3]	10

In this benchmark only the first two parameters are meaningful as the medium is fully saturated. Computed total heads are shown in fig.4.8. The analytical solution is visualized in fig.4.9.
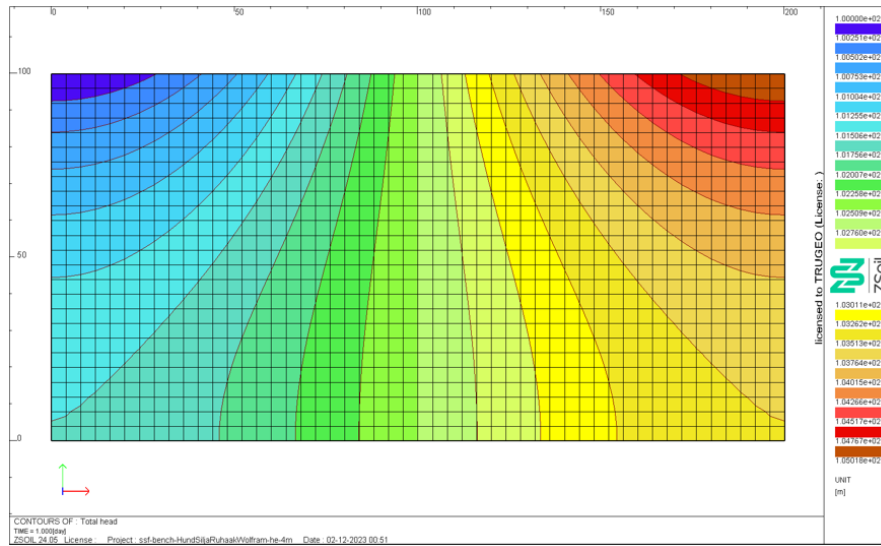
Figure 4.8: Computed total heads contours
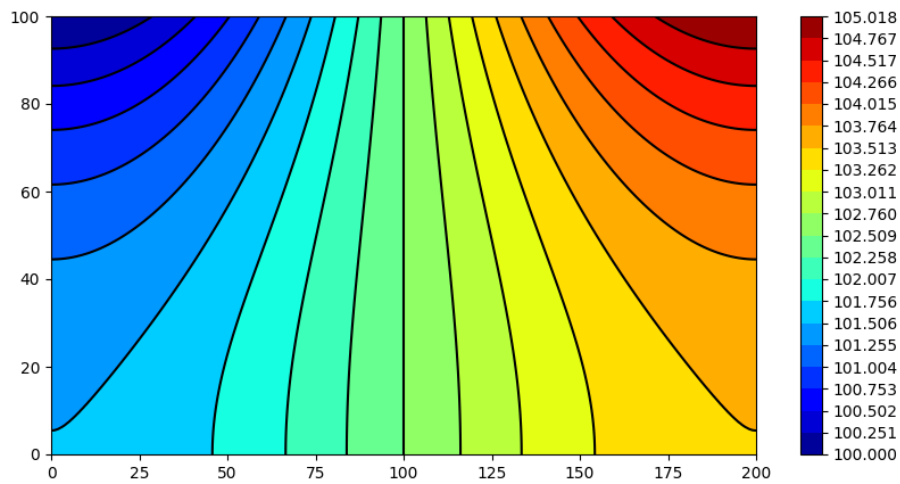
Figure 4.9: Analytical total heads contours

Chapter 5

HEAT PROBLEMS

TRANSIENT HEAT PROBLEM

STEADY STATE HEAT TRANSFER WITH ADVECTION

5.1 TRANSIENT HEAT PROBLEM

Data file: heatTR01.inp

The transient heat problem is analyzed here. The geometry, boundary conditions and the initial condition are illustared in Fig. 5.1.
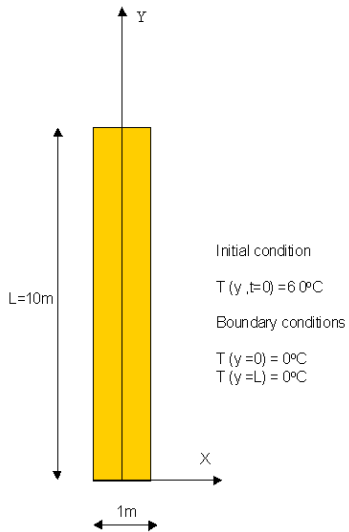
Figure 5.1: One-dimensional transient heat problem
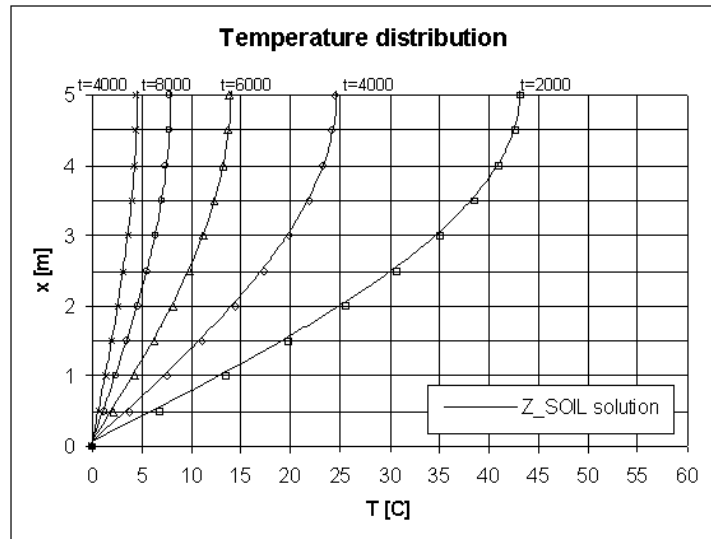
Figure 5.2: Temperature profiles

The analytical solution has the form:

$$T\left(y,t\right) = \sum_{n=0}^{\infty} \frac{4T_o}{(2n+1)\pi} \exp\left(-\frac{\lambda/c\,\pi^2(2n+1)^2}{L^2}t\right)\sin\left(\frac{(2n+1)\pi y}{L}\right)$$

Due to symmetry of the problem (with respect to axis y=L/2) the half-scheme is considered here. Material parameters are listed in table below.

Material	Model	Data group	Properties	Unit	Value
1 concrete bar	Heat transfer	Heat	λ	[kN/m^2/C]	8.64
			c	–	3000

Both the analytical and the numerical solutions are given in Fig. 5.2 for time instances $t = 2000, 4000, 6000, 8000, 10000$ [h].

5.2 STEADY STATE HEAT TRANSFER WITH ADVECTION

Data files: ssf-bench-Domenico-he-4m-A.inp, ssh-advection-bench-Domenico-he-4m-A.inp

The steady state heat transfer problem with advection, in a rectangular domain 200mx100m, is analyzed here. The seepage problem is illustrated in fig.5.3. The left, right and bottom boundaries are assumed as impermeable, while at the top boundary pressure head boundary condition is enforced. The pressure head $h(x)$ at $z = z_o = 100$ m is defined as follows

$$h(x) = A - B \, \cos{(\pi x/L)}$$

where:

$$
\begin{aligned}
B &= \cosh{(\pi \, z_o/L)} \\
A &= L/2 + B
\end{aligned}
$$

In the considered case $L = 200$ m and $z_o = 100$ m.
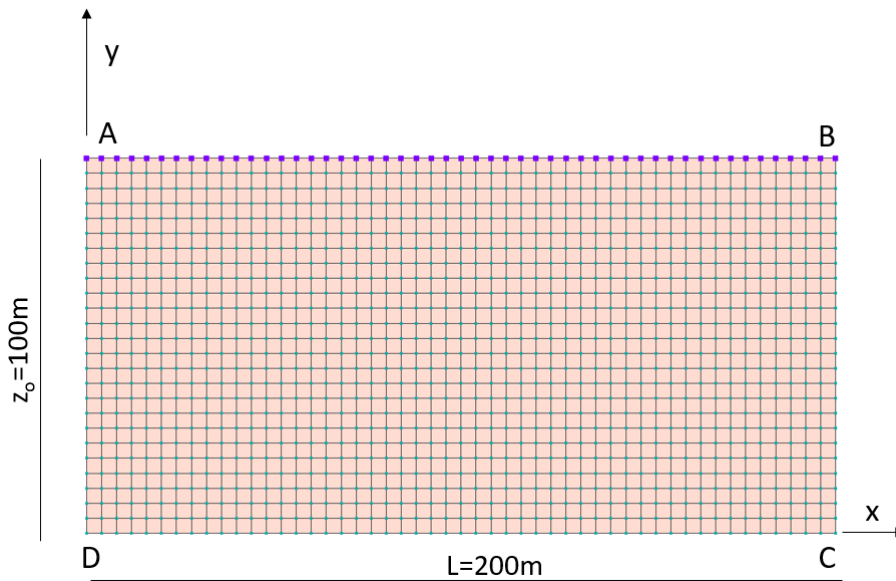
Figure 5.3: Geometry and BC for the benchmark

The analytical solution for spatial distribution of total heads $h(x, y)$, derived by Domenico and Palciauskas (Domenico, P.A. and Palciauskas, V.V. (1973). Theoretical Analysis of Forced Convective Heat Transfer in Regional Ground- Water Flow. Geol Soc Am Bull, 84, pp. 3803-3814.), is as follows (z is equivalent in 2D to y coordinate)

$$h(x, z) = A - B \frac{\cosh{(\pi \, z/L)}}{\cosh{(\pi \, z_o/L)}} \, \cos(\pi \, x/L) \tag{5.1}$$

Seepage properties used in this benchmark are given in the following table

Material	Model	Data group	Properties	Unit	Value
1 soil	Elastic	Unit weights	γ^{F}	[kN/m^3]	10
		Flow	$k_{x'}$	[m/day]	0.00432
			$k_{y'}$	[m/day]	0.00432
			β	–	0
			S_r	–	0
			α	[1/m]	2
			n	–	2
			k_r after	–	Irmay
			K^{F}	[kN/m^2]	2000000
			K_{air}	[kPa]	100
		Density	e_{o}	–	0.428571
			γ^{F}	[kN/m^3]	10

Comparizon of the computed total heads and analytical ones is given in section 4.4, therefore, it is not repeated here. The resulting fluid velocities are mapped then onto heat transfer mesh using superconvergent patch recovery method (this is an automatic procedure once the seepage project is associated with the heat transfer one). The steady state heat transfer problem is illustrated in fig.5.4. The left and right boundaries are isolated, at the top boundary temperature $T_o = 10^o$ C is enforced, while at the bottom boundary, a uniform distributed heat flux $q_b = 0.03$ [W/m^2] is applied .
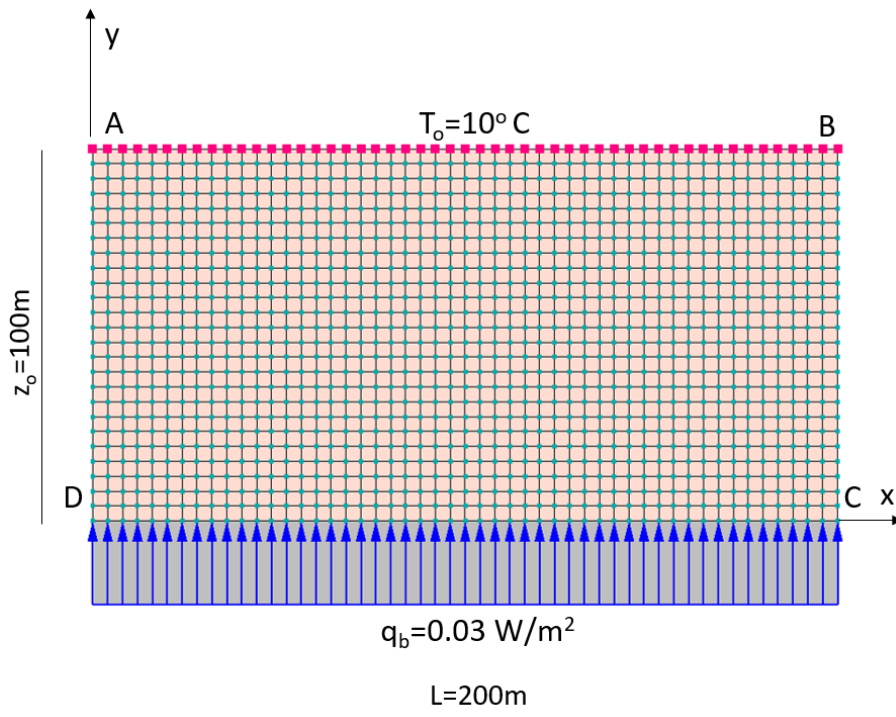
Figure 5.4: Geometry and BC for the benchmark

The analytical solution for spatial distribution of temperatures $T(x, y)$, derived by Domenico and Palciauskas (Domenico, P.A. and Palciauskas, V.V. (1973). Theoretical Analysis of Forced Convective Heat Transfer in Regional Ground- Water Flow. Geol Soc Am Bull, 84, pp. 3803-3814.), is as follows (z is equivalent in 2D to y coordinate)

$$
\begin{aligned}
T(x,z) \;=\;\; & T_o + \frac{q_b}{\lambda}(z_o - z) + \\
+ \;\; & \frac{c^* \, q_b \, k \, B}{2\lambda^2} \, \frac{\cos(\pi \, x/L)}{\cosh(\pi \, z_o/L)} \left((z_o - z)\cosh(\pi \, z/L) + \frac{L}{\pi}\frac{\sinh(\pi(z - z_o)/L)}{\cosh(\pi \, z_o/L)} \right)
\end{aligned}
$$

Thermal and unit weight properties used in this benchmark are given in the following table

Material	Model	Data group	Properties	Unit	Value
		Heat	λ^s	[kN/day/C]	43.2
			$c^{s,*}$	[kN/m^2/C]	1650.0
			λ^f	[kN/day/C]	43.2
			$c^{f,*}$	[kN/m^2/C]	1650.0
		Density	e_o	–	0.428571
			γ^F	[kN/m^3]	10

Computed temperatures are shown in fig.**??**. The analytical solution is visualized in fig.5.6.
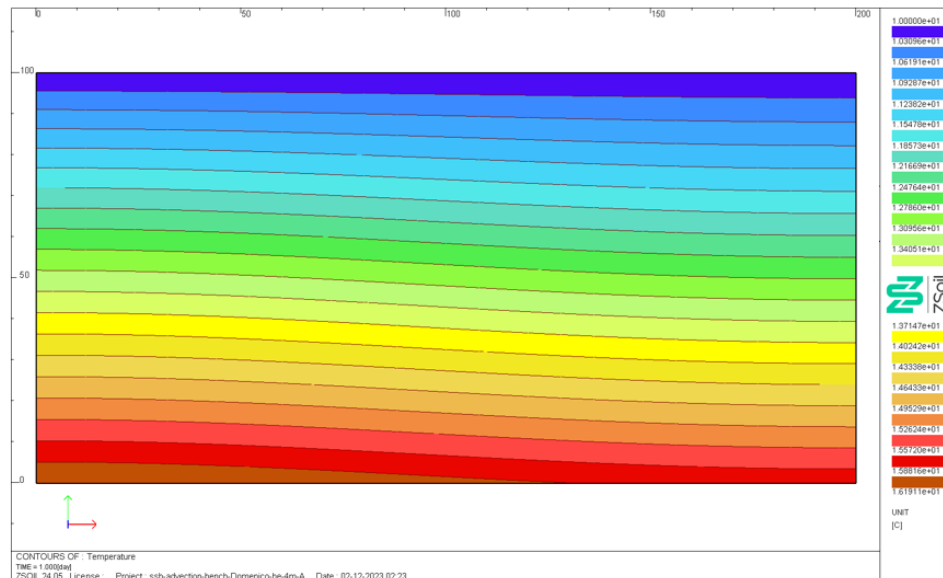
Figure 5.5: Computed temperature field
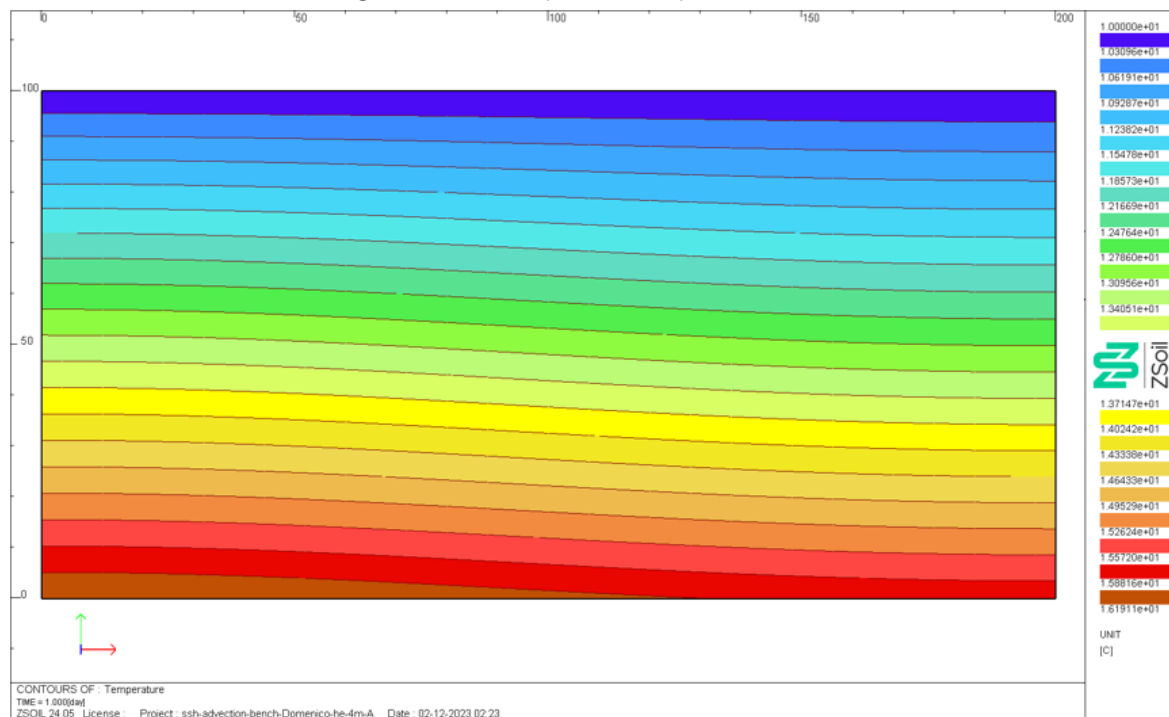
Figure 5.6: Analytical temperature contours

Chapter 6

STRUCTURAL BENCHMARKS

BEAMS

AXISYMMETRIC SHELLS

SHELLS

MEMBRANES

NONLINEAR BEAM HINGES

NONLINEAR SHELL HINGES

6.1   BEAMS

ELASTO-PLASTIC FIXED-END BEAM

ELASTO-PLASTIC BEAM WITH SUPPORTS VARIABLE IN TIME

REINFORCED CONCRETE 2-SPAN BEAM

REINFORCED CONCRETE 2-FLOOR FRAME

PRESTRESSED BEAM

TWISTED BEAM

RING

6.1.1   ELASTO-PLASTIC FIXED-END BEAM

Data file: EPLBEAMF.INP

Problem description:

Elasto–plastic, fixed-end beam loaded with concentrated force at the mid–span. Flexibility based formulation is used. Beam geometry, BC, load as well as results such as M,Q graphs , deflections are shown in Fig. 6.1
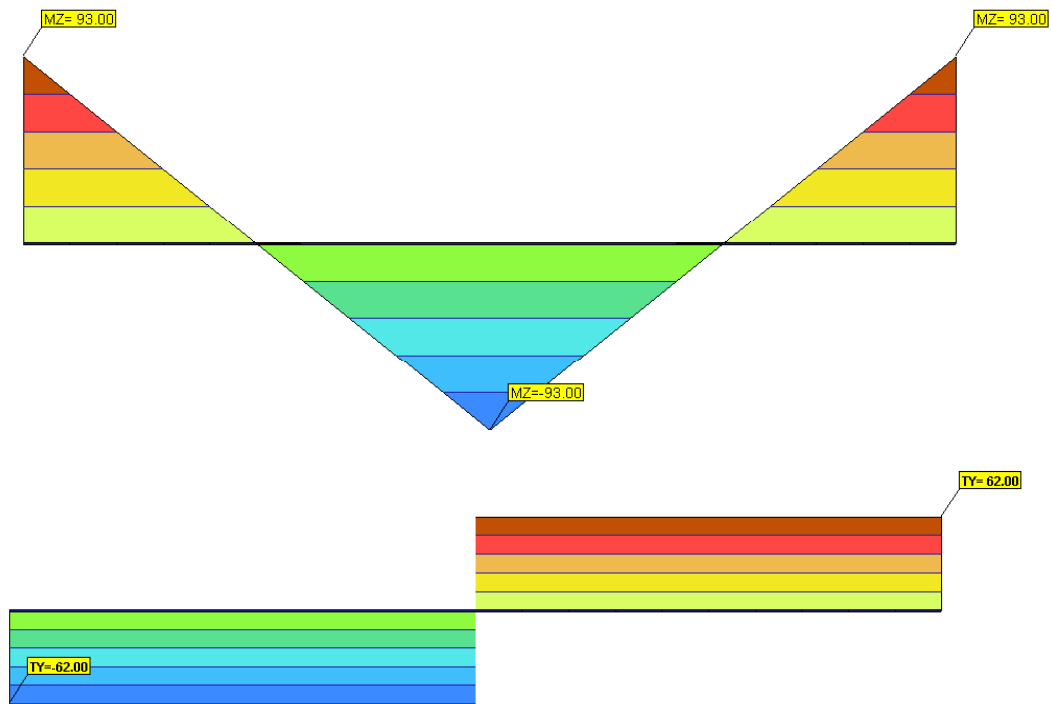
Figure 6.1: Elasto-plastic beam. Data and results

Cross–section data: I-shaped section, layered approach.

Material data: (Uni–axial elastoplastic model)

$E = 2.1 \cdot 10^8$[kPa], $\nu = 0.3$, $f_y = 3.0 \cdot 10^5$[kPa]

Results:

Item:	Unit:	Z_SOIL:	exact:
Elastic limit moment	kNm	78.75	78.31
Plastic limit moment	kNm	93.0	93.0
Disp. at el .limit load	m	2.06e-2	2.01e-2
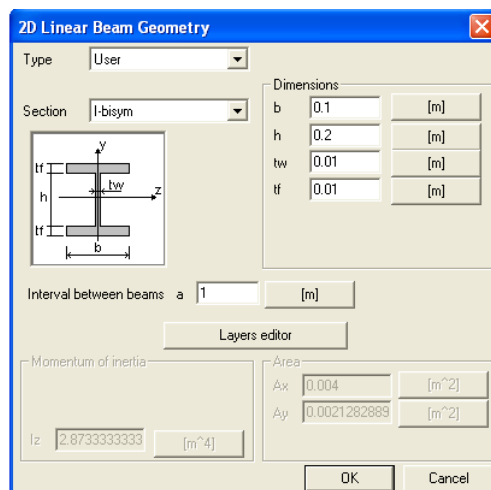
Figure 6.2: Cross sectional data $[m]$
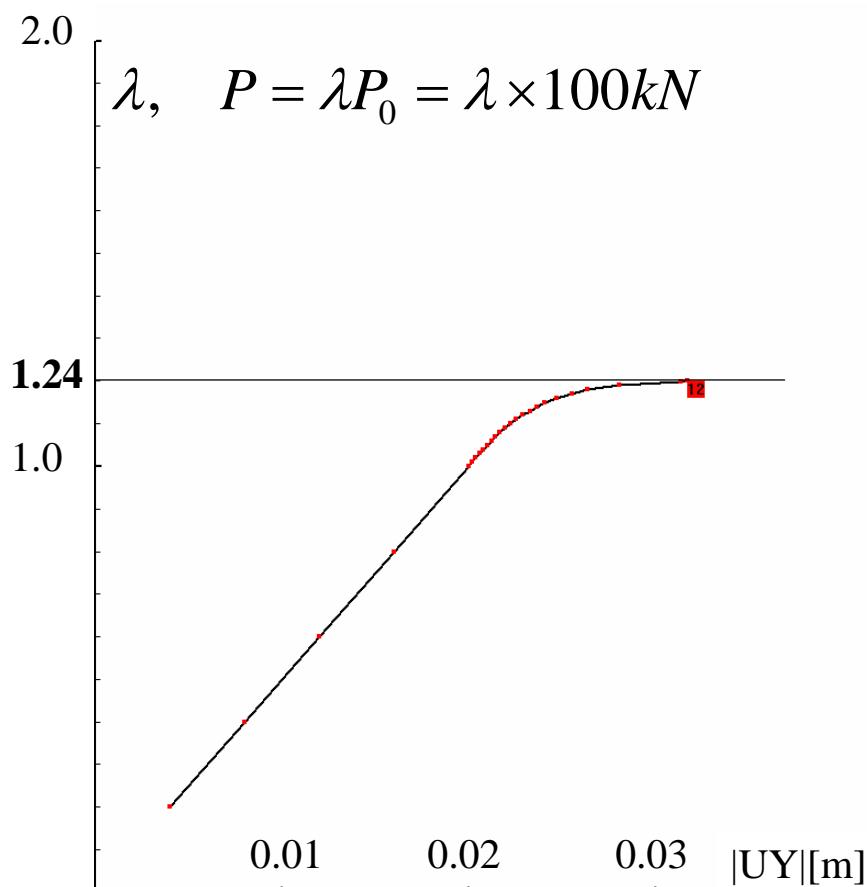
Figure 6.3: Load-displacement graph

6.1.2 ELASTO-PLASTIC BEAM WITH SUPPORTS VARIABLE IN TIME

Data file: VARBEAMBC.INP, VARBEAMH.INP

Problem description:

Elasto-plastic beam under uniform load. Support conditions are variabe in time, i.e. at time $0 < t \leq 1$, the beam is clamped at both end, then, for time $1 < t \leq 2$, under constant load, rotation constraints are removed and central support is applied (to already deformed structure). Removal of rotational constrains is performed by:

- applying existence function ($0 < t \leq 1$ active) to RZ rotation BC (file **VARBEAMBC.INP**)

- keeping RZ constraint permanently active in BC, but releasing it at the element level by means of hinges (file **VARBEAMH.INP**) also controlled by existence function ($t > 1$ active)

Both data sets give identical results.
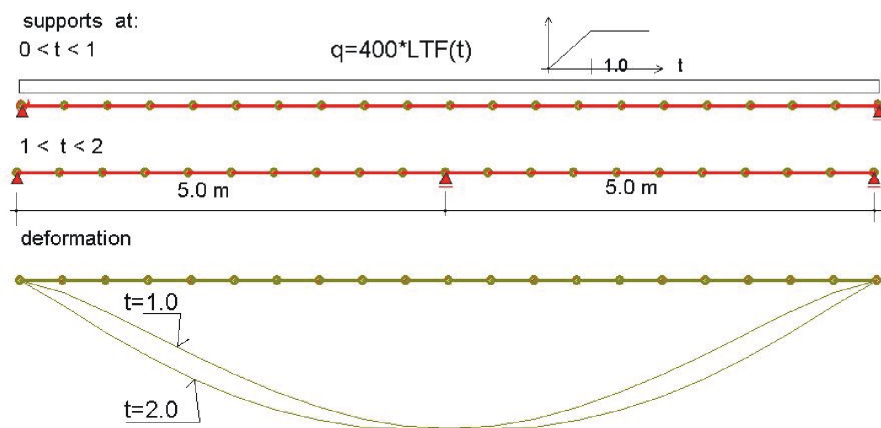
Figure 6.4: Beam geometry, load, supports in 2 time steps. Deformation patterns

Cross-section data: uniform rectangular, $b = h = 1.0$

Material data: (uniaxial elastoplastic model)

$E = 10000$, $\nu = 0.3$, $f_t = f_c = 10000$

Results:
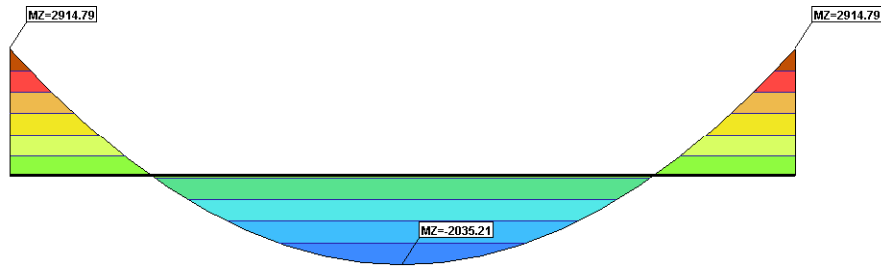
Figure 6.5: M_z graph at $t = 1.0$ (clamped 1-span beam, uniform load)
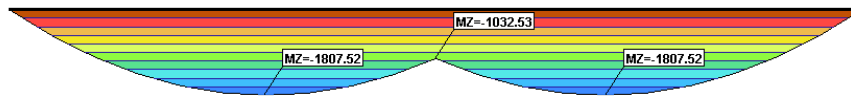
Figure 6.6: M_z graph at $t = 2.0$ (free-supported 2-span beam, load as for $t = 1.0$)

The theoretical ultimate bending moment for this cross section is equal to $\dfrac{bh^2}{4}f_c = 2500$ kNm. For given mesh ZSoil will yield 2513 kNm.

6.1.3 REINFORCED CONCRETE 2-SPAN BEAM

Data files: RCBEAM-STD.INP, RCBEAM-FLEX.INP

Reference: Michanovic A., Marovic P., Dvornik J.: Nonlinear calculus of reinforced concrete structures ,ed. DHGK, Zagreb, 1993

Problem description:

Elasto–plastic (reinforced concrete section), 2-span beam is loaded with a uniform load until failure state is detected. Beam geometry, boundary conditions and loading are shown in Fig. 6.7.
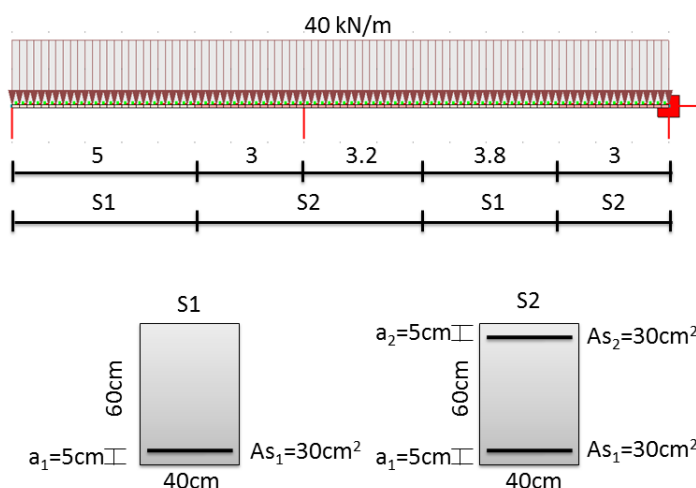
Figure 6.7: Reinforced concrete beam

Material data:

- **concrete**(uni-axial elasto-plastic): $E = 39000$ [MPa], $G = 16250$ [MPa], $f_c = 40.0$ [MPa], $f_t = 0.0$ [MPa]

- **reinforcement** (uni–axial elasto–plastic) $E = 210000$ [MPa], $f_y = 400$ [MPa]

In both data files the reinforced concrete cross section is defined by activating ⊠ **Additional layers** option, at the material level. This setting is shown in the Fig. 6.8. The two beam formulations are tested here, the standard displacement one (2 node beam elements with a single integration point)(file: RCBEAM-STD.INP) and the flexibility based one (2 node element with 5 integration points) (file: RCBEAM-FLEX.INP). Choice of the beam formulation is made under group ⊠ **Main** .

Results:

Item:	Formulation	Z_SOIL:	Ref [MIH]:
Ultimate load factor	Flexibility based	2.47	2.60
Ultimate load factor	Displacement based	2.52	2.60
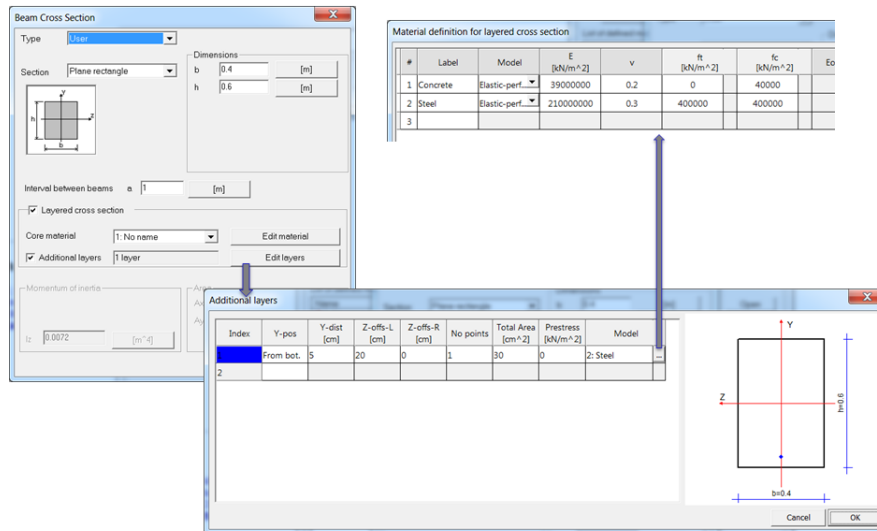
Figure 6.8: Definition of cross section through ⊠ **Additional layers** option

6.1.4   REINFORCED CONCRETE 2-FLOOR FRAME

Data file: RCFRAME.INP

Reference:

Michanovic A., Marovic P., Dvornik J.: Nonlinear calculus of reinforced concrete structures ,ed. DHGK, Zagreb, 1993

Problem description:

Elasto-plastic (reinforced concrete section), 3-flor,1- span frame loaded with uniform vertical and horizontal (wind forces) load. Frame geometry, BC and loads are shown in Fig. 6.9

Cross–section data:

3 reinforced concrete sections, layered approach.
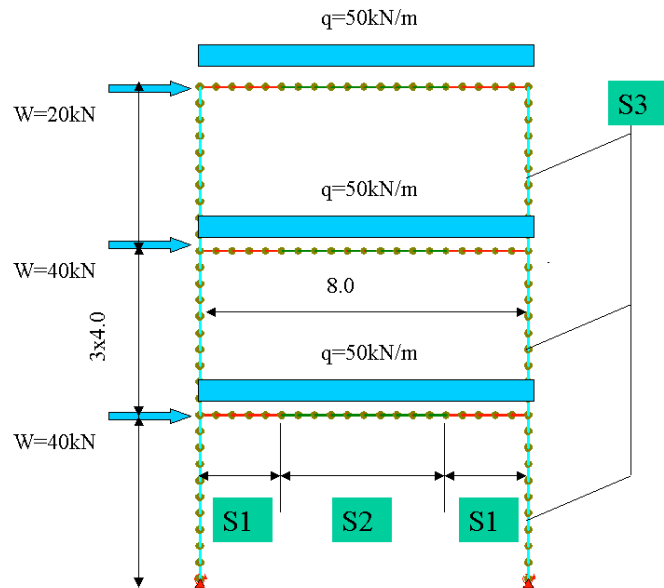
Figure 6.9: RC-frame. Geometry and loads
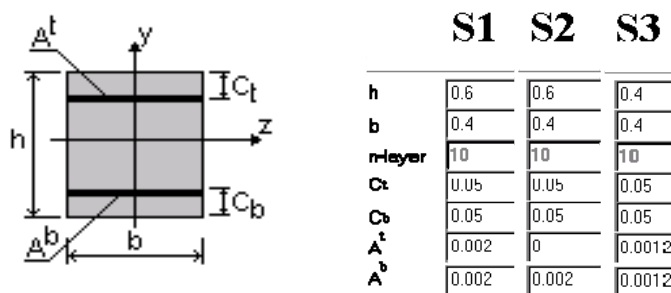
Figure 6.10: Cross-section data

Material data:

concrete (uni-axial elasto-plastic)

$E = 39000$ [MPa], $G = 162504$ [MPa], $f_c = 40.0$ [MPa], $f_t = 0.0$ [MPa]

reinforcement (uni–axial elasto–plastic)

$E = 210000$ [MPa], $f_y = 300.0$ [MPa]

Results:

Item:	Unit:	Z_SOIL:	Ref [MIH]:
Ultimate load factor	-	1.70	1.65
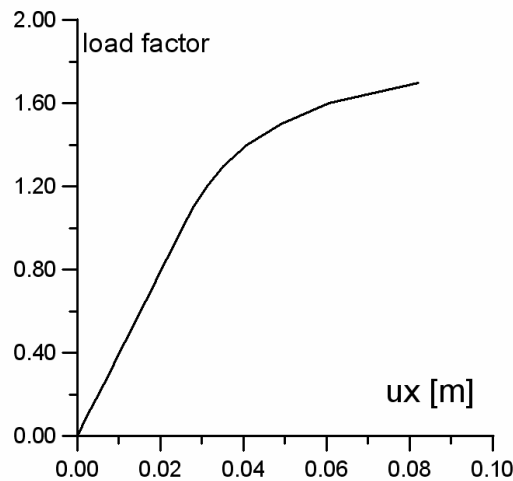
Figure 6.11: Load-displacement graph
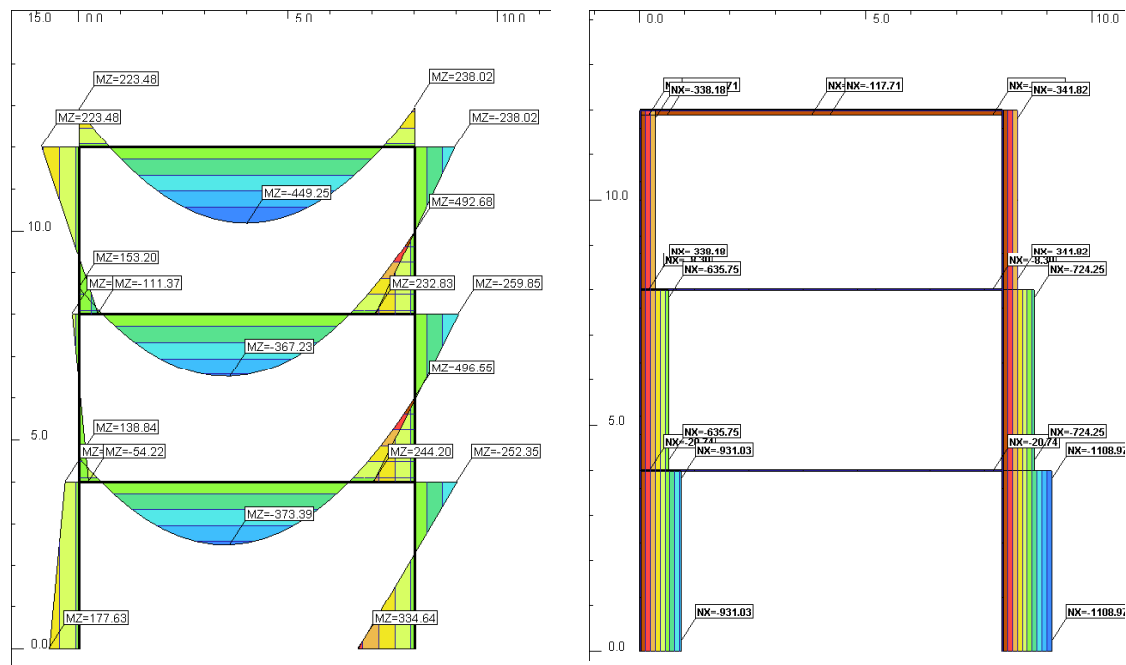
Figure 6.12: M_z , N graphs

6.1.5   PRESTRESSED BEAM

Data files: PRESTRESSEDBEAM-EC2.INP, PRESTRESSEDBEAM-EC2-x4.IN

Problem description:

Ultimate limit load analysis of a partially prestressed beam is analyzed here. Numerical results are compared with the experimental data by Tao and Du (after Chern, You and Bazant, PCI Journal vol. 37, No 1, 1992 p.74-84) for beam A-3.

Beam geometry, boundary conditions and loading are shown in Fig. 6.13.

Prestressed reinforcement ($A_p = 1.568$ cm^2) as well as standard reinforcement ($A_s = 2.36$ cm^2) are placed 6 cm from the bottom fibers. Reinforcing bars are prestressed up to 820
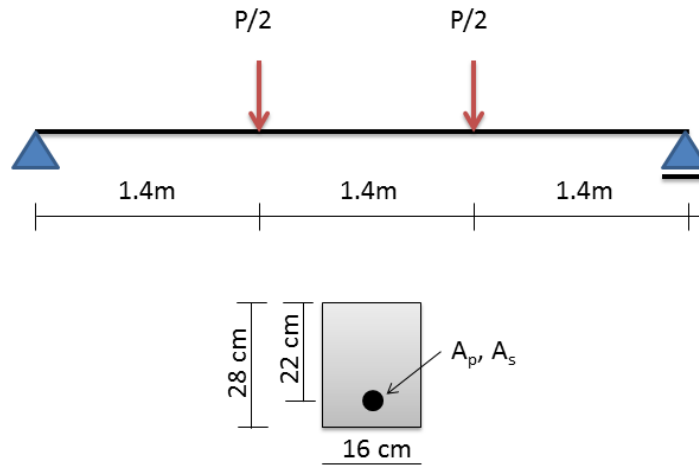
Figure 6.13: Prestressed concrete beam

MPa.

In this example a uniaxial $\sigma - \varepsilon$ relation proposed in the Eurocode-2 will be used to model concrete behavior. It has the following form

$$\sigma_c = f_{cm} \frac{k\eta - \eta^2}{1 + (k-2)\eta} \tag{6.1}$$

$$\eta = \frac{\varepsilon_c}{\varepsilon_{c1}} \tag{6.2}$$

$$k = 1.05 \frac{E_{cm}\varepsilon_{c1}}{f_{cm}} \tag{6.3}$$

As the uniaxial compressive strength is $f_c \approx 30.6$ MPa therefore we assume (following EC2 quidelines) concrete class C30/37 for which $f_{cm} = 38$ MPa, $E_{cm} = 32000$ MPa, $\varepsilon_{c1} = 0.0022$, $\varepsilon_{cu1} = 0.0035$. This yields $k = 1.945$. The stress-strain relation in compression domain is shown in the figure 6.14. The corresponding relation in tensile domain is shown in the figure 6.15. Softening behavior is regularized using softening scaling method for a given characteristic length $L_c = 5$ cm.
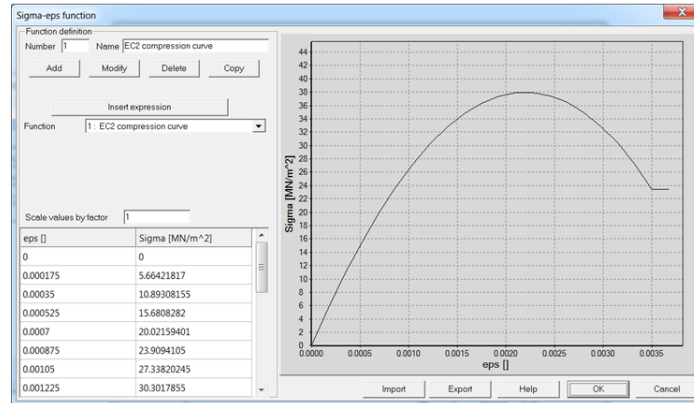
Figure 6.14: $\sigma - \varepsilon$ relation in compression
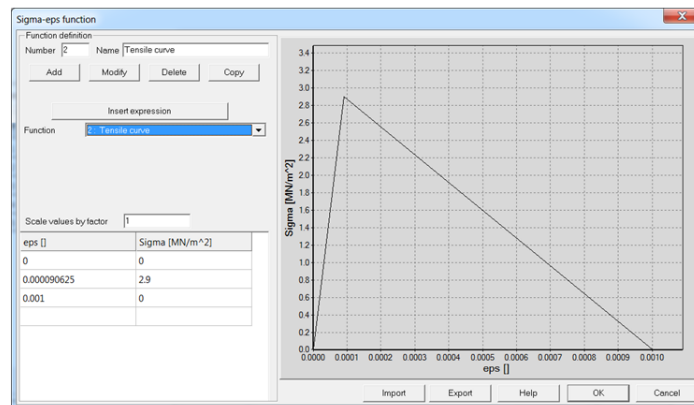
Figure 6.15: $\sigma - \varepsilon$ relation in tension
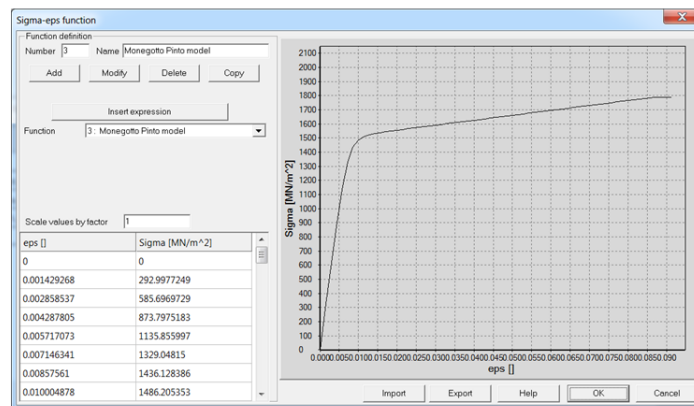
Figure 6.16: $\sigma - \varepsilon$ relation for prestressing bars

To model standard reinforcement an elasto-plastic model is used with the following set of parameters: $E = 200000$ MPa, $f_y = 430$ MPa. Reinforcing bars require little more sophisticated model like the one proposed by Monegotto and Pinto (after Chern, You and Bazant, PCI Journal vol. 37, No 1, 1992 p.74-84). This model expresses nonlinear stress-strain relation and describes hysteresis effect. To use this model a user defined stress-strain law is used and the skeleton curve is described by the following relation

$$
\sigma_p = E_p\,\varepsilon_p\left(Q + \frac{1-Q}{\left(1+\left(\dfrac{E_p\,\varepsilon_p}{K\,f_{py}}\right)^N\right)^{1/N}}\right) \tag{6.4}
$$

$$
Q = \frac{f_{pu} - K\,f_{py}}{E_p\,\varepsilon_{pu} - K\,f_{py}} \tag{6.5}
$$

In the considered case $E_p = 205000$ MPa, $f_{py} = 1465$ MPa, $f_{pu} = 1790$ MPa, $\varepsilon_{pu} = 0.087$, $N = 6.06$, $K = 1.0325$. The resulting Q value is $Q = 0.017$. It has to be mentioned here that the user model assumes (in general) unloading-reloading behavior like in damage models. Therefore one has to be careful when using this model to model prestressing in case of cyclic loadings (in dynamics for instance).

The Monegotto and Pinto relation is shown in the figure 6.16. In both data files flexibility based beam formulation is used (set at group ⊠ **Main**). The reinforced concrete cross section is defined by activating ⊠ **Additional layers** option, at the material level. This setting is shown in the Fig. 6.17.
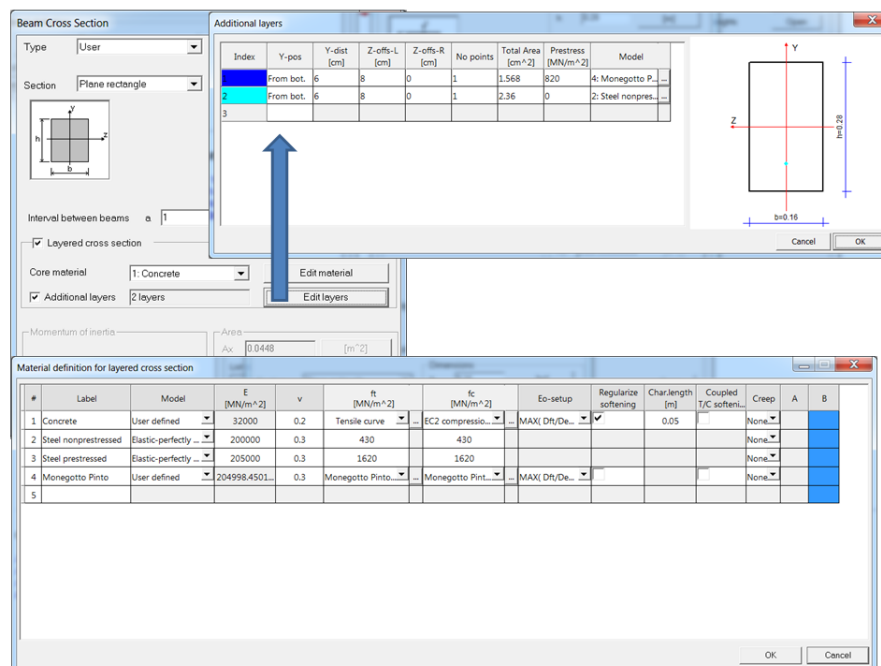
Figure 6.17: Definition of cross section through ⊠ **Additional layers** option

Comparizon of computed and experimental force-displacement diagrams is shown in figure 6.18.
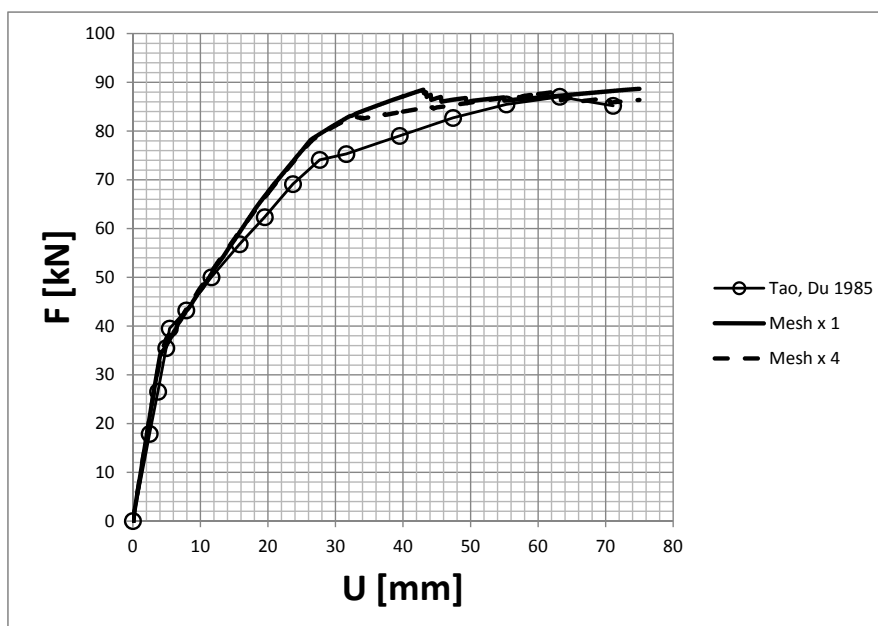
Figure 6.18: Force displacement diagrams

6.1.6 TWISTED BEAM

Data files: TWISTED_BEAM_Y.INP, TWISTED_BEAM_Z.INP

Reference:

Batoz J-L., Dhat G., Modélisation des structures par éléments finis, ed. Hermes , 1993, Vol3 , page 458.

Problem description:

Cantilever twisted beam, loaded with concentrated forces at the free end, after (BATOZ,1993), modelled with **beam** elements .The test is designed to check the performance of the twisted beam elements submitted to shear and bending deformation. _Y / _Z in the file name correspond to the direction of loading force in 2 cases of loads.
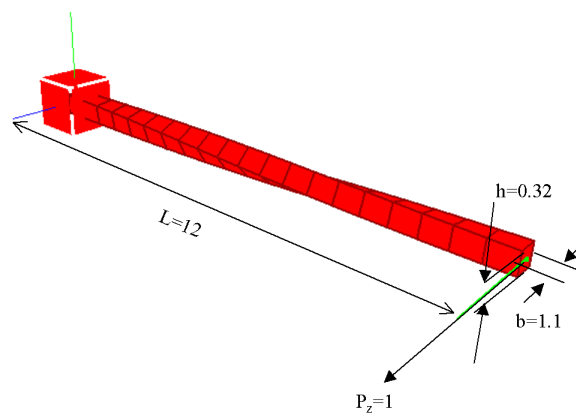
Figure 6.19: Geometry of twisted beam (beam model).

Cross–section data (Elastic model, integral approach):

Area: $A = 1.1 \times 0.32 = 0.352$,

inertia: $I_x = 0.00981221$, $I_y = 0.00300375$, $I_z = 0.0354933$

shear correction factors: $\kappa_y = \kappa_z = 0.83333$

Material data (linear elastic beam):

$E = 29 \cdot 10^6$, $\nu = 0.0$

Results comparison:

File:	V_A^{REF}	$V_A^{\text{Z\_SOIL}}$	W_A^{REF}	$W_A^{\text{Z\_SOIL}}$
..._Y	0.00175	0.001624	-0.00179	-0.001507
..._Z	-0.00172	-0.001507	0.00542	0.00551

6.1.7 RING

Data file: RINGBEAM.INP

Problem description:

Elastic ring supported at 4, two-directionally hinged supports, loaded with out-of plane uniform linear load. Geometry, BC, load are shown in Fig. 6.20
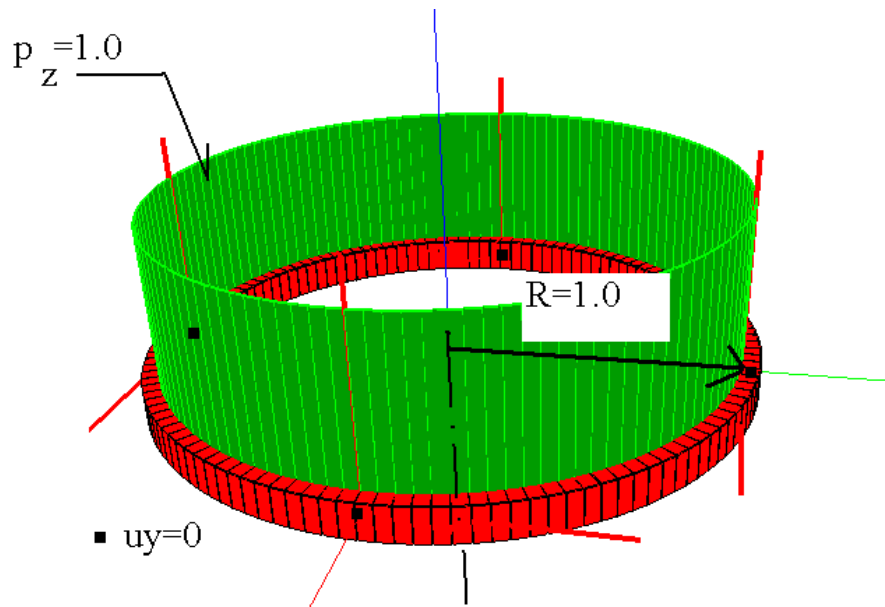
Figure 6.20: Out of plane loaded ring. Geometry and load

Cross–section data (Elastic model, integral approach):

area $A = 0.1$, inertia $I_x = I_y = I_y = 0.001$

Material data (Linear elastic):

$E = 100000$ [kPa], $\nu = 0.3$

Results:
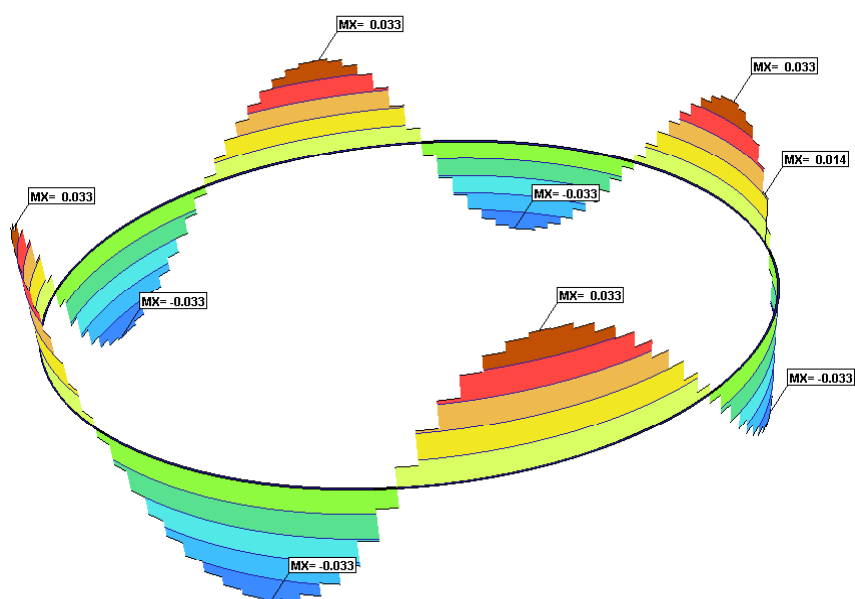
Figure 6.21: Torsional moment (M_x)
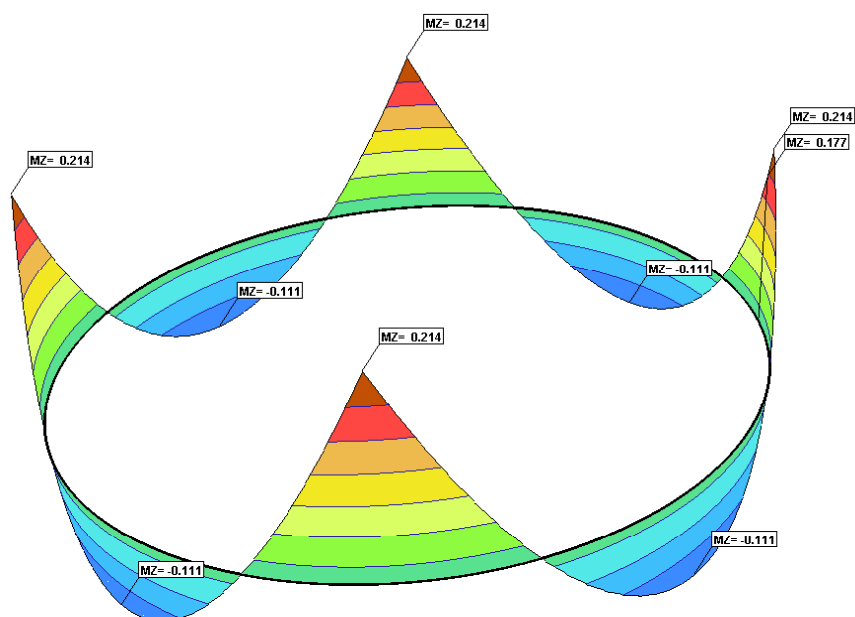
Figure 6.22: Bending moment (M_z)

Results comparison:

Item:	Formula:	Exact value:	Z_SOIL
$M_x =$	$qR^2(\tan(\alpha) - \alpha)$ with $\alpha = \arccos(\frac{n}{\pi}\sin\frac{\pi}{n})$	$= 0.03312$	0.033
$M_z^{\max} =$	$qR^2(-1 + \frac{\pi}{n}/\sin\frac{\pi}{n})$	$= 0.110$	0.111
$M_z^{\min} =$	$0.215 \cdot qR^2$	$= 0.215$	0.214

6.2 AXISYMMETRIC SHELLS

TUBE TO SPHERE CONNECTION

CYLINDER SUBJECTED TO PRESSURE

CIRCULAR ELASTO-PLASTIC PLATE

6.2.1 TUBE TO SPHERE CONNECTION

Data file: TUBULURE.INP

Reference:

Batoz J-L., Dhat G., Modélisation des structures par éléments finis, ed. Hermes, 1993, Vol3, page 207

Problem description:

Axisymmetric shell (cylindrical +spherical) submitted to vertical load (total P=1kN) as shown in Fig 6.23
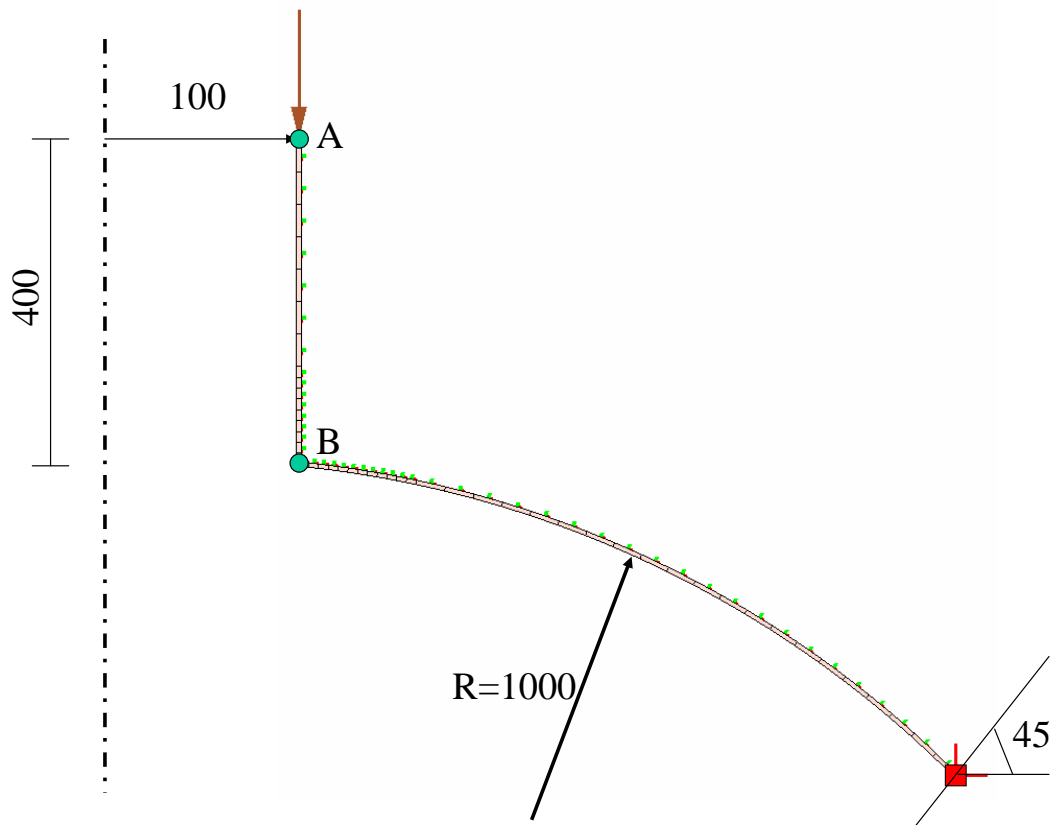
Figure 6.23: Geometrical model

Cross–section data:

Constant thickness $h = 6$ [mm]

Material data (Linear axisymmetric shell):

$E = 210$ [kN/mm^2], $\nu = 0.3$

Results comparison:

	Z_SOIL	Reference
Disp. VA [mm]	-1.384E-2	-1.362E-2
Disp. UB [mm]	-1.038E-3	-1.013E-3
Disp. VB [mm]	-1.353E-2	-1.332E-2
Rot. fB [-]	-2.738E-5	-2.486E-5

6.2.2 CYLINDER SUBJECTED TO PRESSURE

Data file: CYLINDER.INP

Reference:

Batoz J-L., Dhat G., Modélisation des structures par éléments finis, ed. Hermes, 1993, Vol3, page 163.

Problem description:

Cylindrical shell, clamped at the top, loaded by internal pressure. Geometry, load BC. and deformation of the shell are given in Figure 6.24
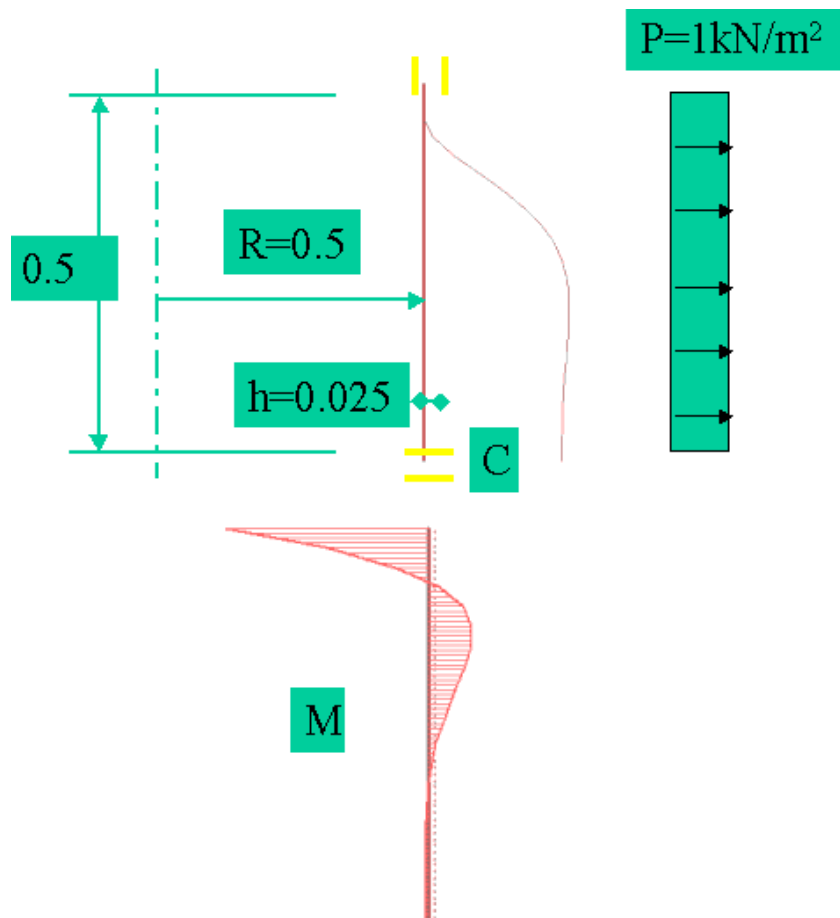
Figure 6.24: meridian deformation and bending moment graph

Cross–section data:

Constant thickness $h = 0.025$ [m]

Material data (Linear axisymmetric shell):

$E = 2 \cdot 10^{11}$ [Pa], $\nu = 0.3$

Results comparison:

	Z_SOIL	Exact
U_{xc}[m]	0.4986-7	0.4989E-7

6.2.3 CIRCULAR ELASTO-PLASTIC PLATE

Data file: CIRCPLATE.INP

Problem description:

Elasto–plastic (Huber–Misès) clamped circular plate under uniform load. The data as well as results (moments at the ultimate state) are shown in the Fig. 6.25
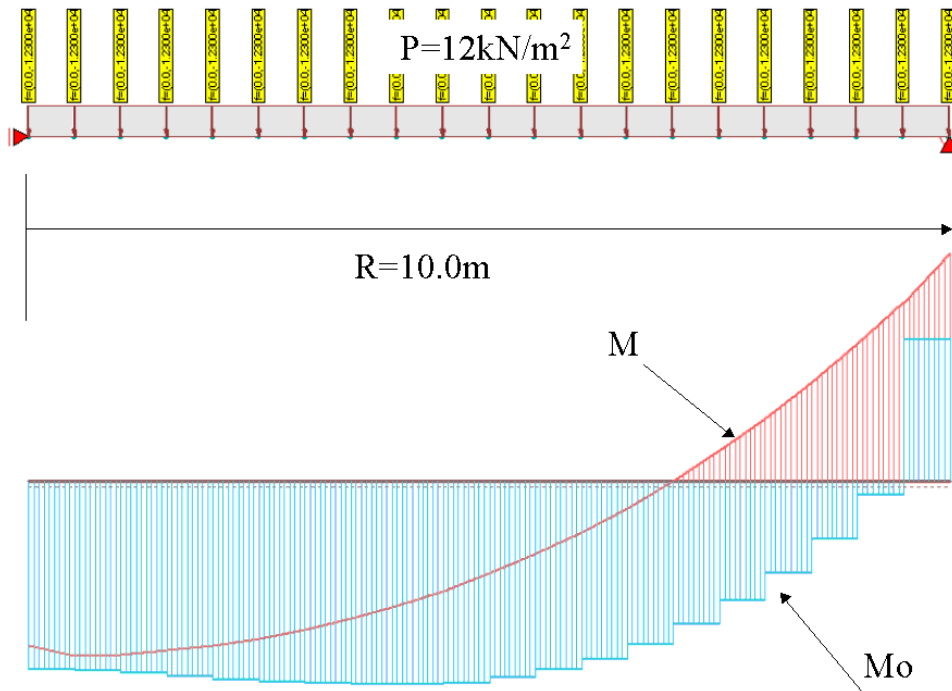
Figure 6.25: BC, load [kN/m^2]. Graphs of radial M_r and circumferential M_o bending moments.

Cross section:

      Uniform thickness $h = 1.0$, layered approach $n_{layer} = 10$

Material data – Elasto–plastic (bi-axial stress state, Huber–Misés criterion):

    $E = 2.1 \cdot 10^8$ [kPa], $\nu = 0.3$, $f_y = 4000000$ [kPa],

Results:

ultimate moment:

$$M_{\text{ult}} = \frac{f_y h^2}{4} = 400000 * 1/4 = 100000 \text{ kNm/m}$$

$$M_{\text{ult}} = \sqrt{M_r^2 + M_o^2 - M_r M_o}$$

	Z_SOIL	exact
max load $q_{\max}$	12200	$12 * M_{\text{ult}}/r^2 = 12000$

6.3 SHELLS

TWISTED BEAM (SHELL MODEL)

SQUARE ELASTOPLASTIC PLATE

SCORDELIS-LO ROOF

HEMISPHERE

ELASTOPLASTIC CYLINDRICAL SHELL

6.3.1   SCORDELIS-LO ROOF

Data file: SCOROOF.INP

Reference:

Batoz J-L., Dhat G., Modélisation des structures par éléments finis, ed Hermes, 1993, Vol3, page 446.

Problem description:

Cylindrical shell roof. Geometry, FE mesh, boundary conditions (for 1/4 of the shell due to dual symmetry) are shown in Fig. 6.26
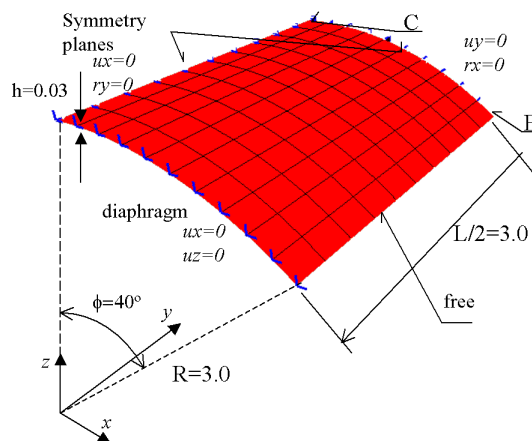
Figure 6.26: Geometry and boundary conditions

Load:

Uniform vertical load $p_z = -6250$ [Pa]

Material (linear elastic with):

$E = 3 \cdot 10^{10}$ [Pa], $\nu = 0.0$

Results:

Comparison with reference BATOZ, 1993, .i.e. exact solution:

	Z_SOIL	reference
W_B	0.0363	0.0361
W_C	0.00543	0.00541
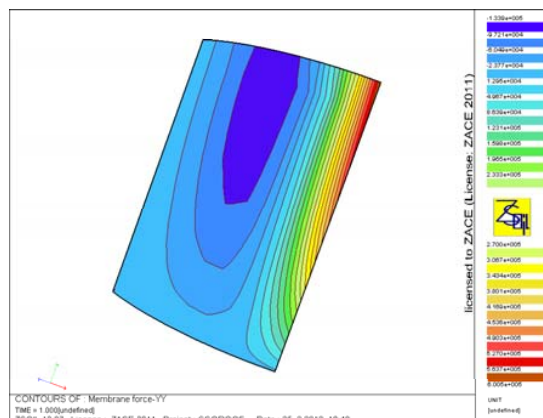
Figure 6.27: Membrane forces in Y direction

6.3.2   TWISTED BEAM (SHELL MODEL)

Data files: TWISTED_SHELL*.INP

Reference:

Batoz J-L., Dhat G., Modélisation des structures par éléments finis, ed Hermes, 1993, Vol3, page 458.

Problem description:

Cantilever twisted beam, loaded with concentrated forces at the free end, after (BATOZ,1993), modeled with shell elements .The test is designed to check the performance of the nonplanar elements submitted to shear and torsional deformation. 4 Files correspond to 2 cases of thickness and 2 cases of loads as specified in the table:

	thickness: $h = 0.32$	thickness $h = 0.0032$
Force: $F_y = 1$ (vertical)	*****_32_Y.INP**	*****_0032_Y.INP**
Force: $F_z = 1$ (horizontal)	*****_32_Z.INP**	*****_0032_Z.INP**

The geometry, FE mesh (12x4 SXQ4 elements), load and boundary conditions are shown in Fig. 6.28
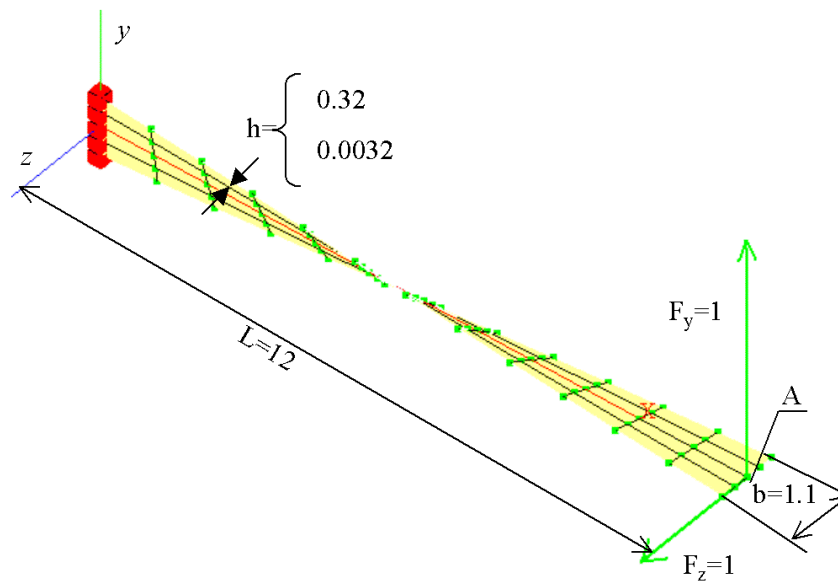
Figure 6.28: Twisted shell, geometry and other data.

Material data (linear elastic shell):

$E = 29 \cdot 10^6$ [MPa], $\nu = 0.0$

Results comparison:

File:	V_A^{REF}	$V_A^{Z\_SOIL}$	W_A^{REF}	$W_A^{Z\_SOIL}$
...32_Y	0.00175	0.00161	-0.00179	-0.00175
...32_Z	-0.00172	-0.00175	0.00542	0.00535
...0032_Y	1296	1258	-1878	-1836
...0032_Z	-1878	-1836	5316	5142

6.3.3   HEMISPHERE

Data files: HEMISPHERE_1L.INP, HEMISPHERE_2L.INP

Reference:

Batoz J-L., Dhat G., Modélisation des structures par éléments finis, ed Hermes, 1993, Vol3, page 462.

Problem description:

Hemispherical shell loaded with 2 concentrated forces. Both types of shell elements (i.e. shell 1 node layer) and shell (two node layers) are used in files **HEMISPHERE_1L.INP** and **HEMISPHERE_2L.INP**, respectively. Geometry and FE mesh (only one quarter is analyzed due to dual symmetry) are shown in Fig. 6.29:
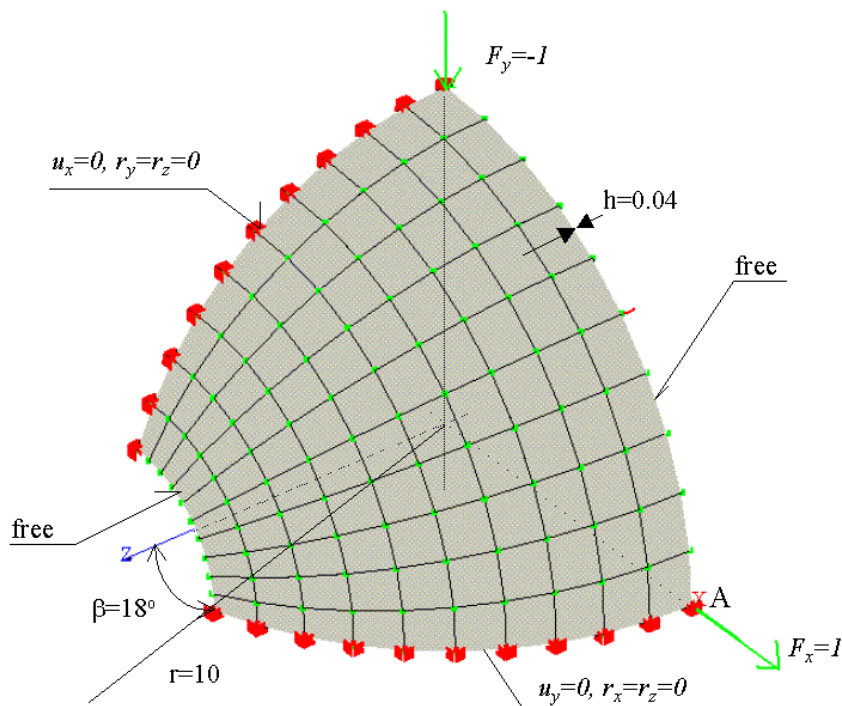
Figure 6.29: Hemispherical shell. Geometry [m] and other data

Material data (Linear elastic shell):

$E = 6.825 \cdot 10^7$, $\nu = 0.3$

Results comparison (Displacement u_{Ax}[m]):

reference	Z_SOIL - 1 node layer	Z_SOIL - 2 node layer
0.094	0.09260	0.09297

6.3.4 SQUARE ELASTOPLASTIC PLATE

Data file: EPSQPLATE.INP

Reference:

Hinton E., Owen D.R.J, Finite Element Software For Plates and Shells, Pineridge Press Ltd., Swansea UK 1984, vol 2 page 317

Problem description:

Elasto-plastic clamped square plate under uniformly distributed load

Material – elasto-plastic Huber-Misès (planes stress in each layer), isotropic, no softening/hardening:

$E = 30000$ [MPa], $\nu = 0.3$, $f_y = 30.0$ [MPa]

Geometry and discretization:

span $L = 6.0$[m], thickness $h = 0.2$[m]

6×6 SXQ4 shell elements (1 node layer) on the 1/4 of the plate as shown in the Fig. 6.30
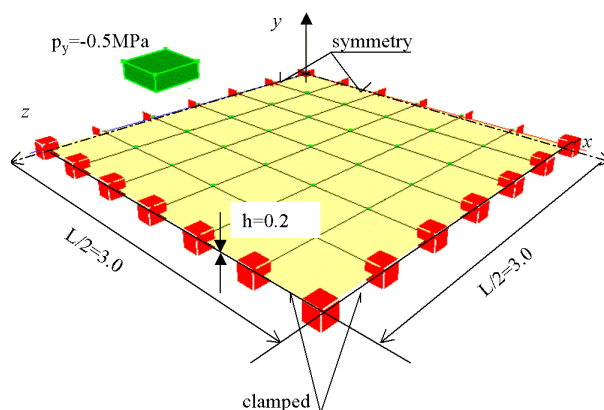
Results comparison
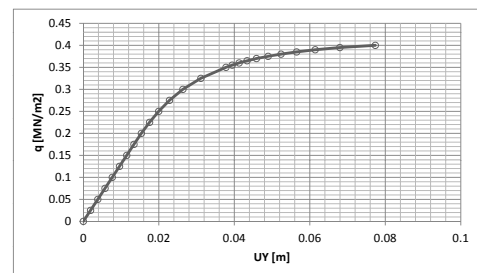
Figure 6.30: Elasto-plastic plate. Geometry and other data

Figure 6.31: Load versus vertical displacement at the plate centre graph.

Cross–sectional discretization:

10 equal layers

Load:

surface load up to $p = gh = 2.5 * 0.2 = 0.5$ [MN/m^2]

6.3.5   ELASTOPLASTIC CYLINDRICAL SHELL

Data file: EPCYLSHE.INP

Reference:

Hinton E., Owen D.R.J, Finite Element Software For Plates and Shells, Pineridge Press Ltd., Swansea UK 1984, vol 2, page 319

Problem description:

Cylindrical shell roof with 2 free edges supported by diaphragm, under self weight p/m^2
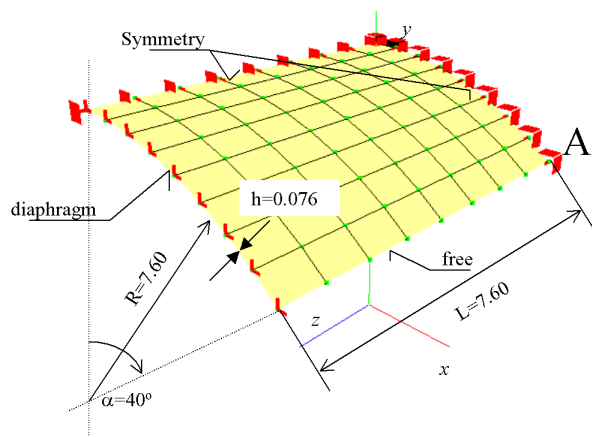
Results comparison
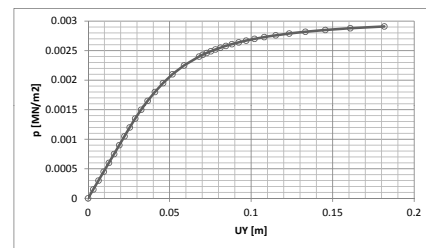
Figure 6.32: Elasto-plastic cylidrical shell roof. Geometry [m] and other data

Figure 6.33: Load density versus free edge mid-point (A) deflection graph

Material – Elasto-plastic Huber-Misès (plane stress in each layer), isotropic, no softening/hardening:

$E = 21000$ [MPa], $\nu = 0$, $f_y = 4.1$ [MPa]

Load:

uniform surface load up to $p_y = -0.003$ [MN/m^2]

Geometry and FE mesh (as shown in the Fig. 6.32

length :$L = 7.60$[m], radius: $R = 7.60$[m], angle: $\alpha = 40°$, thickness :$h = 0.076$[m]

8x8 SXQ4 elements (one node layer) for the 1/4 of the shell due to symmetry

Cross–sectional discretization:

10 equal layers

6.4 MEMBRANES

SOIL SLOPE REINFORCED BY MEMBRANES

6.4.1 SOIL SLOPE REINFORCED BY MEMBRANES

Data file: RFSSLOPE.INP

Reference:

Sawicki A., Lesniewska D., Reinforced Soils. Theory and applications., ed PWN Warsaw 1993

Problem description:

The slope $(10[m]$ height, $60°$ inclination), made of soil treated here as elasto-plastic (Drucker-Prager) continuum, with reinforcement modeled as membrane elements, is loaded by gravity and vertical uniform load. The ultimate value of top load is investigated (*analysis type: plane strain*). First initial state analysis is performed taking into account soil gravity load, then time dependent driven load analysis with increasing value of the load applied at the top of the slope is carried out until the divergence. The base load is $p = 1000[kPa]$. Load time function linearly varying from 0 at time 0 to 1 at time 1, is used to control loading process. Load incrementation result from setting of parameters in *Control / Analysis & Drivers* such us *Start=0, End=1, Increment=0.1.*

Geometry and discretization:

Numerical model is shown in the Fig. 6.34
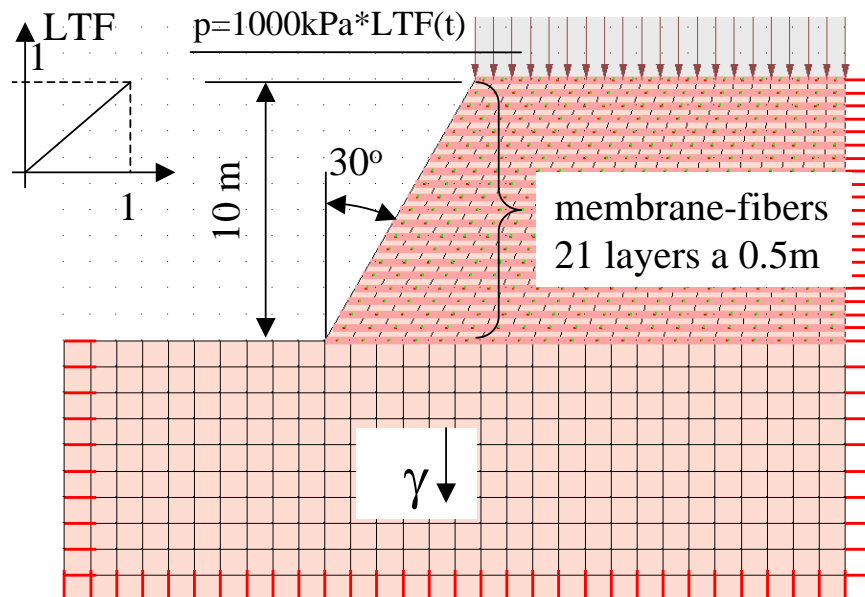
Figure 6.34: Reinforced soil slope. Geometry and reinforcement distribution

Material data

	Material	Model	Data group	Properties	Unit	Value
1	soil	Drucker-Prager	Elastic	E	[kN/m^2]	100000
				ν	—	0.3
			Unit weights	γ	[kN/m^3]	17
			Nonlinear	ϕ	[°]	34
				c	–	0
				Adjustment		Plane strain
2	membrane fiber	Elastic	Elastic	E	[kN/m^2]	1000000
			Nonlinear	f_t	[kN/m^2]	12
				f_c	[kN/m^2]	0
			Geometry	A	[m2/m]	0.005

Load: gravity (applied at time $t = 0$)
surface load up to $p = 1000$[kPa]

Results

At load factor $Ltf = 0.71$ divergence is observed with the failure surface shown at Fig. 6.35.
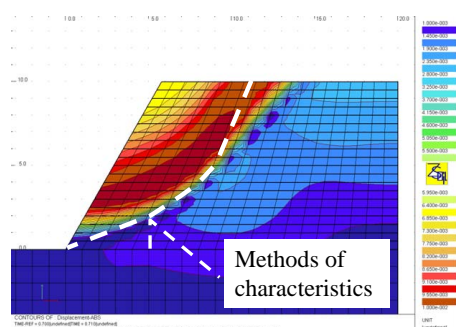
Figure 6.35: Failure surfaces estimated by Z_SOIL and from the reference
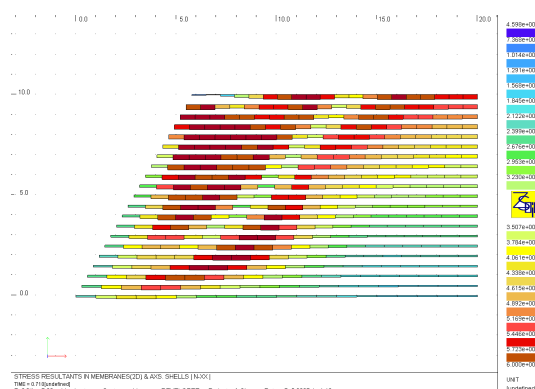
Figure 6.36: Tensile forces in membrane elements

The last converged state is noted at load factor $Ltf = 0.70$ compared with 0.71 obtained from the method of characteristics (perfectly plastic-rigid model) in reference. The forces appearing in membrane elements at the ultimate load are shown in Fig. 6.36

6.5   NONLINEAR BEAM HINGES

UNCOUPLED AXIAL NONLINEAR BEAM HINGE

UNCOUPLED FLEXURAL NONLINEAR BEAM HINGE

COUPLED FLEXURAL NONLINEAR BEAM HINGE FOR SEGMENTAL LININGS

6.5.1   UNCOUPLED AXIAL NONLINEAR BEAM HINGE

Data files:
HINGE-BEAM-2D-UX-L-DAM-1.INP, HINGE-BEAM-2D-UX-L-NL-EL-1.INP,
HINGE-BEAM-2D-UX-R-DAM-1.INP HINGE-BEAM-2D-UX-R-NL-EL-1.INP

Problem description:

The goal of this benchmark is to reproduce complex nonlinear behavior of a joint (connection between beams) subject to the axial imposed displacement applied at the beam endpoint. The resulting normal force-relative axial displacement curve must follow the explicit curves given by the user as a set of piecewise linear segments in axes F-u. The two different joint modes are analyzed i.e. nonlinear elastic and damage type. For nonlinear elastic mode dissipation of the energy does not occur while for damage mode it does and unloading-reloading response curves follow the secant joint stiffness modulus. The imposed axial displacement is applied at the beam endpoint next to the hinge. In all data files displacement based beam finite element is used, as there is no bending (this can be set at the group of parameters Main).
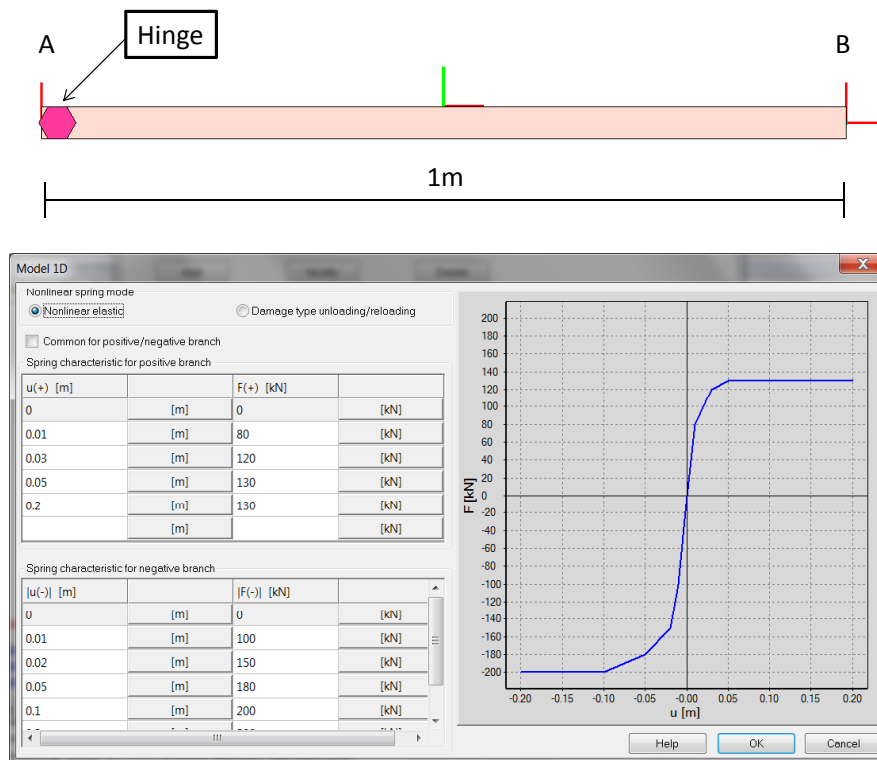
Figure 6.37: Beam geometry and $F - u$ user defined joint chacteristics (different for tension and compression)

Material parameters are as follows

Material	Model	Data group	Properties	Unit	Value
1 Beam	Beam	Elastic	E	[kN/m^2]	200000.0
			ν	—	0.0
		Geometry	b	[m]	0.1
			h	[m]	0.2
		Unit weight	γ	[kN/m]	0.0

Figure 6.38: Load time function for imposed displacement

The evolution of the normal force with respect to the imposed displacement for nonlinear elastic hinge is shown in the figure below. It can easily be recognized that the maximum achieved tensile force is equal to 130 kN while the compressive one one is 200 kN.
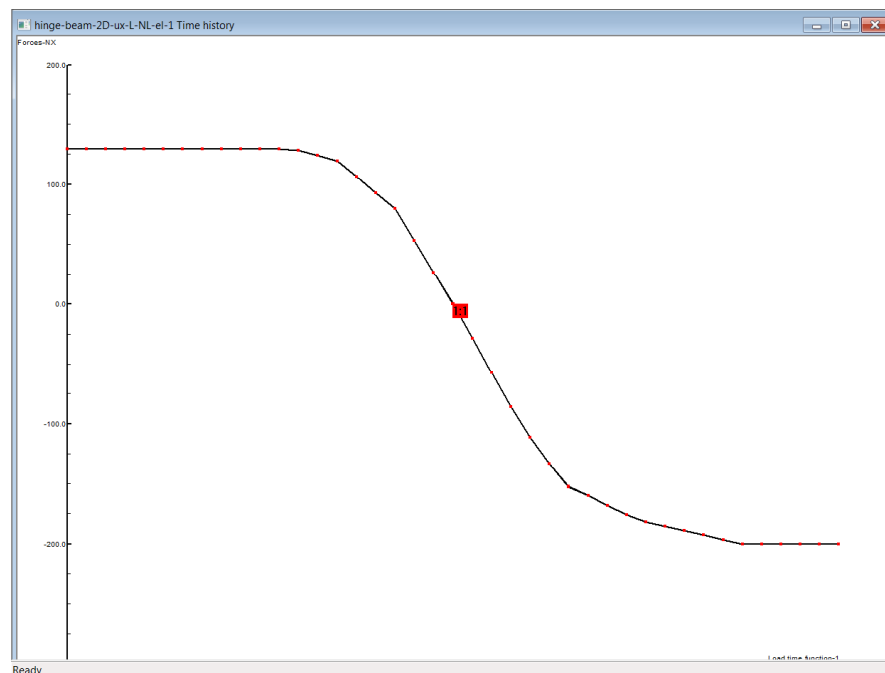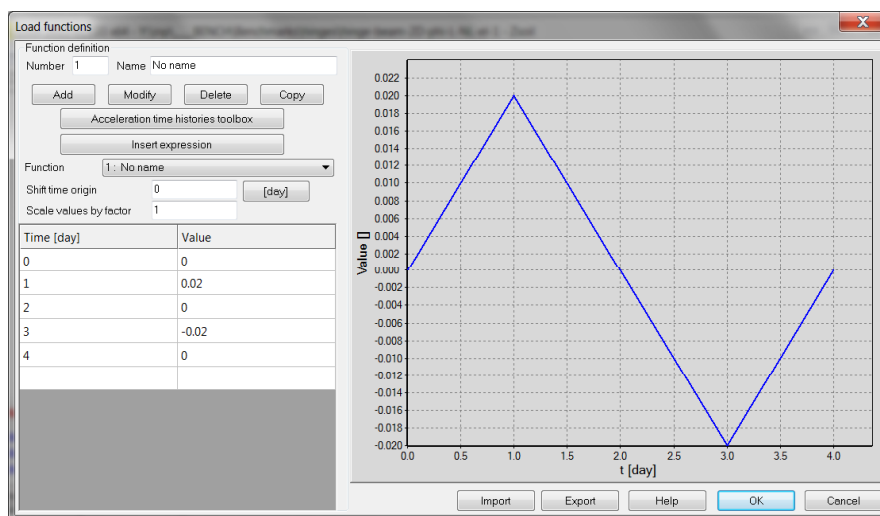

Figure 6.39: Resulting force-displacement diagram for nonlinear elastic hinge mode

The evolution of the normal force with respect to the imposed displacement for damage type hinge is shown in the figure below. It can easily be recognized that the maximum achieved tensile force is equal to 130 kN while the compressive one one is 200 kN but virgin loading and unloading/reloading paths do not coincide.
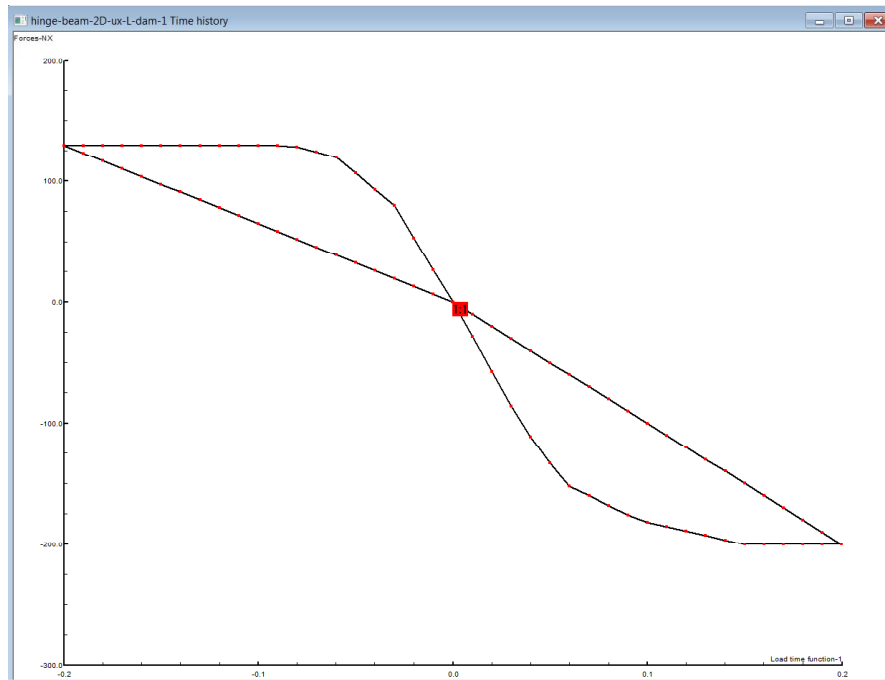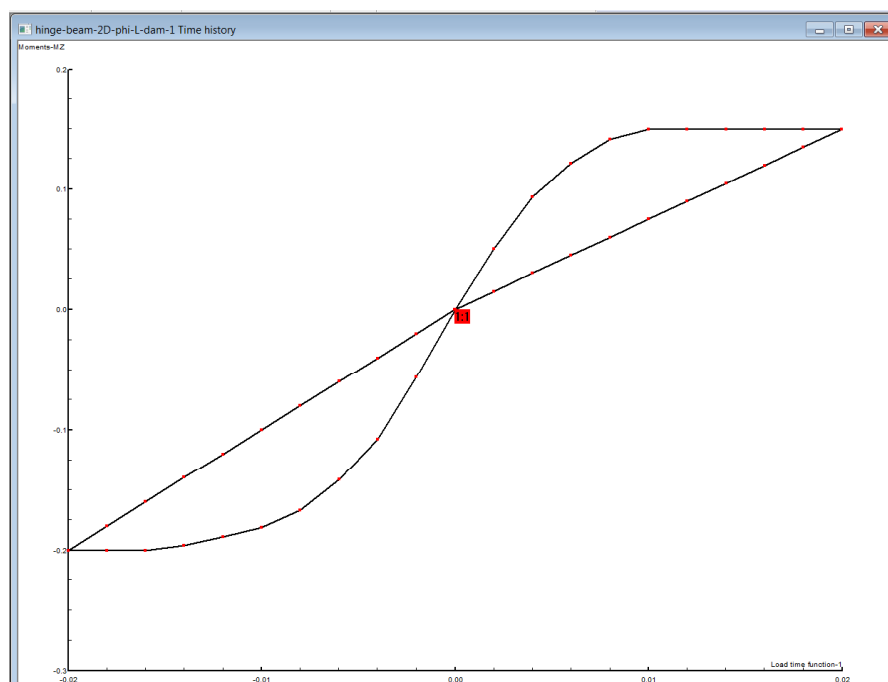
Figure 6.40: Resulting force-displacement diagram for damage type mode

6.5.2   UNCOUPLED FLEXURAL NONLINEAR BEAM HINGE

Data files:
HINGE-BEAM-2D-PHI-L-DAM-1.INP, HINGE-BEAM-2D-PHI-L-NL-EL-1.INP,
HINGE-BEAM-2D-PHI-R-DAM-1.INP HINGE-BEAM-2D-PHI-R-NL-EL-1.INP

Problem description:

The goal of this benchmark is to reproduce complex nonlinear behavior of a joint (connection between beams) subject to the imposed rotation applied at the beam endpoint. The resulting bending moment-relative rotation curve must follow the explicit curves given by the user as a set of piecewise linear segments in axes F-u. The two different joint modes are analyzed i.e. nonlinear elastic and damage type. For nonlinear elastic mode dissipation of the energy does not occur while for damage mode it does and unloading-reloading response curves follow the secant joint stiffness modulus. The imposed rotation is applied at the beam endpoint next to the hinge. It should be emphasized here that the positive bending moment is the one that causes tension in top beam fibers. In all data files flexible based beam element is used to reproduce linear moment distribution with a single beam element (to be set in the group of parameters `Main`).

Material parameters are as follows

Material	Model	Data group	Properties	Unit	Value
1 Beam	Beam	Elastic	E	[kN/m^2]	200000.0
			ν	—	0.0
		Geometry	b	[m]	0.1
			h	[m]	0.2
		Unit weight	γ	[kN/m]	0.0
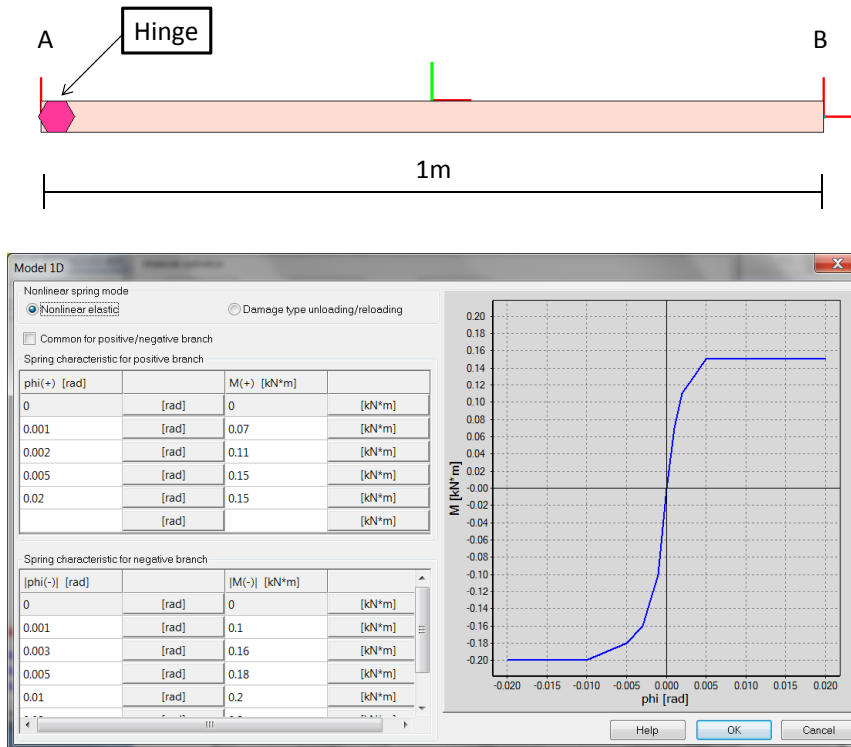
Figure 6.41: Beam geometry and $F - u$ user defined joint chacteristics

Figure 6.42: Load time function for imposed displacement

The evolution of the bending moment with respect to the imposed rotation for nonlinear elastic hinge is shown in the figure below. It can easily be recognized that the maximum achieved positive bending moment is equal to 0.15 kNm while the negative one is 0.2 kNm.

The evolution of the bending moment with respect to the imposed rotation for damage type hinge is shown in the figure below. It can easily be recognized that the maximum achieved positive bending moment is equal to 0.15 kNm while the negative one is 0.2 kNm. As in the example for the uncoupled axial hinge virgin loading/unloading-reloading branches do not
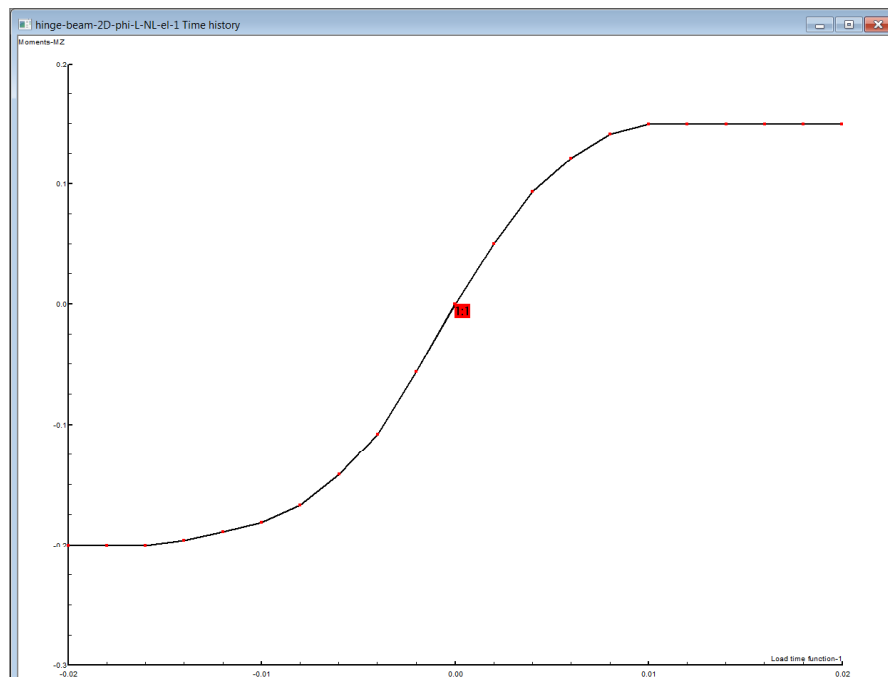
Figure 6.43: Resulting force-displacement diagram for nonlinear elastic hinge mode

coincide.

Figure 6.44: Resulting force-displacement diagram for damage type mode

6.5.3 COUPLED FLEXURAL NONLINEAR BEAM HINGE FOR SEGMENTAL LININGS

Data files:
JANSSEN-2D-BEAM-HINGE-A.INP, JANSSEN-2D-CONTINUUM-MODEL-A.INP,
JANSSEN-2D-BEAM-HINGE-B.INP, JANSSEN-2D-CONTINUUM-MODEL-B.INP

Problem description:

The goal of this benchmark is to reproduce complex nonlinear behavior of a joint (connection between beams), governed by the Janssen theory, subject to the imposed rotation that is applied at both beam endpoints (with opposite signs). To verify Janssen theory a corresponding mechanistic model of a joint was generated using two beam elements connected through the interface discretized with 2D continuum elements and contact interface. In all data files flexible based beam element is used to reproduce linear moment distribution within a single beam element (to be set in the group of parameters Main). The two different loading programs for imposed rotations and normal force are traced.
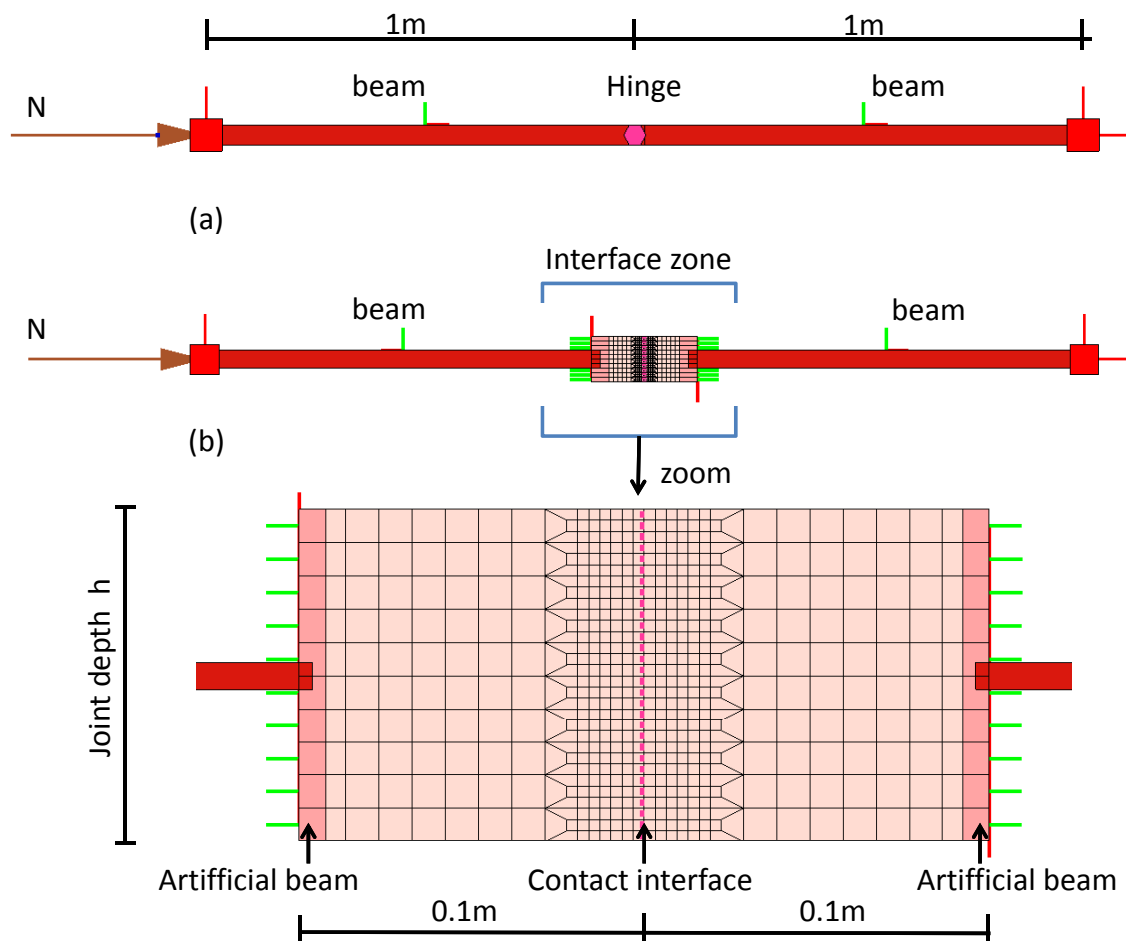
Figure 6.45: (a) beam-hinge model (b) beam-continuum interface model
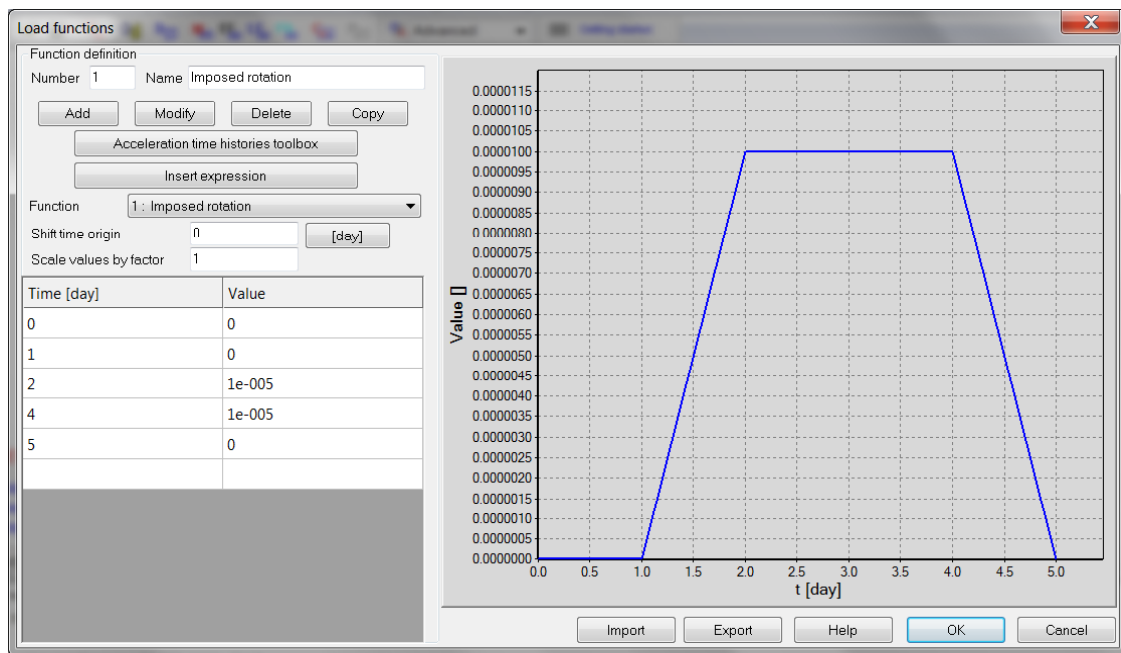
Figure 6.46: Load time function for imposed rotations at both beam endpoints for JANSSEN-2D-BEAM-HINGE-A.INP, JANSSEN-2D-CONTINUUM-MODEL-A.INP data files
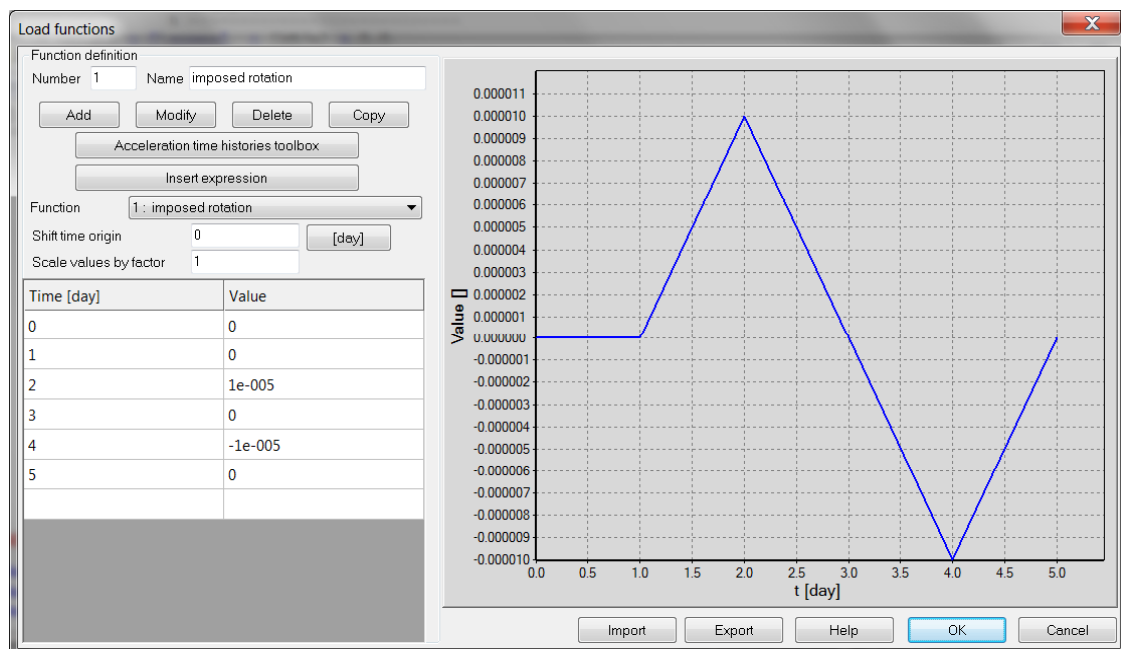
Figure 6.47: Load time function for imposed rotations at both beam endpoints for JANSSEN-2D-BEAM-HINGE-B.INP, JANSSEN-2D-CONTINUUM-MODEL-B.INP data files
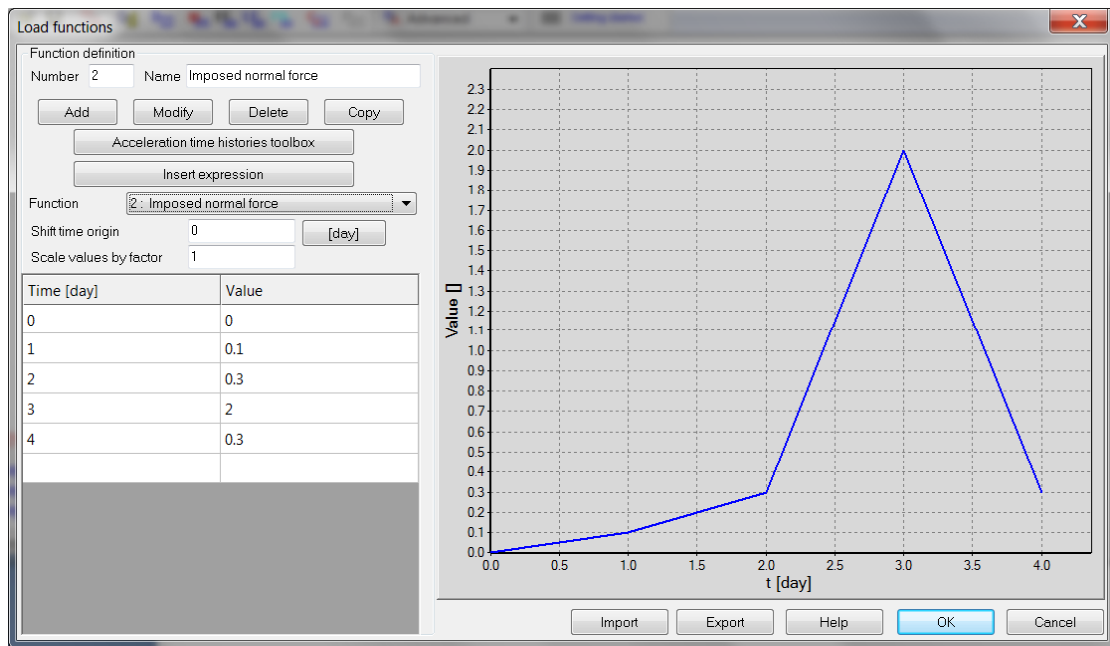
Figure 6.48: Load time function for imposed normal force in beams for JANSSEN-2D-BEAM-HINGE-A.INP, JANSSEN-2D-CONTINUUM-MODEL-A.INP data files
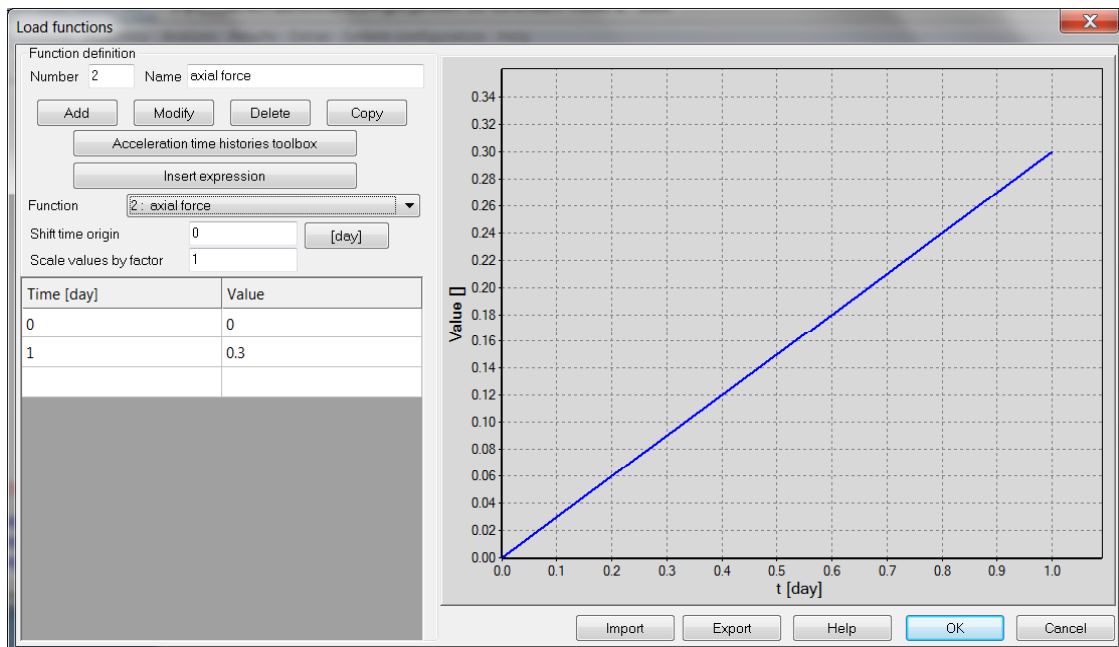

Figure 6.49: Load time function for imposed normal force in beams for JANSSEN-2D-BEAM-HINGE-B.INP, JANSSEN-2D-CONTINUUM-MODEL-B.INP data files

Material parameters for continuum models (files : JANSSEN-2D-CONTINUUM-MODEL-A.INP,JANSSEN-2D-CONTINUUM-MODEL-B.INP) are given in the table

	Material	Model	Data group	Properties	Unit	Value
1	Joint zone	Continuum	Elastic	E	[kN/m^2]	30000000.0
				ν	—	0.2
2	Artifficial beam	Beam	Elastic	E	[kN/m^2]	30000000.0
				ν	—	0.2
			Geometry	b	[m]	1.0
				h	[m]	10.0
			Unit weight	γ	[kN/m]	0.0
3	Interface zone	Contact	Nonlinear	ϕ	[deg]	0.0
4	Std. beams	Beam	Elastic	E	[kN/m^2]	30000000.0
				ν	—	0.2
			Geometry	b	[m]	1.0
				h	[m]	0.2
			Unit weight	γ	[kN/m]	0.0

Material parameters for beam-hinge models (files : JANSSEN-2D-BEAM-HINGE-A.INP,JANSSEN-2D-BEAM-HINGE-B.INP) are as follows

	Material	Model	Data group	Properties	Unit	Value
1	Std. beams	Beam	Elastic	E	[kN/m^2]	30000000.0
				ν	—	0.2
			Geometry	b	[m]	1.0
				h	[m]	0.2
			Unit weight	γ	[kN/m]	0.0
2	Joint	Flexural coupled hinge	Elastic	E	[kN/m^2]	30000000.0
				ν	—	0.2
			Geometry	Joint depth h	[m]	0.1
				Joint width b	[m]	1.0
			Main	Janssen theory flag	—	◎ **ON**
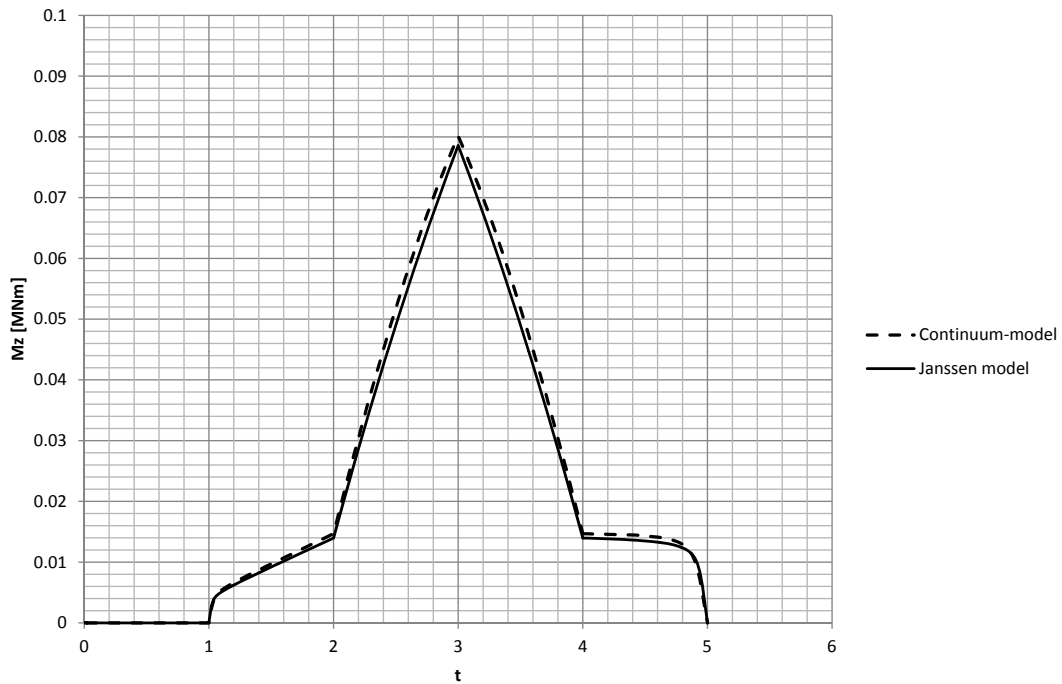
Figure 6.50: Bending moment time history for first loading program of imposed rotations and normal force
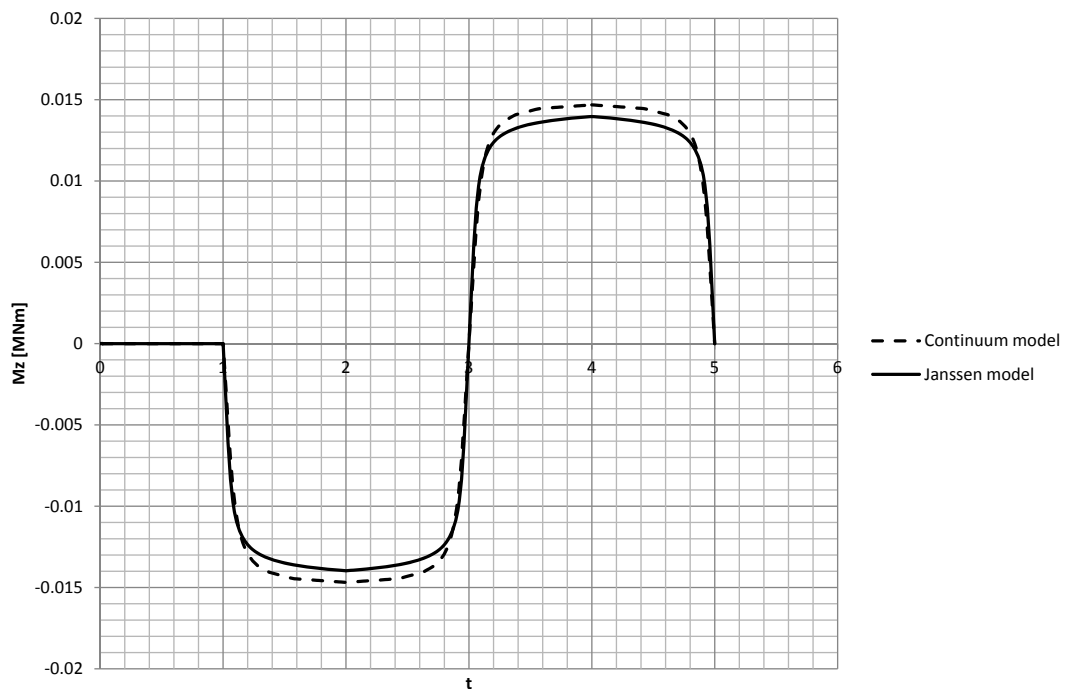
Figure 6.51: Bending moment time history for second loading program of imposed rotations and normal force

These two results prove that complex joint behavior is well approximated by the simple Janssen theory.

6.6   NONLINEAR SHELL HINGES

UNCOUPLED AXIAL NONLINEAR SHELL HINGE

UNCOUPLED FLEXURAL NONLINEAR SHELL HINGE

COUPLED FLEXURAL NONLINEAR SHELL HINGE FOR SEGMENTAL LININGS

6.6.1 UNCOUPLED AXIAL NONLINEAR SHELL HINGE

Data files:
HINGE-SHELL-UYL-NEL.INP, HINGE-SHELL-UYL-DAM.INP

Problem description:

The goal of this benchmark is to reproduce complex nonlinear behavior of a joint (connection between two shell elements) subject to the in plane imposed displacement applied at the right edge. The resulting membrane force-relative axial displacement curve must follow the explicit curves given by the user as a set of piecewise linear segments in axes F-u. The two different joint modes are analyzed i.e. nonlinear elastic and damage type. For nonlinear elastic mode dissipation of the energy does not occur while for damage mode it does and unloading-reloading response curves follow the secant joint stiffness modulus. It is important to note that shell hinges are defined in local coordinate system shown in figure below. It has to be emphasized here that the local hinge axis X is always aligned along shell element edge at which hinge is defined. Therefore, in this example, the hinge is defined for UY local degree of freedom.
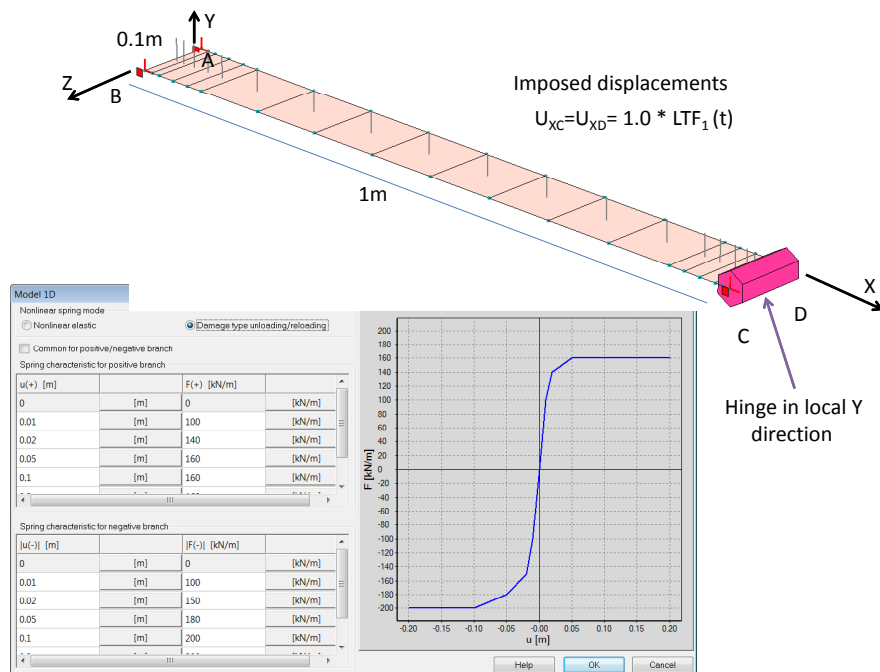
Figure 6.52: Shell geometry and $F - u$ user defined joint chacteristics (different for tension and compression)

Material parameters are as follows

Material		Model	Data group	Properties	Unit	Value
1	Shell	Shell	Elastic	E	[kN/m^2]	200000.0
				ν	—	0.0
			Geometry	h	[m]	0.1
			Unit weight	γ	[kN/m]	0.0
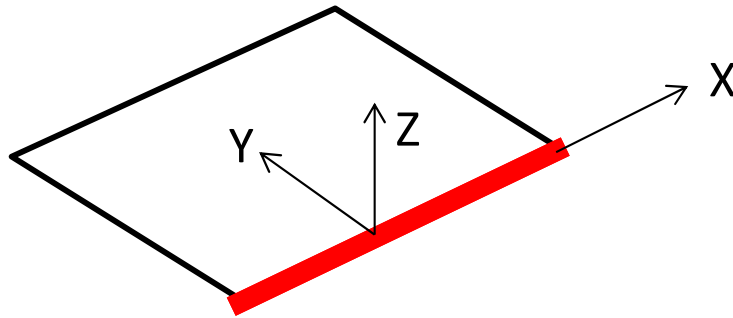
Figure 6.53: Local coordinate system for shell hinge
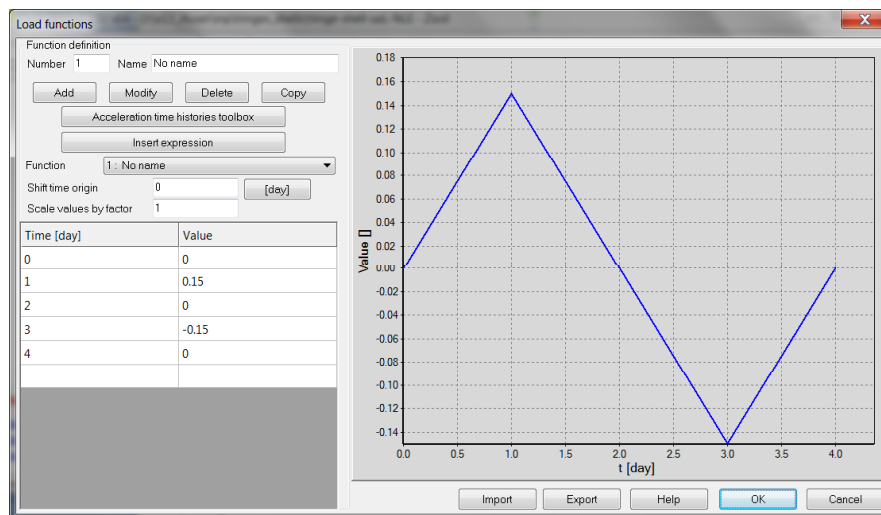
Figure 6.54: Load time function for imposed displacement

The evolution of the membrane force with respect to the imposed displacement for nonlinear elastic hinge is shown in the figure below. It can easily be recognized that the maximum achieved tensile membrane force is equal to 160 kN/m while the compressive one one is 200 kN/m.

The evolution of the membrane force with respect to the imposed displacement for damage type hinge is shown in the next figure. It can easily be recognized that the maximum achieved tensile force is again equal to 160 kN/m while the compressive one one is 200 kN/m but virgin loading and unloading/reloading paths do not coincide.
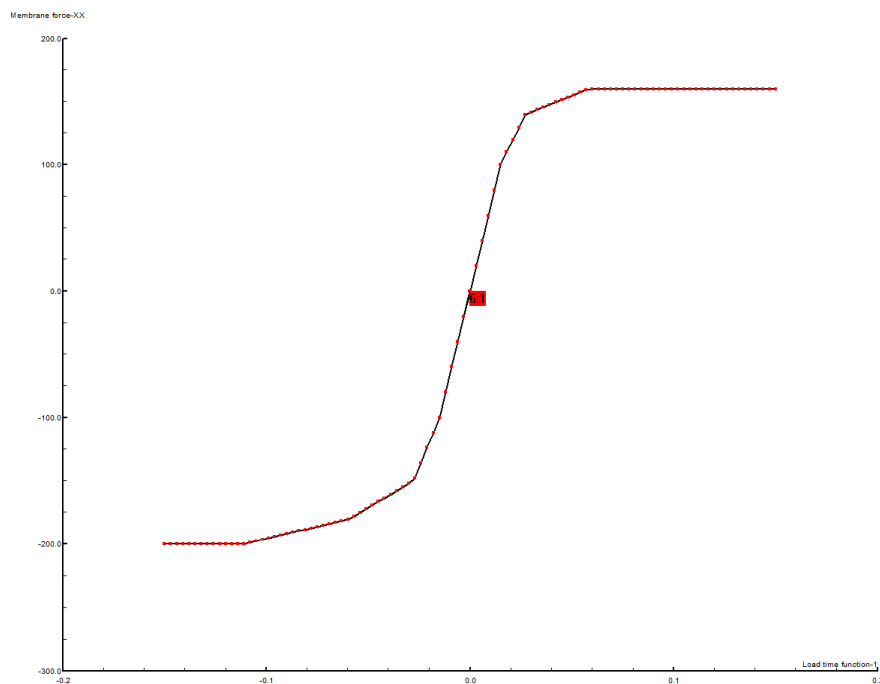
Figure 6.55: Resulting membrane force-displacement diagram for nonlinear elastic hinge mode
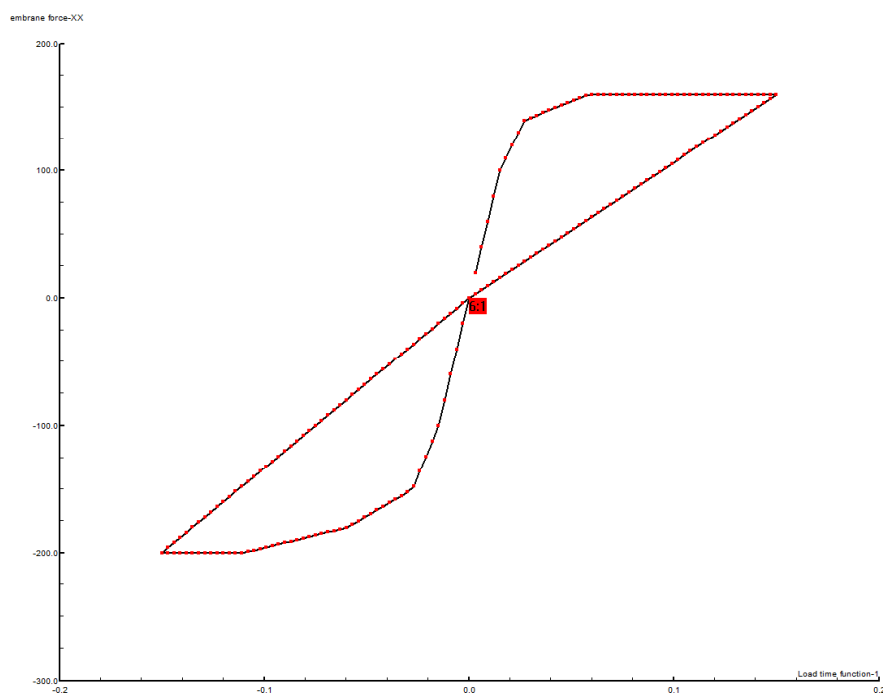
Figure 6.56: Resulting force-displacement diagram for damage type mode

6.6.2   UNCOUPLED FLEXURAL NONLINEAR SHELL HINGE

Data files:
HINGE-SHELL-MXL-DAM.INP, HINGE-SHELL-MXL-NEL

Problem description:

The goal of this benchmark is to reproduce nonlinear behavior of a joint (connection between two shell elements) subject to the imposed rotation applied at the right structure boundary. The resulting bending moment-relative rotation curve must follow the explicit curves given by the user as a set of piecewise linear segments in axes M-ϕ. The two different joint modes are analyzed i.e. nonlinear elastic and damage type. For nonlinear elastic mode dissipation of the energy does not occur while for damage mode it does and unloading-reloading response curves follow the secant joint stiffness modulus. It should be emphasized here that the positive bending moment is the one that causes tension in top shell fibers (see orientation of shell elements) and that the shell hinge local axis Z always coincides with the normal to the shell midsurface.
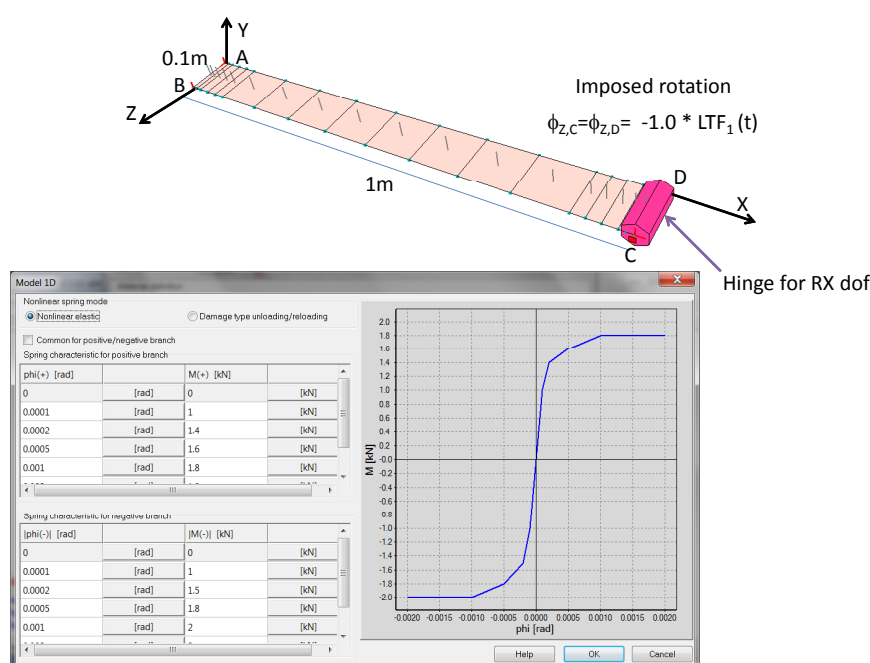
Figure 6.57: Shell geometry and $M - \phi$ user defined joint chacteristics

Material parameters are as follows

Material	Model	Data group	Properties	Unit	Value
1 Shell	Shell	Elastic	E	[kN/m^2]	200000.0
			ν	—	0.0
			h	[m]	0.1
		Unit weight	γ	[kN/m]	0.0

The evolution of the bending moment with respect to the imposed rotation for nonlinear elastic hinge is shown in the figure below. It can easily be recognized that the maximum achieved positive bending moment is equal to 1.8 kNm/m while the negative one is 2 kNm/m.
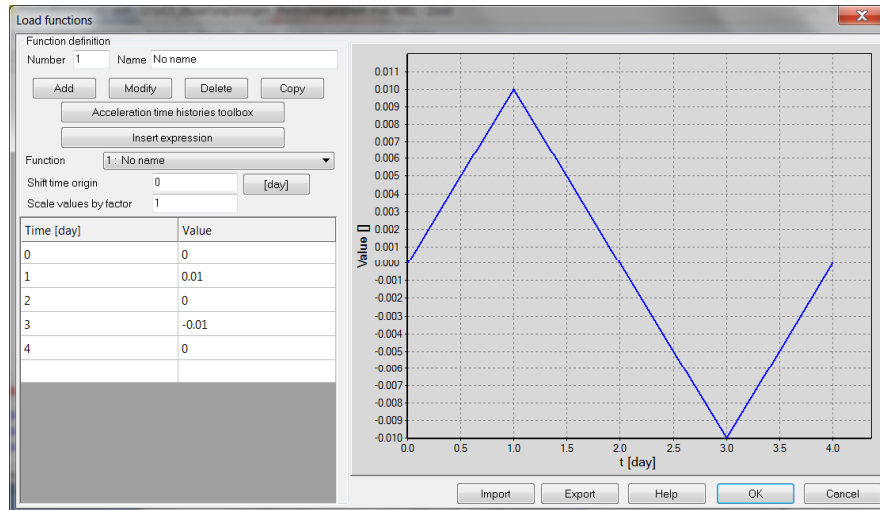
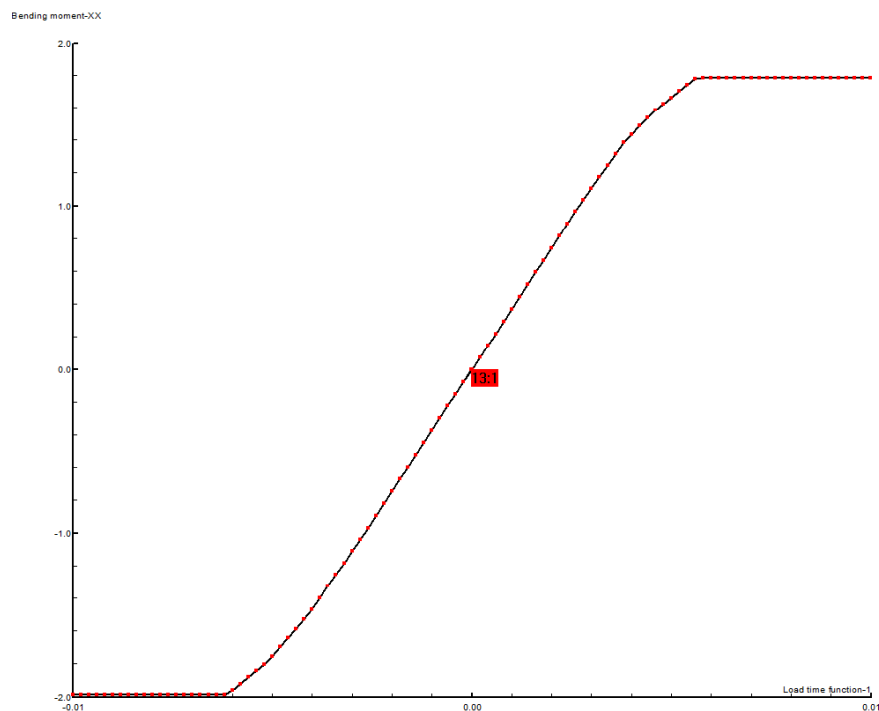Figure 6.58: Load time function for imposed displacement

Figure 6.59: Resulting moment-imposed rotation diagram for nonlinear elastic hinge mode

The evolution of the bending moment with respect to the imposed rotation for damage type hinge is shown in the figure below. It can easily be recognized that the maximum achieved positive bending moment is again equal to 1.8 kNm/m while the negative one is 2 kNm/m. The virgin loading/unloading-reloading branches do not coincide.
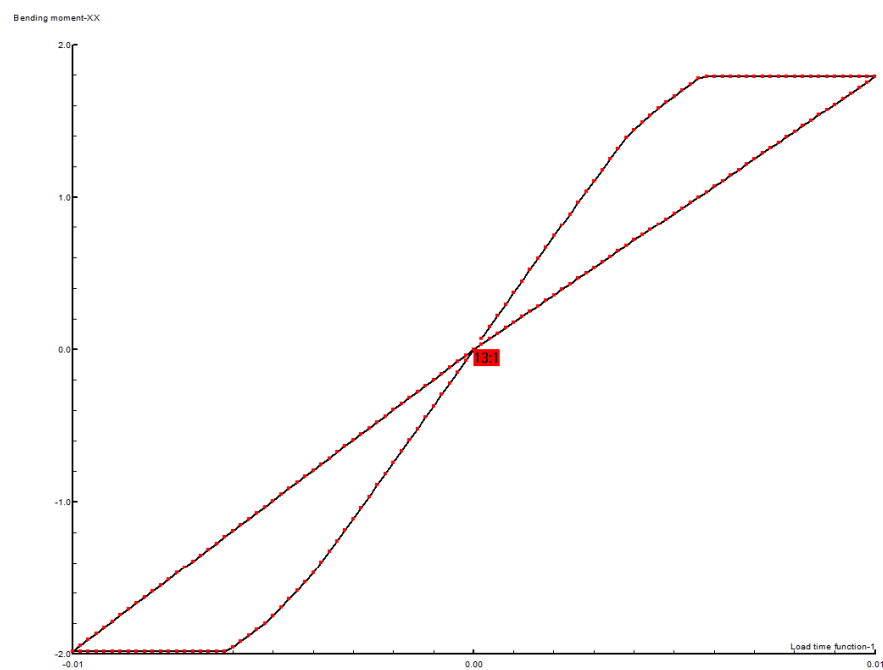
Figure 6.60: Resulting moment-imposed rotation diagram for damage type mode

6.6.3   COUPLED FLEXURAL NONLINEAR SHELL HINGE FOR SEGMENTAL LININGS

Data files:
HINGE-SHELL-JANSSEN-A.INP, HINGE-SHELL-JANSSEN-B.INP,

Problem description:

The goal of this benchmark is to reproduce complex nonlinear behavior of a joint (connection between two shell elements), governed by the Janssen theory, subject to the imposed rotation that is applied at both shell structure boundaries. The reference solutions for this benchmark can be found in subsection 6.6.3. The two different loading programs for imposed rotations and membrane force are traced.
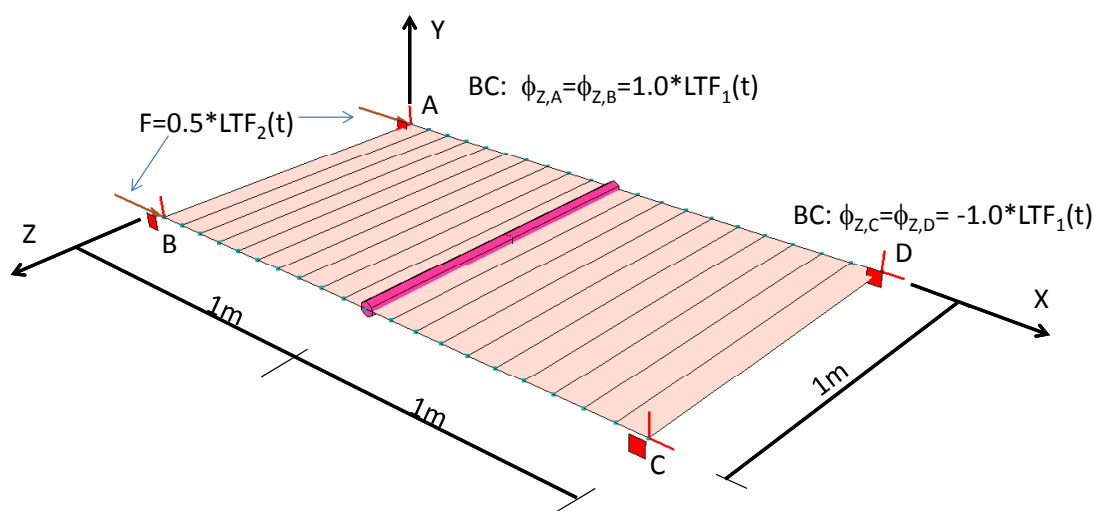
Figure 6.61: Shell-hinge model

Material parameters for shell-hinge models are as follows:

Material	Model	Data group	Properties	Unit	Value
1 Shells	Shell	Elastic	E	[kN/m^2]	30000000.0
			ν	—	0.0
			h	[m]	0.2
		Unit weight	γ	[kN/m]	0.0
2 Joint	Flexural coupled hinge	Elastic	E	[kN/m^2]	30000000.0
			ν	—	0.0
		Geometry	Joint depth h	[m]	0.1
		Main	Janssen theory flag	—	◎ **ON**

Figure 6.62: Load time function for imposed rotations at shell bounding edges
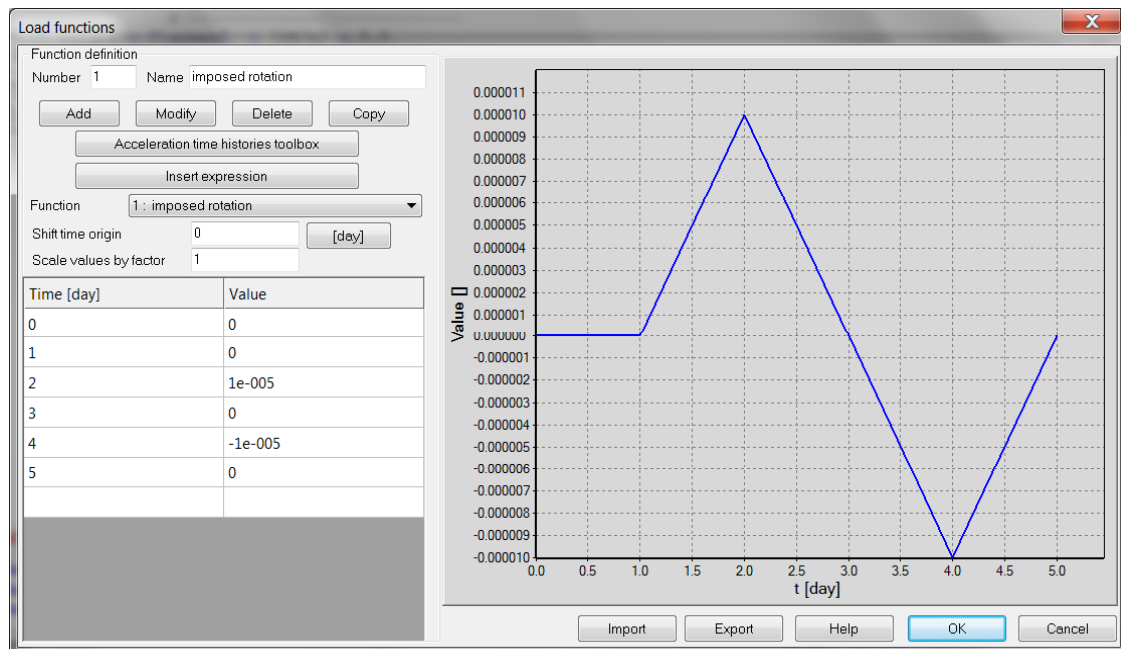
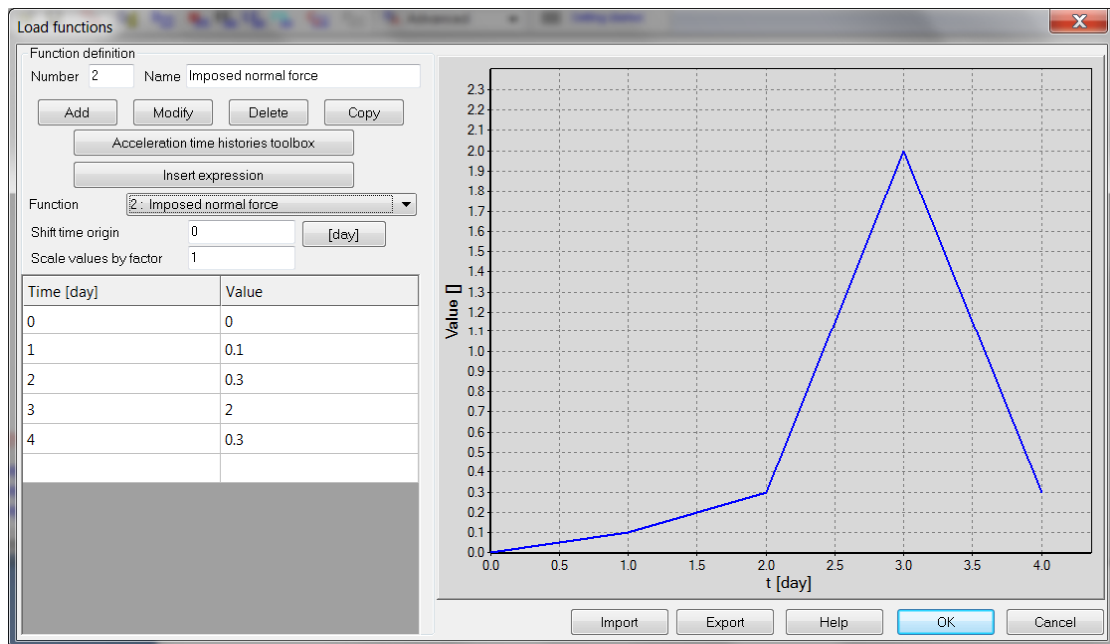Figure 6.63: Load time function for imposed rotations at shell bounding edges

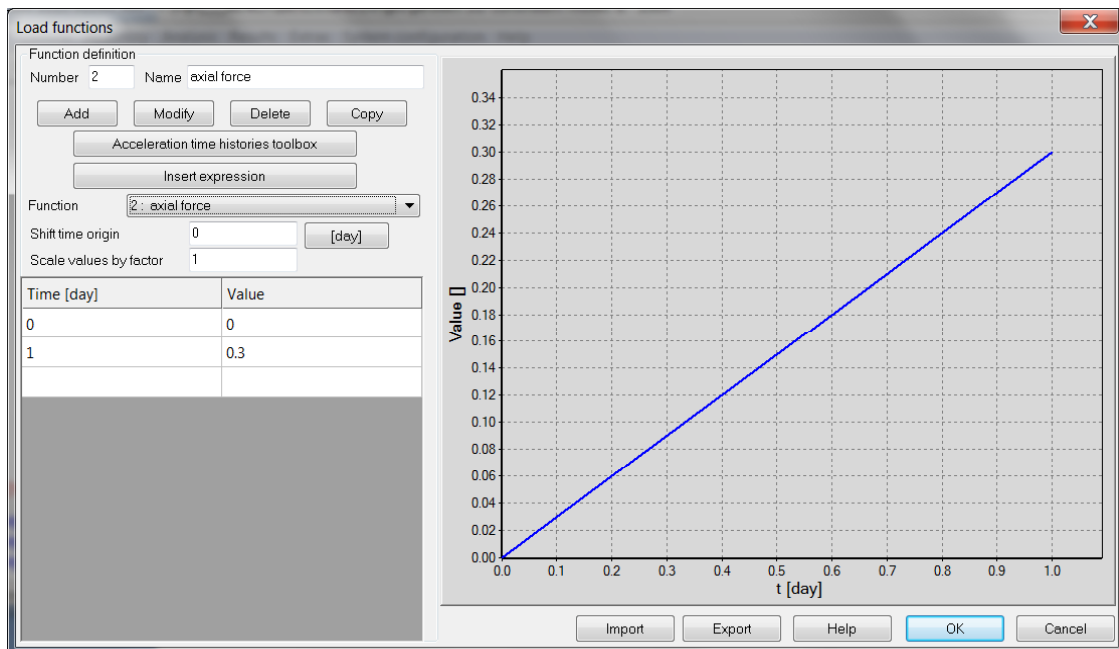Figure 6.64: Load time function for imposed membrane force

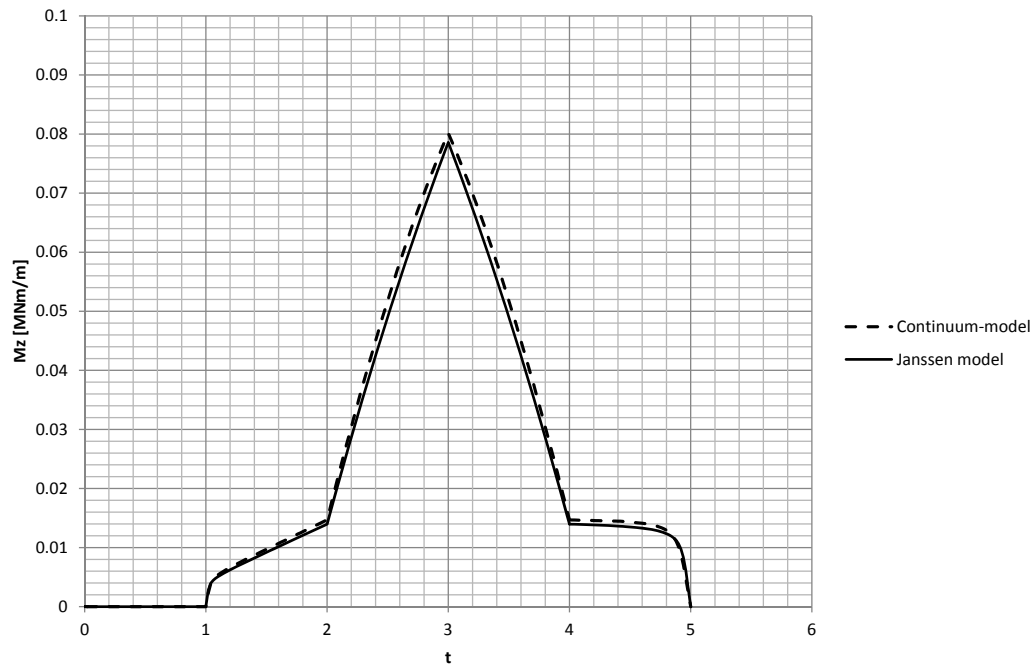Figure 6.65: Load time function for imposed membrane force

Figure 6.66: Bending moment time history for first loading program of imposed rotations and membrane force
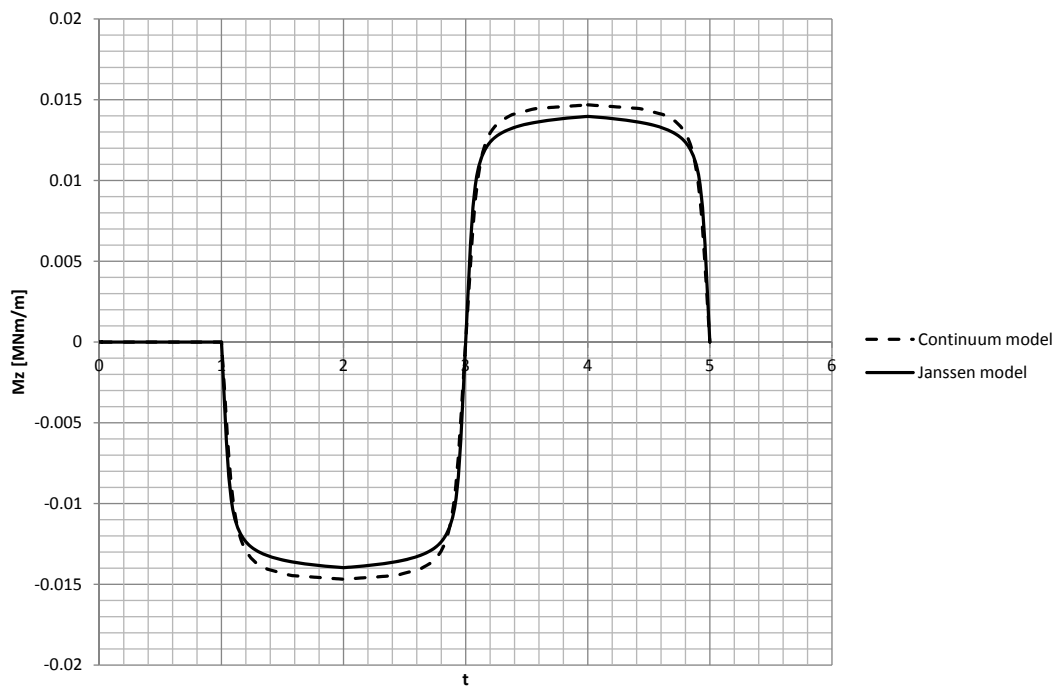

Figure 6.67: Bending moment time history for second loading program of imposed rotations and membrane force

This result is fully compatible with the one obtained for beam elements and beam Janssen hinge.

Chapter 7

SOIL-STRUCTURE INTERACTION BENCHMARKS

BURRIED PIPE

PILE 3D

NAIL

7.1 BURRIED PIPE

Data file: CATONA.INP
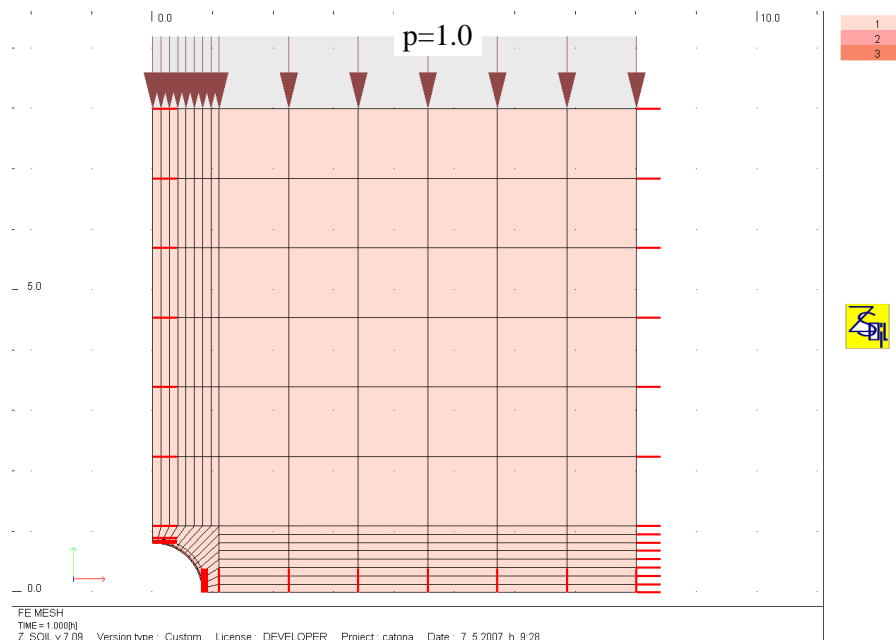
Figure 7.1: of the structure

The geometry of the problem, load and boundary conditions are shown in figure 7.1. Due to the double symmetry of the problem only the quadrant has been discretized.

The material properties for soil, steel pipe and interface are as follows[1]:

Material	Model	Data group	Properties	Unit	Value
1 soil	Elastic	Elastic	E	[kN/m^2]	1000
			ν	—	0.33
2 pipe	Elastic	Elastic	E	[kN/m^2]	335410
			ν	—	0.33
3 interface		Nonlinear	ϕ	[°]]	0°/14.036°/89°

Lining radius and thickness are $r = 0.84m$ $t = 0.0375659m$ respectively.

The normal and shear contact stress distribution is shown in Fig. 7.2. All these results are in a good agreement with theoretical solution.

---

[1]Kisu Lee, An efficient solution method for frictional contact problems, Comp.& Struct., pp.1–11, (1989).
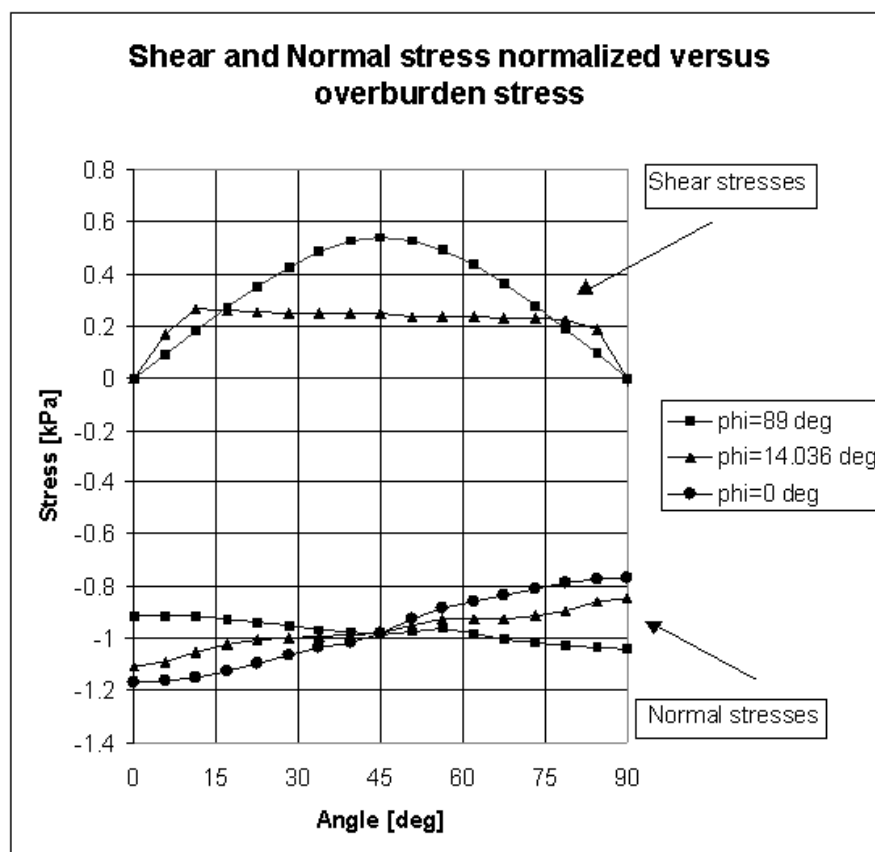
Figure 7.2: normal stresses
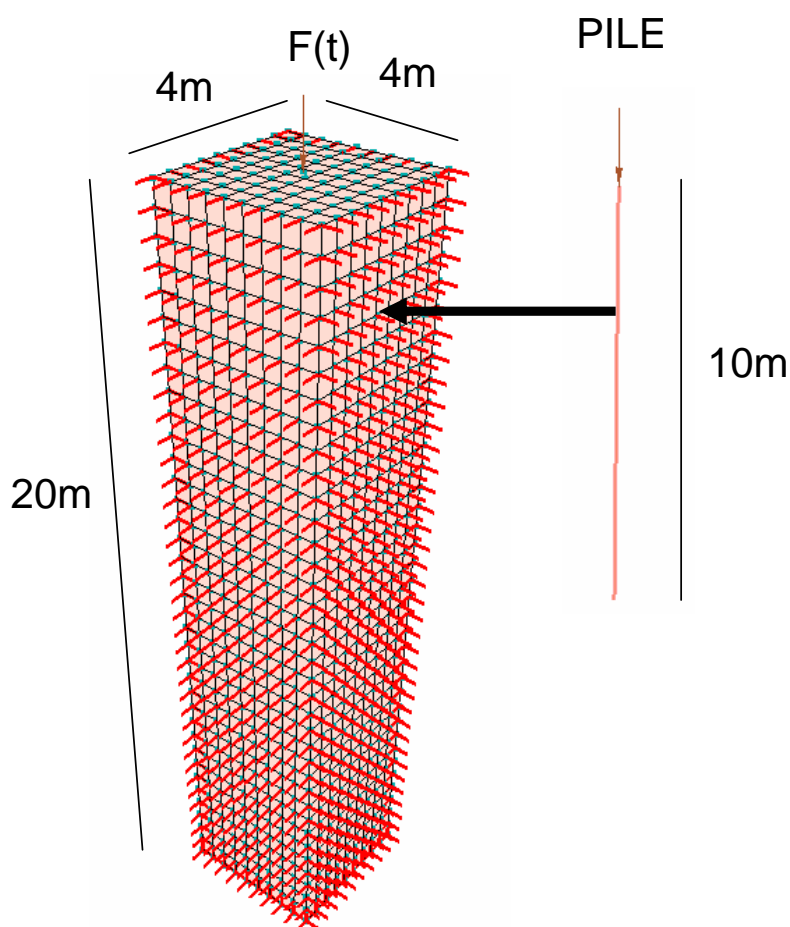
7.2 PILE 3D

Data file: PILE-3D.INP

Figure 7.3: FE model

The geometry of the problem, load and boundary conditions are shown in figure 7.3. This pile bearing capacity problem is modeled with aid of beam elements embedded in the 3D continuum including both pile interface and the interface between foot of the pile and continuum. In this test we assume that the medium is elastic, pile interface is purely adhesive and pile tip interface compressive bearing capacity is limited by q_c value. All material properties are summarized in the table below:

	Material	Model	Data group	Properties	Unit	Value
1	clay	Elastic	Elastic	E	[kN/m^2]	80000
				ν	–	0.3
			Density	γ_D	[kN/m^3]	18
				γ^F	[kN/m^3]	10
				e_o	–	0.0
			Initial state K_o	K_{ox}	[-]	0.6
				K_{oz}	[-]	0.6

2	Pile	Beams	Elastic	E	[kN/m²]	20000000
				ν	–	0.2
			Density	γ	[kN/m³]	0
			Geometry	Diameter	[m]	0.8
3	Pile interface	Pile interface	Non-linear	ϕ	[°]	0
				ψ	[°]	0
				C	[kN/m²]	14
4	Pile ti int.	Pile tip int.	Non-linear	q_t	[kN/m²]	0.0
				q_c	[kN/m²]	2500

The force-settlement diagram is shown in the figure below. It indicates the limit force equal to 1600 kN. The analytical solution for a 10m long pile is as follows: $F = F_s + F_c = \pi \, D \, L \, c + \pi \dfrac{D^2}{4} \, q_c = 3.14 * 0.8 * 10 * 14 + 3.14 * \dfrac{0.8^2}{4} * 2500 = 351.9 + 1256.6 = 1608.5$kN
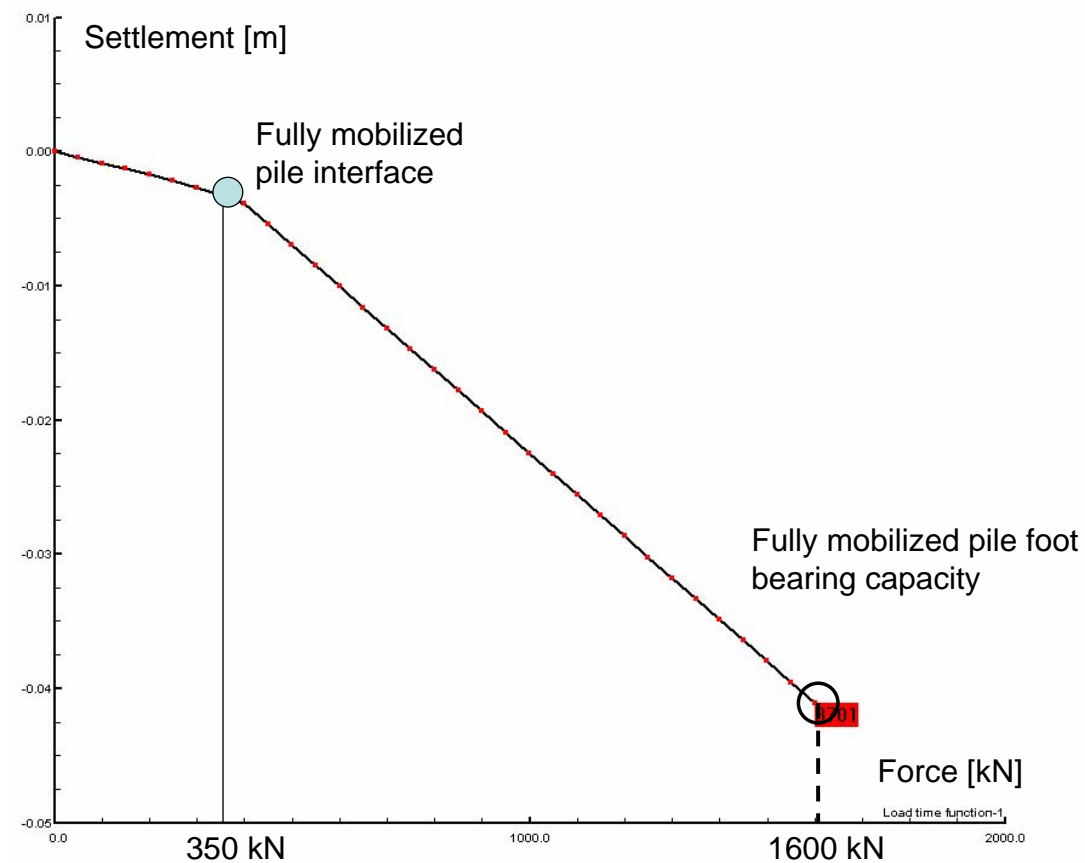
Figure 7.4: Force-settlement diagram

7.3 NAILING

Data file: NAIL-PULLOUT-3D-1_5m.INP, NAIL-PULLOUT-2D-1_5m.INP
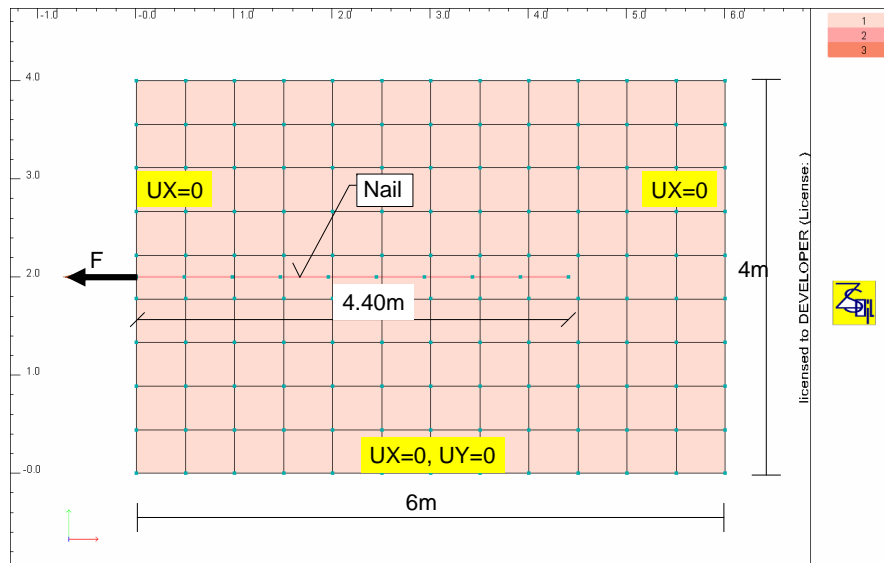
Figure 7.5: FE model

Evaluation of the pullout force for 4.40m long nail constructed in the confined subsoil is the aim of this benchmark. Geometry of the problem (in 2D), point load and boundary conditions (box type), for the test, are shown in figure 7.5. This problem is modeled with aid of beam elements embedded in the 2D continuum, with distance 1.5m in third direction, including adhesive nail interface. Such a complex discretization is created automatically by the preprocessor by using option `Nail` at the macromodelling level. In this test we assume that soil is elastic, while nail interface is purely adhesive. All material properties are summarized in the table below:

Material	Model	Data group	Properties	Unit	Value
1 soil	Elastic	Elastic	E	[kN/m^2]	100000
			ν	–	0.3
		Density	γ_D	[kN/m^3]	20
			γ^F	[kN/m^3]	10
			e_o	–	0.0
		Initial state K_o	K_{ox}	[-]	0.5
			K_{oz}	[-]	0.5
2 Nail core	Beams	Elastic	E	[kN/m^2]	200000000
			ν	–	0.2
		Density	γ	[kN/m^3]	0
		Geometry	Diameter	[m]	0.025
3 Nail interface	Nail interface	Non-linear	τ	[kN/m^2]	120
			Diameter	[m]	0.1

The resulting force-settlement diagram is shown in the figure below. It indicates the limit force equal to 110 kN. The analytical solution is as follows: $F_{ult} = \pi \, D \, L \, \tau = 3.14 * 0.1 * 4.4 * 120/1.5 = 110.58$kN
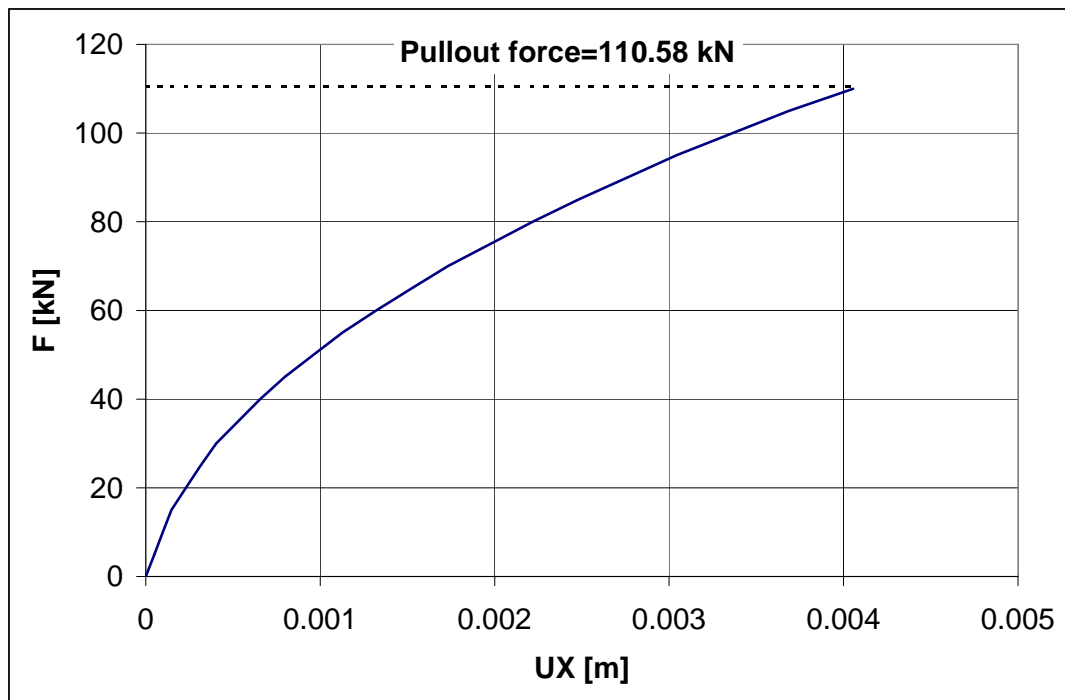

Figure 7.6: Force-settlement diagram

Index